Matrix Node Theory / Evans Node Dialect

Computations, Data and Verification

Conservative dynamics, proper time
and ten decisive requirements

Jordan Ryan Evans

Independent research

Volume II: Numerical record and executable methods

6 September 2026

The complete record distinguishes mathematical identities, simulated experiments, supplied-input benchmarks and published-summary comparisons. It contains 946 passed assertions across six suites. That number is not an experimental accuracy percentage. All new model coefficients and all empirical inputs are identified, and unfavorable physical benchmark results remain in the record.

Abstract

This volume reports the executed calculations accompanying the conservative MNT/EQEF reconstruction. A finite six-node, three-reserve-mode Hamiltonian conserves energy to approximately 3×10^{-13} relative numerical error. Its directly integrated reserve force agrees with a separately evaluated exact memory equation to approximately 3×10^{-14}. Reciprocal threshold dynamics, clock reparameterization, time reversal, full hybrid spectra, directional acoustic corrections and response–fluctuation identities are tested under explicit assumptions.

Three retained suites supply additional phase and threshold checks, clock-corrected synthetic universality tests and selected published-data comparisons. The clock correction restores consistency in generated data known to share one efficiency, while a deliberately nonuniversal control remains incompatible. Published clock, free-fall and wave-speed summaries are compatible with the specified conventional metric branch. The fixed DESI comparison remains $\chi^2 = 28.5062$ for 13 correlated measurements. Collider examples, recoil limits and neutrino propagation retain their limited arithmetic or forecasting scope.

The record contains 172 baseline, 23 retained-audit, 325 clock-and-conversion, 277 conservative-reconstruction, 82 threshold-and-response and 67 coupled-spectrum assertions. All passed their declared software criteria. No new raw detector likelihood, distinctive physical EQEF signal or parameter-free physical constant is claimed. Full inputs, intermediate datasets, tolerances, code and checksums accompany the report.

Contents

Abstract **i**

1 The finite model actually tested **1**

2 Conservative dynamics, memory and reversibility **2**

3 Full spectrum, directional dispersion and nonlinear periods **4**

4 Reciprocal actuation and causal response tests **7**

5 Corrected reference calculations and provenance of a number **8**

6 Purpose, model versions and the meaning of a result **11**

7 The equation-to-data contract **13**

8 Conservation, positivity and closed-system dynamics **14**

9 Frame subdivision and proper-time propagation **18**

10 Identifiability and the cross-channel synthetic experiment **20**

11 Published clock measurements: what can actually be inferred **23**

12 Cosmological covariance, distances and elapsed age **25**

13 Constant and particle-sector expressions after the EQEF clarification **27**

14 Retained mathematical and detector-interface calculations **30**

15 Quantum and gravity constraints beyond rate arithmetic **36**

16 Sensitivity, uncertainty and the avoidance of false improvement **37**

17 Ten decisive requirements and the interpretation of the record **39**

A Input inventory and exact numerical provenance **40**

B Verification ledger **41**

C Reproduction and verification boundaries **47**

D Executable revision analysis **48**

E Complete new verification ledger **55**

F Executable conservative reconstruction **69**

G Executable threshold and causal-response checks **75**

H Executable coupled-spectrum checks **77**

External references **79**

1. The finite model actually tested

1.1 A reproducible Hamiltonian, not an adjusted residual

The reconstruction adds three numerical suites to the retained record. The primary one tests a finite compact-phase network coupled to reserve oscillators. The second checks a reciprocal threshold readout and a separately declared exponential-memory response. The third retains the reserve in the full linear spectral problem. No measured particle mass, electromagnetic coupling or cosmological residual is used to choose their illustrative microscopic coefficients.

The model is based on a positive Hamiltonian,

$$H = \sum_i \frac{p_i^2}{2I} + K \sum_e (1 - \cos \delta_e) \tag{1.1}$$

$$+ \sum_{e,a} \left[\frac{P_{ea}^2}{2m_a} + \frac{m_a \Omega_a^2}{2} \left(x_{ea} - \frac{c_a \sin \delta_e}{m_a \Omega_a^2} \right)^2 \right], \qquad \delta = B^{\mathsf{T}} \theta. \tag{1.2}$$

The canonical equations are $\dot{z} = \mathbb{J} \nabla H$. The same I, K, m_a, Ω_a, c_a are used on every link. The graph and initial state distinguish experimental preparations; they are not independently adjusted particle couplings. The construction uses conventional conservative-reservoir methods [41, 45, 44] and tests their proposed physical interpretation, not a claim that these methods were invented here.

For the principal example there are six vertices, six oriented ring edges, three reserve coordinates per edge and forty-eight first-order state variables. Model units are used throughout. The constants are

$$I = K = m_a = 1, \quad (\Omega_1, \Omega_2, \Omega_3) = (0.65, 1.15, 2.4), \quad (c_1, c_2, c_3) = (0.22, 0.13, 0.07). \tag{1.3}$$

Let $a_i = 2\pi i/6$, with $i = 0, \ldots, 5$, and $B_{i,e} = 1$, $B_{(i+1) \bmod 6, e} = -1$ for edge $e = i$. Initial values are

$$\theta_i = 0.35 \sin a_i, \qquad p_i = 0.08 \cos a_i + 0.015, \tag{1.4}$$

$$x_{ea} = \frac{c_a \sin \delta_e}{\Omega_a^2} + 0.03 \cos a_e \, (1, 0.5, -0.4)_a, \tag{1.5}$$

$$P_{ea} = 0.02 \sin a_e \, (1, -1, 0.3)_a. \tag{1.6}$$

These values and all tolerances appear in the executable script. Integration uses DOP853, relative tolerance 2×10^{-12} and absolute tolerance 2×10^{-14} over $0 \le \tau \le 60$. A tolerance is a numerical control setting, not an estimated error bar on a physical observable.

1.2 The energy convention

The resolved energy is $H_A = \sum p_i^2/(2I) + K \sum (1 - \cos \delta_e)$. The reserve energy $H_R = H - H_A$ includes the interaction through its shifted square. Both are nonnegative in this convention, and $H_A + H_R$ is conserved. A free-reserve-plus-interaction partition would give different separate values but the same total. The printed term "reserve" must not be identified with an observed missing-energy channel without a physical detector map.

1.3 Verification summary

Suite	Passed / executed
Retained phase, lattice and benchmark suite	172/172
Retained constant-expression audit	23/23
Retained clock and conversion suite	325/325
New conservative reconstruction	277/277
New threshold and causal response	82/82
New full coupled spectrum	67/67
Total software and mathematical assertions	946/946

The six suites test different models and approximations. Passing all assertions means their implementations satisfy the recorded criteria. It does not mean that every construction is one unified microscopic law, that every criterion is an independent test, or that 946 physical observations confirm EQEF. Some assertions verify the failure of an intentionally incorrect formula or control.

2. Conservative dynamics, memory and reversibility

2.1 Energy and symmetry checks

The initial total energy is 0.19613734418624293 in model units. The largest relative drift is 3.0354×10^{-13}. The global phase momentum changes by less than 6.7×10^{-16}. Shifting every phase by a common angle leaves forces unchanged, and shifting one phase by 2π leaves the Hamiltonian unchanged. Finite-difference gradients at three distinct recorded states independently check the Hamiltonian vector field.

Reversing every final momentum and integrating for the same duration recovers the initial positions and reversed initial momenta with maximum discrepancy 1.6675×10^{-13}. This is a test of time reversibility of the autonomous finite model. It is not evidence that an arbitrary coarse-grained dissipative equation can be reversed without restoring the unobserved reservoir state.

Table 1: A regularly sampled subset of the conservative six-node trajectory. All 1,201 samples are supplied in CSV.

τ	H_A	H_R	H_*	Relative error
0	0.19262247	0.0035148788	0.19613734	0
5	0.091393488	0.10474386	0.19613734	5.25×10^{-14}
10	0.11958053	0.076556815	0.19613734	7.43×10^{-14}
15	0.10546088	0.090676469	0.19613734	-2.73×10^{-14}
20	0.017750388	0.17838696	0.19613734	-2.72×10^{-14}
25	0.044196423	0.15194092	0.19613734	-3.45×10^{-14}

τ	H_A	H_R	H_*	Relative error
30	0.065954692	0.13018265	0.19613734	-4.75×10^{-14}
35	0.043082734	0.15305461	0.19613734	-1.52×10^{-13}
40	0.12412399	0.072013359	0.19613734	-2.09×10^{-13}
45	0.12334556	0.072791785	0.19613734	-2.13×10^{-13}
50	0.10864142	0.087495929	0.19613734	-2.09×10^{-13}
55	0.17758804	0.018549305	0.19613734	-1.41×10^{-13}
60	0.070663892	0.12547345	0.19613734	-9.42×10^{-14}

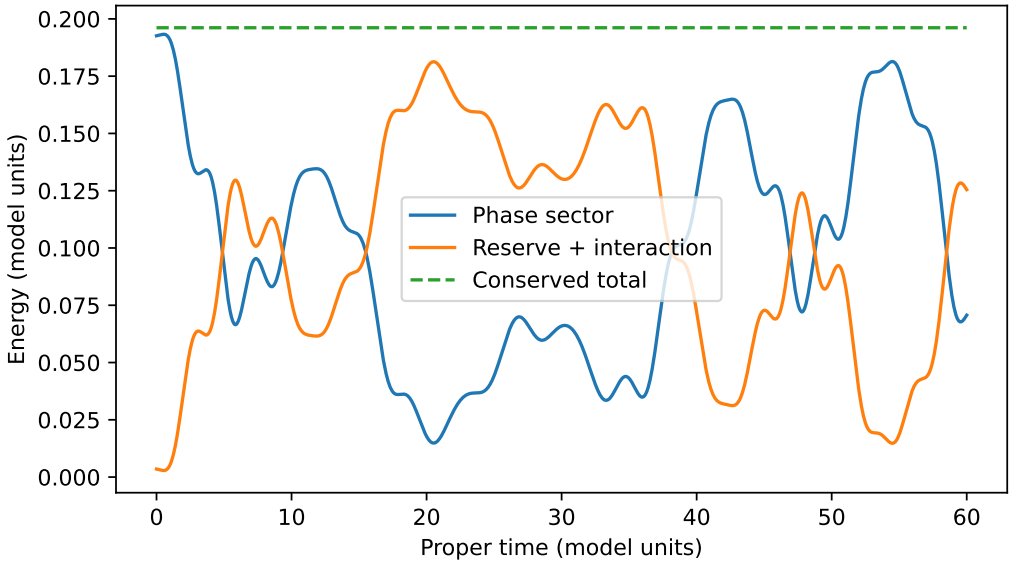

Figure 1: The resolved and reserve energies exchange while their sum stays constant in the declared numerical example. The result is simulated, not detector data.

2.2 An independent memory-equation evaluation

Set $y_{ea} = x_{ea} - c_a \sin\delta_e/(m_a\Omega_a^2)$. The force $R_e = \sum_a c_a y_{ea}$ obtained by direct integration must equal

$$R_e(\tau) = \zeta_e(\tau) - \int_0^\tau M(\tau - s)\cos\delta_e(s)\,\dot{\delta}_e(s)\,\mathrm{d}s, \tag{2.1}$$

$$M(u) = \sum_a \frac{c_a^2}{m_a\Omega_a^2}\cos(\Omega_a u), \tag{2.2}$$

$$\zeta_e(\tau) = \sum_a c_a\left[y_{ea}(0)\cos\Omega_a\tau + \frac{P_{ea}(0)}{m_a\Omega_a}\sin\Omega_a\tau\right]. \tag{2.3}$$

Independent quadrature at seven times on all six edges gives 42 comparisons. The largest absolute difference is 3.1503×10^{-14} in model-force units. The initial preparation term and nonlinear $\cos\delta$ factor are retained. Omitting either would change the equation.

This demonstrates the actual mechanism represented by the reconstruction: apparent resistance is a history-dependent response of conservative stored modes. A finite bath is not assumed to produce exact permanent exponential damping. Its discrete frequencies permit recurrence and return.

2.3 Clock reparameterization

For a positive prescribed comparison factor $q(t) = \mathrm{d}\tau/\mathrm{d}t$, the reference-time trajectory solves $\mathrm{d}z/\mathrm{d}t = q(t)\mathbb{J}\nabla H$. The code compares this solution to the original trajectory evaluated at the integrated proper time. Their maximum difference is 6.64×10^{-13}. It does not alter H or retune the reserve constants.

The transformation test does not derive Einstein's clock rule from a microscopic network. It verifies covariance under the specified change of parameter. Physical clock experiments in the later sections separately test the retained metric branch against published summaries.

2.4 Thermal preparation and fluctuation checks

A conditional Gaussian thermal preparation of the shifted reserve coordinates gives $\langle \zeta_e(\tau)\zeta_{e'}(s)\rangle = \delta_{ee'}k_BTM(\tau - s)$. The code checks the algebraic and sampled consequences in the declared ensemble. The ensemble is an additional assumption and not an assertion of fundamental randomness. This fluctuation–response relationship is established physics [43, 42]; the useful restriction is that the same coupling spectrum governs both sides.

3. Full spectrum, directional dispersion and nonlinear periods

3.1 The same reserve parameters enter the spectrum

For a positive eigenvalue ℓ of BB^{T}, the mass-weighted linear problem has a resolved coordinate and three reserve coordinates. Its squared frequencies solve the matrix eigenproblem and, away from the bare reserve poles, the Schur-complement equation

$$K\ell - I\omega^2 - \ell \sum_a \frac{c_a^2}{m_a\Omega_a^2}\frac{\omega^2}{\Omega_a^2 - \omega^2} = 0. \tag{3.1}$$

The code checks both descriptions at eight specified graph eigenvalues, along with positive eigenvalues and inertia-orthonormal eigenvectors. On the six-node ring the complete twenty-four-coordinate Hessian agrees with five positive graph-mode blocks, three uncoupled cycle-reserve modes and one global-phase zero mode. The tiny nonzero numerical eigenvalue of the latter is a floating-point artifact, not a generated physical mass.

Table 2: All computed four-branch spectra at the eight declared graph eigenvalues. The resolved weight is $I|Q_j|^2$ in an inertia-normalized eigenvector.

ℓ	Branch	ω	Resolved weight
1.0000×10^{-5}	0	0.003162273218	0.99999719
1.0000×10^{-5}	1	0.6500008812	$2.71150988 \times 10^{-6}$

ℓ	Branch	ω	Resolved weight
1.0000×10^{-5}	2	1.150000056	9.66279961×10^{-8}
1.0000×10^{-5}	3	2.400000002	1.47690592×10^{-9}
1.0000×10^{-4}	0	0.009999859496	0.999971893
1.0000×10^{-4}	1	0.650008814	2.71259220×10^{-5}
1.0000×10^{-4}	2	1.150000556	9.66432761×10^{-7}
1.0000×10^{-4}	3	2.400000018	1.47695853×10^{-8}
0.001	0	0.03161832506	0.999717828
0.001	1	0.6500883219	2.72344648×10^{-4}
0.001	2	1.150005561	9.67962739×10^{-6}
0.001	3	2.400000177	1.47748475×10^{-7}
0.01	0	0.09985652103	0.997065008
0.01	1	0.6509017452	0.00283516257
0.01	2	1.150056054	9.83461980×10^{-5}
0.01	3	2.400001776	1.48276242×10^{-6}
0.1	0	0.3106551975	0.955398825
0.1	1	0.6613044708	0.0434248594
0.1	2	1.1506092	0.00116094422
0.1	3	2.400018081	1.53713014×10^{-5}
1	0	0.5984212882	0.0787939658
1	1	1.056118344	0.668889422
1	2	1.182637364	0.252087097
1	3	2.400220949	2.29515466×10^{-4}
3	0	0.6110349697	0.0163407682
3	1	1.140146773	0.00992473213
3	2	1.857413568	0.971064246
3	3	2.401306654	0.00267025315
4	0	0.6122495694	0.0115819824
4	1	1.141387634	0.00571974975
4	2	2.136342018	0.969534663
4	3	2.403366484	0.0131636045

3.2 The acoustic coefficient is predicted before diagonalization

Let $A_1=\sum_a c_a^2/(m_a\Omega_a^4)$. On an identical-edge cubic lattice,

$$\frac{\omega}{c_*k}=1+b(\widehat{k})(ka)^2+O((ka)^4),\quad b(\widehat{k})=-\frac{1}{24}\sum_j \widehat{k}_j^4-\frac{A_1}{2I},\quad c_*=a\sqrt{K/I}. \tag{3.2}$$

For the declared reserve, $A_1/I=0.2809492855807269$. The coefficients along the axis, face diagonal and body diagonal are respectively -0.1821413094570, -0.1613079761237 and

−0.1543635316793. The independent differences are

$$b_{\mathrm{axis}} - b_{\mathrm{body}} = -1/36, \qquad b_{\mathrm{axis}} - b_{\mathrm{face}} = -1/48. \tag{3.3}$$

The isotropic reserve contribution cancels in these differences. The formulas assume a gapped reserve and sufficiently low frequency. They are not bounds from GW170817 or predictions for a photon until the measured field is identified with this branch.

Table 3: Convergence of the coupled acoustic phase-speed coefficient. The analytic coefficient is not fitted to the numerical eigenvalues.

Direction	ka	$(\omega/(c_* k) - 1)/(ka)^2$	Analytic coefficient
axis	0.02	−0.18225213067	−0.18214130946
axis	0.01	−0.18216900033	−0.18214130946
axis	0.005	−0.18214823128	−0.18214130946
face	0.02	−0.16142247026	−0.16130797612
face	0.01	−0.16133658433	−0.16130797612
face	0.005	−0.16131512723	−0.16130797612
body	0.02	−0.15447922699	−0.15436353168
body	0.01	−0.15439243987	−0.15436353168
body	0.005	−0.15437075775	−0.15436353168

3.3 The bathless limit

With all reserve couplings set to zero, $\omega^2 = (4K/I) \sum_j \sin^2(k_j a/2)$. Independent graph and plane-wave calculations check this result. At fixed small $|k|$, the leading axial correction is three times the body-diagonal correction. That ratio belongs to the bathless limit. It is not incorrectly carried over to the full spectrum, for which the coefficient differences above are the appropriate invariant geometric statement.

3.4 A dimensionless nonlinear prediction

Two equal phase inertias with the single cosine link obey $\ddot{\delta} + (2K/I) \sin \delta = 0$. The period at turning amplitude $A < \pi$ obeys

$$\frac{T(A)}{T(0)} = \frac{2}{\pi} \mathrm{K}\left(\sin^2(A/2)\right). \tag{3.4}$$

Here K uses the elliptic-integral parameter convention. At $A = \pi/2$ the predicted ratio is 1.180340599016096. This number needs no particle mass or fine-structure input. It is a conditional prediction of the cosine interaction, familiar from pendulum dynamics, not a newly observed constant of nature. Numerical trajectories at five amplitudes verify the analytic relation.

4. Reciprocal actuation and causal response tests

4.1 A conservative threshold, not a deleting reset

The auxiliary readout has a coordinate z, momentum p_z and Hamiltonian

$$H_D = \frac{p_z^2}{2M_D} + E_D\left[\frac{(z^2-1)^2}{4} - (u_0 + \lambda_C C)z\right], \quad C = \frac{1}{N^2}\left|\sum_j e^{i\theta_j}\right|^2. \tag{4.1}$$

Its phase dependence is included reciprocally in the phase momenta. In particular,

$$\frac{\partial C}{\partial \theta_i} = -\frac{2}{N^2}\sum_j \sin(\theta_i - \theta_j). \tag{4.2}$$

The phase equations receive $+E_D\lambda_C z\,\partial C/\partial\theta_i$. Without this term the readout would act as an unexplained external energy source or sink. Four-node evolution with the specified parameters conserves the total energy to 7.18×10^{-12} absolute error. The readout spans $z \simeq -1.000003$ to 1.86944; it is not falsely described as having settled irreversibly in a model without a dissipative reservoir.

Stationary points satisfy $z^3 - z - u = 0$. The negative-well fold is fixed by $3z^2 - 1 = 0$, giving $z_c = -1/\sqrt{3}$ and $u_c = 2/(3\sqrt{3})$. The code checks the stationary points and their curvatures on both sides of the fold.

Table 4: Stationary points of the declared quartic readout. Stability here means positive curvature of the one-coordinate potential.

Tilt u	Real stationary coordinates		Stable coordinates
0	-1, 0, 1		-1, 1
0.2	-0.87888506625, 1.08803391469	-0.209148848441,	-0.87888506625, 1.08803391469
0.38	-0.629752934699, 1.15306405431	-0.523311119607,	-0.629752934699, 1.15306405431
0.4	1.15970485276		1.15970485276
0.55	1.20657947975		1.20657947975

4.2 A separate exponential-memory limit

For the declared reduced response $\widetilde{M}(\omega) = \zeta_0/(1 - i\omega\tau_b)$, with positive ζ_0 and τ_b, a graph mode has

$$\chi(\omega) = \frac{1}{K\ell - I\omega^2 - i\omega\ell\widetilde{M}(\omega)}. \tag{4.3}$$

The demonstration uses $\zeta_0 = 0.12$, $\tau_b = 0.7$, $k_BT = 0.4$ in model units. These are parameters of this reduced example, not numbers inferred from the finite three-mode bath or experimental measurements. The checks verify positive dissipation, the response identity and stable poles for the specified cases.

For $\omega > 0$, with the $e^{-i\omega t}$ convention,

$$S_F(\omega) = 2\ell k_B T \,\mathrm{Re}\,\widetilde{M}(\omega), \qquad S_Q(\omega) = |\chi(\omega)|^2 S_F(\omega) = \frac{2k_B T}{\omega}\,\mathrm{Im}\,\chi(\omega). \tag{4.4}$$

These identities link attenuation and fluctuations rather than allowing an independent fitted correction for each. A three-variable memory embedding gives the characteristic polynomial

$$I\tau_b s^3 + Is^2 + (K\ell\tau_b + \ell\zeta_0)s + K\ell = 0. \tag{4.5}$$

Its nontrivial Routh–Hurwitz inequality reduces to $I\ell\zeta_0 > 0$. The five tested positive graph modes have stable roots. This check validates the approximation where it is defined; it does not establish that all reserve spectra reduce to this exponential kernel.

4.3 Quantum transfer as an explicitly added description

An independently declared two-state Hermitian Hamiltonian has detuning Δ and off-diagonal coupling g. Its exact transfer probability is

$$P_A(\tau) = \frac{|g|^2}{|g|^2 + \Delta^2/4}\sin^2\left(\frac{\sqrt{|g|^2 + \Delta^2/4}\,\tau}{\hbar}\right). \tag{4.6}$$

The matrix exponential and analytic solution agree across the parameter cases in the dataset. A common real energy shift changes only an overall phase and leaves this probability unchanged. The quantum state space and Born rule are assumptions of this example, not conclusions from classical conservation alone. The short-time transfer is quadratic, in contrast with a memoryless population law's linear onset.

5. Corrected reference calculations and provenance of a number

5.1 The reference input set

The reference calculations use exact SI c, h, e, k_B, N_A and the explicitly stated CODATA 2022 central values of G, α and particle masses [38, 13, 39]. These physical inputs are not deduced from the demonstration Hamiltonian. Their derived combinations test arithmetic and conventions, not a prediction of their inputs. The numerical source uses high-precision arithmetic to avoid confusing roundoff with physical uncertainty.

A constant listed to many digits is not thereby measured to those digits. The CODATA covariance would be needed for a full uncertainty propagation among correlated constants. This appendix does not treat dependent combinations as independent measurements. For example, the Compton wavelength, Bohr radius and Rydberg constant share the electron mass and electromagnetic coupling; three successful recalculations do not yield three independent microscopic alignments.

Table 5: Reference calculations from declared inputs. Extra printed digits expose arithmetic, not experimental precision or independent MNT predictions.

Quantity	Computed value	Unit / dependencies
hbar	$1.05457181765 \times 10^{-34}$	J s exact h and pi
mu0	$1.25663706126 \times 10^{-6}$	N A^-2 alpha and exact h,e,c
epsilon0	$8.85418781884 \times 10^{-12}$	F m^-1 alpha and exact h,e,c
Rydberg constant	$1.09737315680 \times 10^{7}$	m^-1 alpha, electron mass and exact h,c
Bohr radius	$5.29177210547 \times 10^{-11}$	m alpha, electron mass and exact h,c
Hartree energy	$4.35974472216 \times 10^{-18}$	J alpha, electron mass and exact c
Rydberg energy eV	13.6056931228	eV alpha and electron mass; infinite nuclear mass
electron Compton wavelength	$2.42631023538 \times 10^{-12}$	m electron mass and exact h,c
classical electron radius	$2.81794032045 \times 10^{-15}$	m alpha and electron mass; not measured particle size
Thomson cross section	$6.65245870499 \times 10^{-29}$	m^2 alpha and electron mass; low-energy free electron
Bohr magneton	$9.27401006574 \times 10^{-24}$	J T^-1 electron mass and exact e,h
nuclear magneton	$5.05078373927 \times 10^{-27}$	J T^-1 proton mass and exact e,h
electron rest energy	0.510998950692	MeV electron mass and exact c,e
proton rest energy	938.272089428	MeV proton mass and exact c,e
neutron rest energy	939.565421934	MeV neutron mass and exact c,e
proton electron mass ratio	1836.15267342	1 two measured masses; not predicted

Quantity	Computed value	Unit / dependencies
neutron proton mass ratio	1.00137841946	1 two measured masses; not predicted
Planck length	$1.61625502442 \times 10^{-35}$	m G and exact h,c
Planck time	$5.39124644831 \times 10^{-44}$	s G and exact h,c
Planck mass	$2.17643434272 \times 10^{-8}$	kg G and exact h,c
Planck energy	$1.95608163670 \times 10^{9}$	J G and exact h,c
Planck temperature	$1.41678416216 \times 10^{32}$	K G and exact h,c,kB
Stefan Boltzmann constant	$5.67037441918 \times 10^{-8}$	W m^-2 K^-4 exact h,kB,c and pi
gas constant	8.31446261815	J mol^-1 K^-1 exact NA,kB
Faraday constant	96485.3321233	C mol^-1 exact NA,e
flux quantum	$2.06783384846 \times 10^{-15}$	Wb exact h,e; charged condensate interpretation additional
Josephson constant	$4.83597848417 \times 10^{14}$	Hz V^-1 exact h,e; Josephson law additional
von Klitzing constant	25812.8074593	ohm exact h,e; Hall law additional

5.2 Specific repairs with no target adjustment

The wavelength-peak root of Planck's law solves $5(1 - e^{-x}) = x$, with nonzero root $x \simeq 4.96511423$. The frequency-peak root instead solves $3(1 - e^{-x}) = x$ and is about 2.82143937. Using one root in the other definition is an error, not a possible EQEF correction.

For a free spin-half gas at $n = 10^{28}\,\mathrm{m}^{-3}$, the stated formula $E_F = \hbar^2(3\pi^2 n)^{2/3}/(2m_e)$ gives 1.69253219 eV. That is the result for the specified density. It is not rescaled to an unspecified metal's Fermi energy.

For a flat dust-plus-vacuum reference background with $H_0 = 70\,\mathrm{km\,s^{-1}\,Mpc^{-1}}$ and $\Omega_m = 0.3$, the exact age integral gives 13.4669839471 Gyr. Changing it to a different age requires changing the physical input model, not the integration variable.

The dimensional and differentiation checks in Volume I also repair the missing chain factors of a phase-dependent hyperbolic function, the factor of two in the second derivative of

tanh, the energy-density versus energy distinction, and the noncommuting time-dependent propagator. These are mathematical repairs. None selects a physical fine-structure constant.

5.3 Interpreting a retained benchmark failure

The older fine-structure, scalar-mass and muon formulas are kept in the numerical audit with their original printed inputs. Their failures are neither hidden nor assigned to the new Hamiltonian, which is a different specified construction. A physical relation between an old n_c multiplier and a reserve coupling has not been established. A clock factor cannot supply an omitted dimensional normalization or turn an invariant rest-mass mismatch into agreement merely by changing coordinates.

The new construction therefore does not inherit unverified accuracy percentages from historical summaries. Its actual result is a closed conservative initial-value problem, linked response and spectrum, and a transparent calculation-to-observable boundary.

6. Purpose, model versions and the meaning of a result

6.1 The question actually tested

The revised proposal distinguishes available potential from expressed content and treats EQEF as a field-like resistance associated with conversion. A contribution may remain potential because conversion is negated, or return from expression to potential. It is not defined as destroyed energy. The additional correction is that rates must be compared over consistently defined clock intervals.

This volume asks four concrete questions. Do explicit conversion models conserve the enlarged system's content? Does a correctly transformed clock preserve their predictions? Can a common efficiency be recovered across different clock conditions when it is present, and rejected when it is not? Finally, what do the available physical data say without treating an uncalibrated potential rate as known?

The answer is not a single percentage of agreement. The new mathematical checks pass in their stated models. The synthetic shared-efficiency experiment improves greatly when its clock factors are correctly included and rejects a deliberately nonuniversal control. The selected published clock summaries are compatible with the retained relativistic comparison. The DESI fixed-background result remains unchanged. No new parameter-free physical constant or common physical EQEF efficiency is derived in this run.

6.2 The three clock branches

The executed physical comparisons use the *retained-metric branch*: standard proper-time relations provide the reference clock correction. EQEF conversion is a separate potential effect to be inferred only when the independent normalization exists. The alternative branches—a specified EQEF modification to the metric clock law and an EQEF derivation replacing that law—are described in Volume I but are not assigned invented numerical parameters here.

A change of time coordinate is not a change of physical theory. If $\mathrm{d}\tau = q\mathrm{d}t$, a rate per

proper time acquires q when written per reference time. Applying this chain rule to both data and model does not create evidence for a new force. It prevents a false discrepancy. To claim a physical improvement over the retained metric theory, an independently specified EQEF response must predict something different and survive an appropriate comparison.

6.3 Four evidence classes

A *mathematical check* verifies an identity, conservation law, stability condition or numerical implementation. A *synthetic experiment* uses generated observations from a declared model; it tests the inference procedure, not nature. A *published-summary comparison* recomputes a derived result from measured values reported by a collaboration; it is not a reanalysis of their full raw data. An *input-based benchmark* evaluates accepted physics using supplied parameters.

The paper uses these distinctions consistently. In particular, a successful unit test is not an independent experimental confirmation. The record contains 172 retained baseline assertions, 23 retained audit assertions and 325 clock-and-conversion assertions; the three new reconstruction suites add 277, 82 and 67 assertions, giving 946 in total. Many are repeated checks at different times or states. Some deliberately verify that an invalid interpretation fails. Their success count measures execution and consistency, not the truth of the ontology.

6.4 What was run and what was not

All six numerical suites were executed in the present revision. The new Hamiltonian, reciprocal threshold and coupled-spectrum suites are reported first. The three retained suites are described below. The baseline regenerates phase, threshold, clock, lattice, DESI, GW-bound, XENON-table, CERN-kinematic and neutrino-propagation results. The retained audit recomputes the older printed constant and particle-sector formulas. The new suite computes conservative transfers, clock covariance, finite-frame probabilities, identifiability, synthetic universality, published clock comparisons and the invariance of cosmological and wave predictions under time reparameterization.

No new raw gravitational-wave strain likelihood, full collider resonance search, XENON event-level recast, CMB likelihood or observed DUNE oscillation fit was executed. Public data availability is different from use in this run. The complete input and output records accompany the PDFs; missing physical maps and unexecuted analyses are not marked as successful tests.

6.5 Version boundary for the earlier constant tests

The earlier numerical n_c multiplier is not silently identified with the new efficiency η, a proper-time hazard or the field amplitude. The previous tests remain tests of their printed formulas and stated inputs. The clarified EQEF interpretation changes the physical model that would have to be connected to observations; it does not retrospectively change those formulas or justify modifying their dimensions.

A full future test must derive the observable map from a selected field and conversion law. Until then, the present edition reports the exact scope of each calculation rather than repairing

an old result with an adjustable clock or normalization factor chosen from that result itself.

7. The equation-to-data contract

7.1 Conserved transfer and observed intensity

For a closed cell with consistently assigned interaction energy, the new effective balance is

$$\frac{\mathrm{d}E_A}{\mathrm{d}\tau} = \eta J_{\mathrm{pot}} - J_-, \qquad \frac{\mathrm{d}E_P}{\mathrm{d}\tau} = -\eta J_{\mathrm{pot}} + J_-. \tag{7.1}$$

Summing proves conservation of $E_A + E_P$. Negation is the unrealized fraction of a potential forward transfer, while return is a separate reverse transfer. Their numerical effects can differ even when both reduce the observed expressed sector.

For one-way event counts with independently known source normalization and detector response,

$$\lambda(t) = \epsilon_{\mathrm{det}}(t) q(t) \eta(t) r_0(t), \qquad q = \frac{\mathrm{d}\tau}{\mathrm{d}t}. \tag{7.2}$$

This factorization is an explicit effective-model assumption. The mean count over an exposure is its time integral. Background, propagation and energy response must be included for a real experiment. The symbol r_0 denotes attempted events per proper time, not the total reserve energy.

7.2 The exact elementary test model

The new reservoir example takes $J_{\mathrm{pot}} = kE_P$ and $J_- = bE_A$, with $k = 0.3$, $b = 0.07$ and $\eta = 0.9$ in declared proper-time units. Thus $a = \eta k = 0.27$. Starting with total one and $E_A(0) = 0.2$, the exact result is

$$E_A(\tau) = \frac{a}{a+b} + \left(0.2 - \frac{a}{a+b}\right) e^{-(a+b)\tau}. \tag{7.3}$$

All parameters here are illustrative model choices. They were not derived from the microscopic threshold or fitted to a physical clock. Their purpose is to expose whether the clarified conservation and timing interpretation can be implemented correctly.

The lapse used for a nonuniform-clock control is

$$q(t) = 0.8 + 0.1\cos t, \qquad \tau(t) = 0.8t + 0.1\sin t. \tag{7.4}$$

It stays positive. Three calculations are compared: the exact solution evaluated at $\tau(t)$, a numerical differential equation in proper time, and the correctly transformed equation in reference time. A fourth calculation intentionally omits q to show the error that the revision is meant to prevent.

7.3 Parameter roles are fixed before scoring

The input record distinguishes exact unit definitions, measured reference values, inherited benchmark choices and new synthetic settings. The seed identifies a reproducible random

stream; it does not make the study prospectively blind. The physical values used here were already published and in several cases already discussed in the earlier manuscript.

The synthetic calibration channel is separate from its holdouts. That separation tests the implementation of an out-of-sample procedure, but all synthetic channels come from our own declared generating model. No source is described as unseen experimental evidence. A hash of the code proves which code was used, not that it was committed before the relevant physical measurement.

7.4 Numerical precision and tolerances

Exact integer arithmetic is used in the retained first-passage recursion. Symbolic differentiation is used for the scalar potential. Ordinary floating point is used for matrix exponentials, integration and likelihood arithmetic, with independent formulations as cross-checks. The small optical-clock fractional shift is computed without subtracting nearly equal machine-precision numbers; otherwise $1 + 10^{-17}$ would round to one in ordinary double precision.

Tolerances are attached to the algorithms and their expected errors. They are not changed to make physical residuals pass. A covariance matrix is checked for symmetry and positive definiteness before a Gaussian residual is evaluated. A rate at a physical boundary requires a constrained sampling distribution; an asymptotic chi-square value is labeled as such. Sparse data and extreme tails are not converted automatically into discovery claims.

7.5 One-command numerical reproduction

From the delivered package root, the numerical sequence is

```
python baseline/src/run_analysis.py
python legacy/code/run_new_tests.py
python legacy/code/run_cp_forward.py
python code/run_eqef_tests.py
```

The scripts write machine-readable outputs before document tables are created. No paid API, detector account or network download is required to repeat those recorded calculations after the stated dependencies are installed. The software-version snapshot belongs to the computation, while the bibliography and provenance record identify the external measurements and inherited small input tables.

8. Conservation, positivity and closed-system dynamics

8.1 Paired transfers in 200 independently generated states

For each random state, positive expressed and potential contents are drawn. A forward transfer f is restricted to $0 \le f \le E_P$ and a reverse transfer r to $0 \le r \le E_A$. The state update is

$$E'_A = E_A + f - r, \qquad E'_P = E_P - f + r. \tag{8.1}$$

Positivity follows directly from the bounds, and adding the two equations proves exact total conservation. The numerical test checks both properties for all 200 cases. The maximum

computed total discrepancy is 2.665×10^{-15} in the arbitrary energy units. This is floating-point roundoff around an algebraic identity, not a bound on physical energy nonconservation.

The test is a useful regression against the earlier disappearance interpretation. Removing a returned amount from the expressed sector without adding it to potential would fail the paired sum. Subtracting an unconverted amount from the potential reserve would likewise misrepresent negation. The current code implements neither error.

Table 6: Selected paired-transfer checks; all values are arbitrary model energy units.

Case	E_A	E_P	f	r	$E'_A + E'_P$
0	3.0707	4.4741	3.5902	1.7865	7.5448
1	0.86647	1.5303	0.080369	0.10008	2.3967
2	3.9196	4.8984	4.5017	1.884	8.818
3	1.1037	4.7959	3.9272	0.50725	5.8995
4	7.6413	2.6627	0.22031	5.5916	10.304
5	7.5392	0.55552	0.40259	1.6358	8.0948

8.2 Exact and numerical exchange agree

The equilibrium expressed content of the declared reservoir is

$$E_A^* = \frac{0.27}{0.34} = 0.7941176470588235. \tag{8.2}$$

The analytic solution, proper-time integration and reference-time integration agree over the complete sampled trajectory. Their maximum differences are 3.100×10^{-13} and 3.664×10^{-12}, respectively. Intentionally using the reference interval as though it were proper time produces a maximum discrepancy of 0.0528872 in expressed content.

This demonstrates an actual correction to the implementation of the illustrative model: changing the clock convention without transforming the evolution equation gives the wrong state. It is not yet a measurement of an EQEF field. The exact trajectory and full 201-row numerical record are supplied so the distinction can be reproduced.

8.3 Markov positivity and relaxation

For probabilities or normalized contents, the two-state generator is

$$M = \begin{pmatrix} -b & a \\ b & -a \end{pmatrix}. \tag{8.3}$$

Its exact propagator has nonnegative entries and columns summing to one. The stationary distribution is $\pi = (a, b)^T/(a + b)$. Detailed balance holds because $b\pi_A = a\pi_P$. The test checks normalization and positivity at 31 proper times and verifies that the relative entropy

$$D(p\|\pi) = \sum_i p_i \log(p_i/\pi_i) \tag{8.4}$$

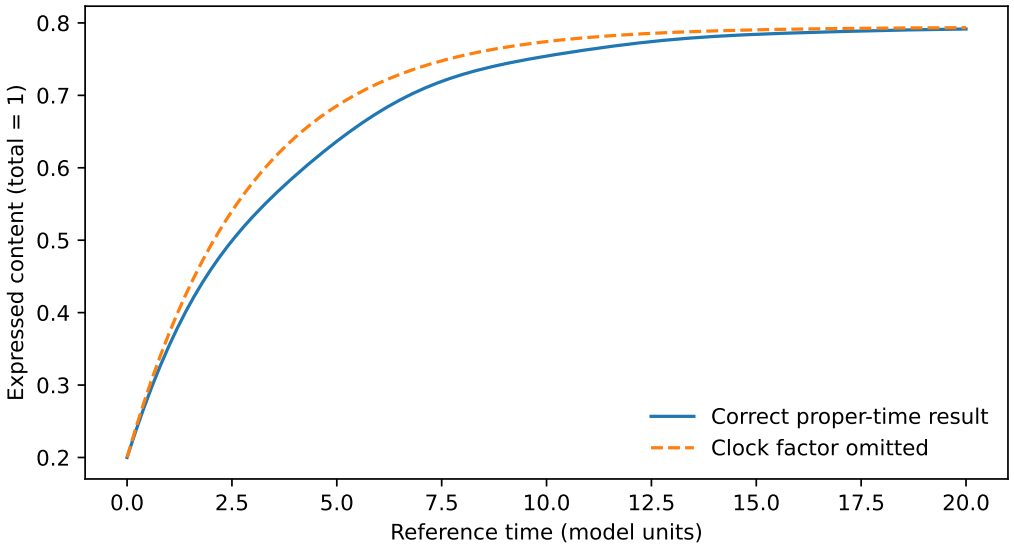

Figure 2: Illustrative conservative exchange. The proper-time analytic curve and transformed numerical solution agree. The curve computed with the omitted clock factor differs. All parameters are declared model inputs; no physical data are plotted.

does not increase along the chosen trajectory.

The assertion is about a finite Markov model with a positive stationary distribution. It is not a proof that a thermodynamic entropy or arrow of time emerges from all possible node dynamics. Assigning physical energy levels and temperature would add a further statistical-mechanical interpretation. The exact generator already suffices for the mathematical positivity and convergence check.

Table 7: Markov exchange and relative entropy. These are model probabilities, not observed particle populations.

τ	p_A	p_P	$D(p\|\pi)$
0	0.2	0.8	0.810063
2.5	0.540183	0.459817	0.161329
5	0.685582	0.314418	0.0323748
7.5	0.747728	0.252272	0.00625493
10	0.77429	0.22571	0.00117512
12.5	0.785643	0.214357	0.000217455
15	0.790495	0.209505	3.99516×10^{-5}

8.4 A coherent model with interaction energy

A second construction tests a conservative system without Markov dissipation:

$$H = \frac{1}{2}(p_A^2 + \omega_A^2 x_A^2) + \frac{1}{2}(p_P^2 + \omega_P^2 x_P^2) + g x_A x_P. \tag{8.5}$$

The declared values are $\omega_A = 1$, $\omega_P = 1.4$ and $g = 0.2$. The quadratic potential is positive definite because $g^2 < \omega_A^2 \omega_P^2$. Diagonalizing its stiffness matrix gives normal frequencies 0.9797958971 and 1.4142135624.

Starting from $(x_A, p_A, x_P, p_P) = (1, 0, 0, 0.3)$, the initial total energy is 0.545. Exact matrix-exponential evolution conserves it to maximum error 1.748×10^{-13} over the sampled interval. The subsystem energies exchange, and the interaction term is explicitly retained. Omitting it would create a spurious total change.

This example proves that observed subsystem exchange and exact enlarged-system conservation are compatible. It does not uniquely identify a physical EQEF oscillator, nor derive friction from a two-mode reversible system. A dissipative effective description would require additional reservoir degrees of freedom or a justified coarse-graining.

Table 8: Coherent two-reservoir accounting, including interaction energy.

τ	E_A	E_P	E_{int}	E_{total}
0	0.5	0.045	0	0.545
10	0.405843	0.202119	-0.0629621	0.545
20	0.469804	0.116272	-0.0410757	0.545
30	0.513431	0.0211759	0.0103928	0.545
40	0.395053	0.147802	0.00214516	0.545
50	0.414072	0.121011	0.00991673	0.545

8.5 Trace preservation is not automatically energy conservation

The quantum transfer example uses

$$K_0 = \begin{pmatrix} \sqrt{s} & 0 \\ 0 & 1 \end{pmatrix}, \qquad K_1 = \begin{pmatrix} 0 & 0 \\ \sqrt{1-s} & 0 \end{pmatrix}, \quad s = e^{-\Gamma\tau}. \tag{8.6}$$

Since $K_0^\dagger K_0 + K_1^\dagger K_1 = I$, the map $\rho \mapsto \sum_j K_j \rho K_j^\dagger$ preserves trace and positivity. Acting locally on one side of an entangled state, the unconditioned map leaves the other side's reduced density matrix unchanged. The code checks these properties at seven times.

The labels may be interpreted as expressed and potential populations only after a physical Hilbert-space mapping is supplied. If their energies differ, trace preservation does not prove that energy is conserved: the energy difference must be carried by a bath or interaction field. The test deliberately keeps this distinction instead of claiming that a probability identity alone completes the conservation mechanism.

Table 9: Specified trace-preserving transfer channel. Probability conservation alone is not an energy-conservation proof.

τ	p_A	p_P	Remote change
0	1	0	0
0.1	0.993024	0.00697556	0
0.5	0.965605	0.0343946	5.55112×10^{-17}
1	0.932394	0.0676062	0
2	0.869358	0.130642	5.55112×10^{-17}
5	0.704688	0.295312	5.55112×10^{-17}
10	0.496585	0.503415	1.11022×10^{-16}

9. Frame subdivision and proper-time propagation

9.1 The finite-interval law

For a constant proper-time hazard $\Gamma = 0.07$ and total proper duration $T = 5$, the exact survival probability is

$$S(T) = e^{-\Gamma T} = 0.7046880897187134. \tag{9.1}$$

Dividing the interval into m frames gives $\Delta\tau = T/m$ and per-frame transition probability

$$p_m = 1 - e^{-\Gamma T/m}. \tag{9.2}$$

Then $(1 - p_m)^m = e^{-\Gamma T}$ for every positive integer m. This is the exact implementation of a universal rate with a frame-dependent fraction. A fixed per-frame probability such as 0.01 instead gives 0.99^m, which changes with the number of numerical frames.

The first-order Euler approximation $(1 - \Gamma T/m)^m$ converges toward the exact survival as m increases, provided the steps are admissible. Its finite-step error is a numerical approximation, not a change in the physical hazard. The recorded table includes all three cases so the universal-rate claim cannot be hidden by a discretization convention.

9.2 A nonuniform clock and a tensor-wave equation

Consider a specified effective tensor-mode equation in proper time,

$$h'' + (3H + \dot{F}/F)h' + k^2 e^{-2H\tau} h = 0, \tag{9.3}$$

with constant illustrative $H = 0.05$, $\dot{F}/F = 0.02$ and $k = 1.3$. These are not measured gravitational-wave parameters. With $\mathrm{d}\tau = q\mathrm{d}t$,

$$\frac{\mathrm{d}^2 h}{\mathrm{d}t^2} + \left[q(3H + \dot{F}/F) - \frac{\dot{q}_t}{q}\right]\frac{\mathrm{d}h}{\mathrm{d}t} + q^2 k^2 e^{-2H\tau(t)} h = 0. \tag{9.4}$$

The derivative on q is with respect to t, while the displayed $\dot{F}/F$ belongs to proper time. The extra $-\dot{q}_t/q$ term comes from differentiating the clock factor, not from a new physical damping force.

Table 10: A universal proper-time hazard under different numerical frame subdivisions.

Frames	$\Delta\tau$	$p(\Delta\tau)$	Exact S	Euler S	Fixed-step S
1	5	0.295312	0.704688	0.65	0.99
2	2.5	0.160543	0.704688	0.680625	0.9801
5	1	0.0676062	0.704688	0.695688	0.95099
10	0.5	0.0343946	0.704688	0.700282	0.904382
20	0.25	0.0173478	0.704688	0.702508	0.817907
50	0.1	0.00697556	0.704688	0.703821	0.605006
100	0.05	0.00349388	0.704688	0.704256	0.366032
1000	0.005	0.000349939	0.704688	0.704645	4.31712×10^{-5}
10000	0.0005	3.49994×10^{-5}	0.704688	0.704684	2.24877×10^{-44}

The script solves the proper-time equation and the transformed equation independently over 101 common physical endpoints. Their maximum difference is 2.2505×10^{-12}. This is a propagation covariance check. It does not use detector strain, estimate a source distance, or constrain an EQEF interaction strength.

9.3 Quantum evolution under a time change

A fixed Hermitian three-state generator is evolved both as $\mathrm{d}\psi/\mathrm{d}\tau = -\mathrm{i}H\psi$ and as $\mathrm{d}\psi/\mathrm{d}t = -\mathrm{i}q(t)H\psi$. At matching endpoints, the maximum amplitude difference is 4.5831×10^{-12}. The norm and corresponding probabilities are checked separately.

Adding a real multiple of the identity changes only a common phase, and the probabilities remain unchanged. This is important for the neutrino interpretation: a common timing or phase factor cannot be counted as a predicted change in flavor mixing. A physical effect must enter the relevant differences or a specified nonunitary channel. The parameter is laboratory evolution time, not the proper time of a massless propagation path.

9.4 Lorentz transformations do not change invariant mass

A supplied timelike four-vector is boosted through six velocities from $-0.99c$ to $0.99c$. The invariant squared mass remains 86 in the declared units, within floating-point rounding. A second identity test verifies that a common multiplicative clock factor cancels from two frequency ratios. Both checks prevent using a clock conversion as a universal repair to particle rest masses or dimensionless couplings.

9.5 What these checks resolve

The author's expectation that a per-frame value changes when the elapsed time changes is correct for a rate-based transition law. The tests establish an explicit way to account for it. They also identify the boundary: consistent timing changes preserve the same physical prediction. They do not automatically generate a new spectrum, adjust an arbitrary coupling or create additional evidence from a coordinate relabeling.

Table 11: Lorentz boost identity test on a supplied timelike four-vector.

β	γ	M^2	Numerical error
-0.99	7.08881	86	-1.81899×10^{-12}
-0.5	1.1547	86	2.84217×10^{-14}
0	1	86	0
0.1	1.00504	86	2.84217×10^{-14}
0.9	2.29416	86	-1.13687×10^{-13}
0.99	7.08881	86	-4.54747×10^{-13}

10. Identifiability and the cross-channel synthetic experiment

10.1 What one count can determine

For a single count with mean $\mu = T\epsilon_{\mathrm{det}} q\eta r_0$, observing μ identifies a product. If q and η are both unknown, the transformations $q \mapsto cq$, $\eta \mapsto \eta/c$ leave the mean unchanged wherever both parameter values are admissible. There is no unique separate estimate from that count alone.

In log parameters, a Poisson model with mean 1000 has a two-parameter information matrix proportional to

$$I = 1000 \begin{pmatrix} 1 & 1 \\ 1 & 1 \end{pmatrix}. \tag{10.1}$$

Its eigenvalues are 0 and 2000. The zero eigenvalue is a genuine identifiability failure, not a shortage of numerical precision. A table of distinct lapse–efficiency pairs with the same predicted product provides a direct numerical check.

Table 12: Different lapse and efficiency pairs with the same intensity ratio.

q	η	$q\eta$
0.72	0.972222	0.7
0.75	0.933333	0.7
0.8	0.875	0.7
0.9	0.777778	0.7
1	0.7	0.7

10.2 The generated four-channel test

Four independent Poisson channels are generated from one efficiency, $\eta = 0.98$, with deliberately different proper/reference clock factors. Potential rates, observation durations and detector efficiencies are known by construction. They are not fitted from the generated counts. Channel A is used once for calibration; B, C and D are held out from that calibration.

The effective exposure is $w_i = r_{0i} T_i q_i \epsilon_i$. The count mean is ηw_i. A naive estimator which ignores time dilation divides by $r_{0i} T_i \epsilon_i$, causing channels with different q_i to appear to have different efficiencies. The corrected estimator divides by w_i.

Table 13: Generated experiment inputs. A is the calibration channel; B–D are held out from that calibration.

Channel	r_0	T	q	ϵ_{det}	w
A	50000	2	1	0.9	90000
B	80000	3	0.8	0.85	163200
C	200000	1.5	0.6	0.92	165600
D	100000	4	0.95	0.8	304000

Table 14: Generated observations and corrected efficiencies. The final column changes only the D efficiency in the control.

Channel	Counts	Naive η	Corrected η	Count SE	Control counts
A	87718	0.9746444	0.9746444	0.003290803	87718
B	160119	0.7848971	0.9811213	0.002451892	160119
C	161440	0.5849275	0.9748792	0.002426304	161440
D	296569	0.9267781	0.9755559	0.001791386	273429

10.3 One calibration and three predictions

Channel A gives

$$\widehat{\eta}_A = 0.9746444444, \qquad \sigma_A \simeq 0.0032908027. \tag{10.2}$$

The three holdout means are $\widehat{\eta}_A w_i$. The covariance used for their residuals includes both their Poisson count variance and the common calibration term $w_i w_j \sigma_A^2$. It is therefore not diagonal merely because the holdout counts were generated independently.

The recorded quadratic residual is 4.6169114. Using the conditional three-dimensional Gaussian reference gives a tail probability 0.202096. This value is an approximate consistency diagnostic for the synthetic holdout calculation, not the probability that the model is true. The estimated efficiency need not equal the injected value exactly because channel A itself has finite counting noise.

10.4 A likelihood check using all four channels

For independent Poisson means ηw_i, the unconstrained common-efficiency maximum-likelihood estimator is

$$\widehat{\eta} = \frac{\sum_i N_i}{\sum_i w_i}. \tag{10.3}$$

The homogeneity deviance relative to one fitted mean per channel is

$$D = 2 \sum_i \left[N_i \log \frac{N_i}{\widehat{\eta} w_i} - (N_i - \widehat{\eta} w_i) \right], \tag{10.4}$$

with the continuous zero-count convention. Here the fitted value is inside the physical interval. The asymptotic degrees of freedom are three because one common parameter replaces four separate means.

Including the clock factors gives $D = 4.6030583$ and the asymptotic tail 0.203280. A 5000-draw parametric simulation of the same null model gives 0.209758, with ordinary Monte Carlo uncertainty of roughly 0.006. Omitting the clock factors gives $D = 26943.6201$. The large change demonstrates recovery from a deliberately incorrect comparison convention in this generated dataset.

This is the clearest improvement produced by the revision. It is evidence that the corrected analysis does what it should when the assumed model generates the data. It is *not* evidence that four unrelated real experiments share a measured EQEF constant.

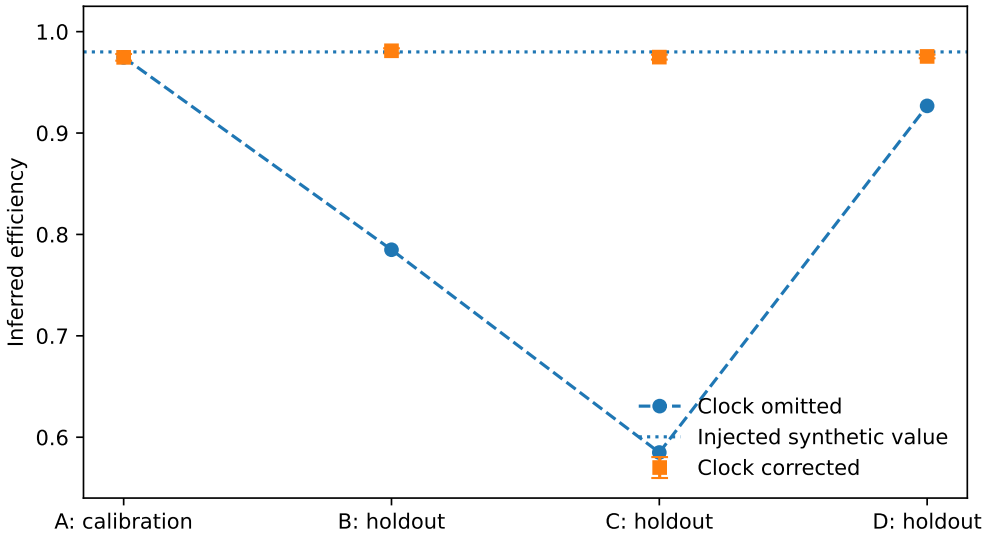

Figure 3: Generated four-channel efficiencies. The naive calculation omits each channel's known clock factor; the corrected calculation uses it. The horizontal reference is the injected efficiency, not an experimentally established constant.

10.5 A control that must remain inconsistent

To test whether clock correction simply forces agreement, channel D is regenerated with efficiency 0.90 while the other channels retain 0.98. The same exposures and clock rules are used. The common-efficiency deviance becomes 1138.8136, so the model is decisively inconsistent in this constructed control.

An asymptotic calculation gives an extremely small tail, but the 5000-draw simulation does not measure such an extreme probability. The result is reported as rejection of the deliberately nonuniversal synthetic model, not as a precision discovery significance. No change to the time factors or response functions is made to hide the injected failure.

10.6 Time-varying efficiencies are exposure weighted

A separate deterministic integral uses varying rate, lapse and efficiency. The expected count is 76.0820656 and effective exposure 80.1416120, giving

$$\eta_{\mathrm{eff}} = 0.9493453363. \tag{10.5}$$

The arithmetic time average is 0.9510880422. Their difference is expected because times with different rates and clock factors contribute different event weights. Replacing the integral by an unweighted average would change the predicted count. The result is an integration benchmark, not an extra fitted physical parameter.

10.7 The condition for a physical universality test

To apply this method to particles or experiments, the attempted rates and field response must be predicted or calibrated independently of the held-out observations. Correct clock factors alone do not supply them. A common efficiency inferred after giving every channel a free normalization would have no discriminating content. The synthetic test instead keeps the normalizations known and demonstrates the valid inference procedure under that condition.

11. Published clock measurements: what can actually be inferred

11.1 Optical clocks at different heights

The primary optical-clock paper reports a height change of 0.33 m and a fractional frequency change $(4.1 \pm 1.6) \times 10^{-17}$ [29]. Using the same weak-field approximation and $g = 9.80$ m s^{-2},

$$\left(\frac{\Delta\nu}{\nu}\right)_{\mathrm{GR}} = \frac{g\Delta h}{c^2} = 3.5983102813 \times 10^{-17}. \tag{11.1}$$

The residual divided by the reported standard error is 0.31356. Under a multiplicative response model, the inferred *relative* efficiency change between the two settings is approximately 5.0169×10^{-18}, with uncertainty dominated by the measurement. It is compatible with zero.

This comparison does not determine an absolute EQEF efficiency, because the intrinsic transition rate and any common response cancel between settings. It tests an additional differential response under the retained gravitational clock law. Only the published summary and the stated small-height approximation are used; no raw optical-clock time series is reanalyzed.

11.2 Moving positive muons and the rest lifetime

The 1977 storage-ring paper reports a positive-muon laboratory lifetime 64.419 ± 0.058 microseconds and quotes a rounded Lorentz factor 29.33 in its abstract [30]. The independent MuLan rest-lifetime input is 2.1969803 ± 0.0000022 microseconds [31]. Multiplication gives

$$\gamma\tau_0 = 64.437432199\ \mu\mathrm{s}. \tag{11.2}$$

The observed minus calculated difference is $-0.018432199\ \mu$s, about -0.318 of the stated laboratory lifetime error when other uncertainties are omitted. This is an illustrative

comparison of published summaries, not a reconstruction of the historical experiment's beam distribution or complete covariance.

If time dilation is omitted, comparing decay rates would create an apparent shortfall

$$1 - \frac{\tau_0}{\tau_{\text{lab}}} = 0.9658954610. \tag{11.3}$$

After correcting for the quoted γ, the inferred moving/rest effective-efficiency ratio is

$$\frac{\eta_{\text{moving}}}{\eta_{\text{rest}}} = \frac{\gamma\tau_0}{\tau_{\text{lab}}} = 1.00028613. \tag{11.4}$$

The propagated uncertainty from the two lifetimes alone is about 0.00090061. The half-last-digit sensitivity of the rounded γ is another 0.00017052 in the ratio; it is not substituted for the unavailable true beam uncertainty. The result is compatible with a ratio of one, not an independently derived absolute efficiency.

The numerical comparison explains why a missing clock factor can dominate a rate residual. It does not prove that ordinary relativistic time dilation is caused by EQEF. Nor can it test equality of an atomic conversion probability and a muon decay probability without deriving how the same field affects those two processes.

11.3 Galileo gravitational redshift

The Galileo analysis reports a fitted redshift-violation parameter $(0.19 \pm 2.48) \times 10^{-5}$ [32]. The retained metric prediction is zero for this additional parameter and is compatible with that reported uncertainty. The value is an experiment-specific coefficient of the gravitational-redshift signal; it is not the same object as $1 - \eta$ in the elementary reservoir model.

We reproduce the summary comparison, not the satellite orbit reconstruction, laser-ranging analysis or full time-series likelihood. An EQEF interpretation would need to predict the coefficient of this particular modulation. Merely assigning the fitted residual to the field would estimate a phenomenological parameter rather than derive it.

Table 15: Published-summary comparisons in their own units. No row estimates an absolute EQEF efficiency.

Observable	Measured	Error	Comparator
Optical fractional shift	4.10000×10^{-17}	1.60000×10^{-17}	3.59831×10^{-17}
Muon lifetime (μs)	64.419	.058	64.4374322
Galileo redshift coefficient	1.90000×10^{-6}	2.48000×10^{-5}	0

11.4 Why these comparisons cannot be pooled into an absolute constant

The optical experiment measures a relative frequency change, the moving-muon example compares lifetimes between two settings, and Galileo fits a gravitational-redshift modulation. They have different response functions, nuisance parameters and observational definitions. Their near-zero residuals do not form three direct measurements of the same absolute η.

A shared-field test becomes possible when a specified interaction determines the response of each apparatus to the same field parameters. The joint likelihood would then retain shared constants and separate calibrated experimental conditions. The present data instead support the narrower statement that no additional discrepancy is required by these selected summary comparisons under the retained clock model.

11.5 Independent baselines and circularity

The measured rest lifetime is a valid independent baseline for a test of relativistic dilation, but it cannot simultaneously be advertised as a lifetime predicted from the same measured Fermi constant when that constant was obtained from muon decay. Similarly, a gravitational potential inferred from the clock anomaly being tested cannot serve as an independent calibration of that anomaly. Each dependency must be traced to its measurement or physical derivation.

The revised analysis uses the sources in the roles explicitly stated above. It does not claim that the potential energy reservoir, attempted conversion rate or EQEF stress tensor has been measured by these clock summaries.

12. Cosmological covariance, distances and elapsed age

12.1 The retained DESI comparison

The retained benchmark uses the 13-entry DESI DR2 compressed distance vector and full covariance [18, 19]. The supplied flat background has $H_0 = 67.4\ \mathrm{km\ s^{-1}\ Mpc^{-1}}$, $\Omega_m = 0.315$, $\Omega_r = 0.000092$ and $r_d = 147.1$ Mpc. These are rounded comparator inputs, not quantities derived from the primitive node dynamics.

The fresh calculation gives

$$\chi^2 = (d-m)^T C^{-1}(d-m) = 28.5062330419. \tag{12.1}$$

For a fixed Gaussian 13-component comparator with no fitted parameter in this run, the conditional upper-tail probability is 0.00768646. This is not a test of every possible cosmological parameter choice and does not establish a preference for EQEF. Uncertainty in the supplied cosmological parameters is not marginalized in this benchmark.

12.2 A coordinate change cannot improve the same residual

Let A be any invertible linear change of the data-vector coordinates. Set $d' = Ad$, $m' = Am$ and $C' = ACA^T$. Then

$$(d'-m')^T (C')^{-1}(d'-m') = (d-m)^T A^T A^{-T} C^{-1} A^{-1} A(d-m) \tag{12.2}$$

$$= (d-m)^T C^{-1}(d-m). \tag{12.3}$$

The new code tests this identity with a specified nonsingular transformation of the same DESI vector. The result remains 28.5062330419, with difference zero at the printed precision.

The transformation is an implementation and units audit. It is not a proposed physical correction to BAO distances. A time-dilation model capable of changing the physical likelihood

Table 16: DESI DR2 compressed measurements and the fixed background comparator. The last column uses only the marginal standard deviation; the reported total statistic uses the full covariance.

z	Quantity	Data	Comparator	$(d-m)/\sigma$
0.295	D_V/r_d	7.941676	8.052478	-1.456
0.510	D_M/r_d	13.587584	13.493042	+0.562
0.510	D_H/r_d	21.862947	22.728555	-2.018
0.706	D_M/r_d	17.350691	17.691228	-1.893
0.706	D_H/r_d	19.455349	20.159663	-2.110
0.934	D_M/r_d	21.575640	21.983313	-2.520
0.934	D_H/r_d	17.641495	17.560878	+0.401
1.321	D_M/r_d	27.600856	28.067504	-1.438
1.321	D_H/r_d	14.176022	14.058516	+0.523
1.484	D_M/r_d	30.511901	30.260459	+0.329
1.484	D_H/r_d	12.817000	12.874213	-0.110
2.330	D_H/r_d	8.631546	8.611984	+0.194
2.330	D_M/r_d	38.988974	39.163346	-0.328

must alter the predicted expansion, sound horizon, photon propagation or observational calibration through independent equations. Simply rescaling the theoretical vector alone would change the comparison inconsistently.

12.3 The clock-corrected age

For the supplied radiation-inclusive background,

$$\tau_0 = \int_0^1 \frac{\mathrm{d}a}{aH(a)} = 13.7906925241 \text{ Gyr}. \tag{12.4}$$

Under the purely illustrative coordinate lapse $q(a) = 0.8 + 0.2a$, the coordinate interval becomes 15.1898253437 in Gyr units. Integrating the proper-time factor through that interval restores exactly the original 13.7906925241 Gyr value. There is only one physical elapsed age in this unchanged background.

This calculation demonstrates the difference between a time label and a changed universe. The standard cosmological benchmark already includes proper-time expansion and redshift conventions. An extra factor cannot be appended to a published age as though the original calculation omitted time dilation. A new physical EQEF background would need its coupled density, pressure, exchange and metric equations solved first.

12.4 The required next cosmological calculation

The conservative field interpretation permits

$$\dot{\rho}_A + 3H(\rho_A + p_A) = Q, \qquad \dot{\rho}_P + 3H(\rho_P + p_P) = -Q. \tag{12.5}$$

Once Q, the equations of state, gravitational action and initial conditions are fixed, the same solution must determine $H(z)$, acoustic scales, elapsed age and growth. The current work does not select these functions from the observed DESI residual. That would be a phenomenological fit and would require fresh holdout data for a predictive claim.

The retained 13 measurements include correlated distance components and overlapping survey information. Their marginal pulls must not be added as independent Gaussian measurements, and successive releases of the same survey must not be multiplied as independent evidence without their overlap covariance. These considerations are part of the statistical test, not merely formatting qualifications.

13. Constant and particle-sector expressions after the EQEF clarification

13.1 Why the earlier substitutions are retained

The author has clarified a physical interpretation different from an arbitrary fixed multiplier: EQEF concerns conversion resistance, and a per-frame fraction can depend on proper duration. The old printed expressions remain useful records of what was previously specified, but their coefficient n_c is not identified with the new efficiency or hazard. The following reexecutions are diagnostic checks on those expressions, not a declaration that every EQEF completion is excluded.

No coefficient is changed here to reproduce a target. Where an inverse calculation is shown, it is labeled as the value required to fit that target in the old numerical convention. It is not installed as a first-principles constant in the revised model.

13.2 The electromagnetic expression

The previously printed numerical expression is

$$A_{\mathrm{lit}} = \frac{\delta n_c}{4\pi}\left(\frac{v}{\hbar c}\right)^2, \quad \delta = 0.00115, \quad n_c = 10^{-6}, \quad \frac{v}{\hbar c} = \frac{246}{0.1973269804}. \tag{13.1}$$

Floating-point and 60-digit evaluations give

$$A_{\mathrm{lit}} = 0.00014222804820718984 28\ldots, \quad A_{\mathrm{lit}}^{-1} = 7030.961983977\ldots. \tag{13.2}$$

The CODATA 2022 inverse fine-structure reference is 137.035999177(21) [13]. With v in GeV and $\hbar c$ in GeV fm, the literal expression has units fm^{-2} when δ and n_c are dimensionless. A common clock transformation does not remove those dimensions.

A valid physical calculation would have to derive an additional scale or a normalized gauge response. The latter has the conventional form $\alpha = q_e^2 g_0^2/(4\pi Z_F)$ after canonical normalization. Determining Z_F is a dynamical calculation, not a correction obtained by adjusting elapsed time in a dimensionless measured ratio. The earlier expression therefore remains unaligned in its stated interpretation; this does not test an as-yet-unprovided EQEF normalization law.

13.3 Inverse values are calibration diagnostics only

Holding the other old printed inputs fixed, numerically matching the electromagnetic reference requires $n_c = 5.1307408463 \times 10^{-5}$ in that code convention. Matching the old 127.3 GeV scalar benchmark with $c_{hs} = 0.1$ requires $n_c = 2328.5670768$. The historical muon-correction range with its stated coefficient interval requires values between 0.00155785 and 0.0233677.

These disjoint values show that changing only that old multiplier does not align those printed benchmarks. They do not determine or constrain a newly defined proper-time transfer rate until an equation connects the two quantities. In particular, the scalar mass is a hypothetical source benchmark, not an observed new resonance, and the historical muon correction is not treated as an unquestioned current discrepancy.

Table 17: Old-n_c inverse substitutions with other printed inputs fixed. These are calibration diagnostics, not the revised efficiency.

Target in old expression	Required old n_c
Electromagnetic decimal, numerical only	$5.130740846 \times 10^{-5}$
127.3 GeV hypothetical scalar benchmark	2328.567077
Historical muon-correction interval	0.00155785 to 0.0233677

13.4 Scalar mass and mixing follow from the potential

For the printed potential

$$V(\Phi, s) = \frac{\lambda_h}{4}(\Phi^2 - v^2)^2 + \frac{\lambda_s}{4}s^4 + \frac{\lambda_{hs}}{2}\Phi^2 s^2, \tag{13.3}$$

expanding at $(\Phi, s) = (v, 0)$ with canonical kinetic terms gives

$$\left.\frac{\partial^2 V}{\partial(\Phi, s)^2}\right|_{v,0} = \begin{pmatrix} 2\lambda_h v^2 & 0 \\ 0 & \lambda_{hs} v^2 \end{pmatrix}. \tag{13.4}$$

The bilinear mixing term is exactly zero at that vacuum. Under the source's illustrative coupling relation and $c_{hs} = 0.1$, the second mass is 2.6380561 MeV rather than the proposed 127.3 GeV benchmark. These are exact differentiation and substitution results for the stated potential.

A different vacuum or an additional operator can change the mass matrix. That would be a new dynamical specification requiring a new stability and phenomenology calculation. A clock relabeling does not turn a diagonal rest-frame Hessian into a mixed one. The revised conversion theory therefore needs its own derivation of the matter potential rather than a hidden adjustment of this example.

13.5 Muon magnetic anomaly: scaling and reference dependence

The old scaling term has the form

$$\Delta a_\mu = C_\mu \delta n_c (m_\mu/\Lambda)^2. \tag{13.5}$$

With its stated $\Lambda = 1$ TeV, the coefficient per unit C_μ is $1.2838246160 \times 10^{-17}$. The displayed range $C_\mu = 10^4$–10^5 therefore gives 1.2838×10^{-13}–1.2838×10^{-12}, not an order-10^{-9} correction. The anomaly is dimensionless, so a common rescaling of the measurement clock does not supply the missing interaction coefficient.

The 2025 experimental world average and the 2025 Standard Model update used here differ by $(38.5 \pm 63.6730) \times 10^{-11}$ under the simple uncorrelated-summary calculation [36, 35]. The corresponding diagnostic is about 0.605 standard deviations. This does not resolve all hadronic-input disagreements; it records the chosen reference and avoids presenting an older discrepancy as a fixed present target. No EQEF coefficient is fitted to that difference.

13.6 The neutrino phase substitution

The earlier central phase expression $(1.2 - 0.05)\pi$ gives 207 degrees, not the quoted 250–290 degree band. The retained forward calculation propagates 207 and 270 degrees separately through the same illustrative matter Hamiltonian. Their different probabilities are predicted consequences of those different supplied phase choices, not a detector preference for either.

A common clock or identity-Hamiltonian correction cancels from flavor probabilities when treated consistently. A genuinely new EQEF phase would need to modify a relevant eigenvalue difference, flavor coupling or open-system term. The current clarification does not select such a matrix and is not represented as doing so.

Table 18: Conditional flavor forecasts for two supplied CP phases; no detector events enter.

δ (degrees)	E (GeV)	$P_{\mu e}$	$P_{\bar{\mu}\bar{e}}$
207	0.5	0.111115	0.0349459
207	1	0.018199	0.013427
207	2	0.0763966	0.0161558
207	2.5	0.0710978	0.0216612
207	3	0.058408	0.0220874
207	5	0.025053	0.0141511
270	0.5	0.13361	0.0010184
270	1	0.0376272	0.0175264
270	2	0.078328	0.007893
270	2.5	0.0788632	0.0160144
270	3	0.0671822	0.0193116
270	5	0.0301014	0.0150799

13.7 The revised conclusion for constants

The new clock treatment repairs the comparison of quantities that are rates per different time standards. It does not repair the old dimensionful electromagnetic expression, the zero scalar mixing term, or the unselected particle spectrum. The useful outcome is a sharper separation of tasks: derive the field response and proper-time conversion law, then derive the normalized

particle and gauge observables. No failure is erased by assigning a new meaning to an old numerical parameter.

14. Retained mathematical and detector-interface calculations

The following calculations were rerun rather than copied as inherited pass labels. They preserve the original declared inputs and remain separate from the new conservative-conversion model. The clock correction does not change these physical benchmarks without an independently specified new interaction. Their results are included in full at the scope supported by the available input data.

14.1 Mathematical implementation checks

14.1.1 Moments and threshold scaling

The uniform-phase simulation uses seed 20260906, independent random streams for separate simulations, and 50,000 paths of length up to 1024. The second and fourth moment checks compare sampled means with N and $2N^2 - N$. Table 19 gives the numerical errors in units of their Monte Carlo standard errors.

Table 19: Uniform-phase moment checks, 50,000 sampled paths at each size. Standardized errors use the estimated Monte Carlo standard error, not an experimental uncertainty.

N	$\widehat{\mathbb{E}\lvert Z\rvert^2}$	Exact $\mathbb{E}\lvert Z\rvert^2$	Error/SE (second)	Error/SE (fourth)
16	15.96864	16	-0.451	+0.078
64	63.83721	64	-0.572	-0.105
256	257.63567	256	+1.422	+1.310
1024	1022.73960	1024	-0.275	-0.087

For the partial-coherence mixture with $m = 0.2$ and $N = 256$, the computed second moment is 2866.194757, compared with the exact 2867.2. The Monte Carlo standard error is 5.602321, giving a standardized discrepancy of −0.1794.

Table 20 distinguishes the regimes below, at and above the random-walk exponent $1/2$. At $p = 1/2$ the crossing probability remains of order one. At $p > 1/2$ it decreases with size, while exact coherence eventually crosses for $p < 1$.

A zero count in 50,000 trials is not a proof of zero probability. Its exact one-sided 95% binomial upper limit is

$$1 - 0.05^{1/50000} = 5.9913 \times 10^{-5}. \tag{14.1}$$

For the all-time threshold in Volume I, Section 7, the analytic noise-crossing budget is $\eta = 0.05$. No crossing occurred in the sampled noise paths through 1024 updates, and a perfectly coherent sequence first crossed at update 49. The proof, rather than the finite simulation, controls all update times.

The R0 exact-prefix calculation and its infinite-horizon certificate are given in Volume I, Section 8. They also make a useful control: removing persistent mean coherence can prevent

Table 20: Instantaneous overflow estimates for amplitude threshold N^p. These are not first-passage or all-time probabilities.

N	$p = 0.4$	$p = 0.5$	$p = 0.6$	$p = 0.75$
16	0.57150	0.37314	0.17522	0.01600
64	0.64818	0.36634	0.09924	0.00028
256	0.72070	0.37260	0.04904	0/50,000
1024	0.78002	0.36666	0.01834	0/50,000

the threshold sequence from supplying a continuing clock. Restoring a declared nonzero mean produces the finite-mean renewal behavior proved there. This is a mechanism check within the specified models, not an experimental discovery.

14.1.2 Seams and discrete propagation

Independent rephasing of the test state sequence changes the raw overlap phase by as much as 3.1168 radians. The corrected transported overlap and the fidelity agree before and after rephasing to 2.23×10^{-16}. An orthogonal overlap produces an undefined phase rather than a fabricated zero. A circular difference straddling the branch cut correctly gives 0.02 radians.

The nearest-neighbor lattice test uses 257 sites, 60 steps and Courant parameter $\nu = 0.5$. The initialized disturbance remains exactly zero outside the finite update cone. The maximum absolute drift of the quadratic modified energy is 5.56×10^{-17}; the corresponding phase charge drift is 1.43×10^{-14}. Halving the wave number in the dispersion comparison reduces the leading continuum error by ratios 4.0074, 4.0019 and 4.0005, as expected for a second-order error. A deliberately unstable $\nu = 1.1$ control has an amplification root of magnitude 2.4282 per step. These checks apply to the explicit quadratic lattice dynamics, not to every possible node update.

14.2 GWOSC and gravitational-wave propagation

14.2.1 A versioned catalog calculation

The GWOSC GW150914 entry in GWTC-1-confident, version 3, reports representative source masses 35.6 and 30.6 $M_\odot$ and final mass 63.1 $M_\odot$ [20]. Their tabulated difference is

$$35.6 + 30.6 - 63.1 = 3.1\, M_\odot, \qquad \frac{3.1}{35.6 + 30.6} = 0.0468278. \tag{14.2}$$

This differs from arithmetic based on older event-table versions because the quoted source inferences differ. The calculation is a catalog consistency check. Marginal posterior summaries are correlated and are not event-by-event independent energy measurements; the inference also uses relativistic waveform models.

14.2.2 Updated massive-mode constraint

A published 2026 reanalysis of modified-dispersion tests gives a 90% upper bound of 2.21×10^{-11} peV, equivalently $2.21 \times 10^{-23}\,\mathrm{eV}/c^2$, for the graviton-mass parameter [21].

This edition uses that particular published bound; it does not claim to have performed the reanalysis or to establish a universal best bound.

For the illustrative massive-mode dispersion,

$$E^2 = p^2c^2 + m_g^2c^4, \qquad \frac{v_g}{c} = \sqrt{1 - \left(\frac{m_gc^2}{hf}\right)^2}. \tag{14.3}$$

Writing $x = (m_gc^2/hf)^2$, numerical cancellation is avoided by using

$$1 - \frac{v_g}{c} = \frac{x}{1 + \sqrt{1 - x}} \simeq \frac{x}{2}. \tag{14.4}$$

The conventional Compton wavelength is then

$$\lambda_g = \frac{hc}{m_gc^2} \geq 5.61014 \times 10^{13}\ \text{km}. \tag{14.5}$$

For a static reference distance $D = 440$ Mpc, the leading travel-time difference is $(D/c)x/2$. The magnitude of the corresponding f^{-1} propagation phase is $2\pi f\Delta t$, with the Fourier sign fixed by convention. Table 21 evaluates these scales.

Table 21: Massive-mode bound conversion at a static reference distance of 440 Mpc. Values saturate a published upper bound; they are not measured delays.

f (Hz)	$1 - v_g/c$	Δt (s)	$\lvert\delta\Psi\rvert$ (rad)
20	3.569×10^{-20}	1.617×10^{-3}	0.203140
35	1.166×10^{-20}	5.278×10^{-4}	0.116080
100	1.428×10^{-21}	6.466×10^{-5}	0.040628
300	1.586×10^{-22}	7.185×10^{-6}	0.013543

A luminosity distance must not be substituted into this static formula and called an exact cosmological result. In the ultrarelativistic limit on an expanding background, with observed frequency f_{obs} and source redshift z_s, the leading delay relative to a massless signal is

$$\Delta t = \frac{(m_gc^2)^2}{2h^2f_{\text{obs}}^2} \int_0^{z_s} \frac{\mathrm{d}z}{(1+z)^2H(z)}. \tag{14.6}$$

The extra redshift factors follow because the locally propagating frequency is $(1+z)f_{\text{obs}}$. The reproduction script also evaluates this integral for its declared reference redshift $z_s = 0.09$: at 100 Hz it gives 5.28402×10^{-5} s when the mass bound is saturated. No emission-time coincidence is inferred from that calculation.

The mass term here is a phenomenological branch, not a prediction of the R0 rule. It is also distinct from the quartic lattice correction of Volume I, Section 10 and the varying-F tensor friction of Volume I, Section 14. These three effects cannot be identified merely because each involves phase or propagation.

14.2.3 Interface to a genuine strain analysis

A detector-level comparison requires a waveform, antenna response, noise model and calibration treatment. With a one-sided noise power spectral density $S_I(f)$,

$$(a|b)_I = 4\,\mathrm{Re}\int_{f_{\min}}^{f_{\max}} \frac{\tilde{a}^*(f)\tilde{b}(f)}{S_I(f)}\mathrm{d}f, \quad \log\mathcal{L} = -\frac{1}{2}\sum_I (d_I - h_I|d_I - h_I)_I + \text{const.} \tag{14.7}$$

A specified phase correction belongs inside h_I, together with nuisance and source parameters. Raw strain, posterior sampling and such a waveform likelihood were not rerun in this revision. The public-bound calculation constrains an explicitly identified effective branch without suggesting otherwise.

14.3 XENONnT: public limits and their correct use

14.3.1 Reconstruction of the released tables

The XENONnT light-dark-matter release supplies spin-independent contact and light-mediator limit tables for masses 3–12 GeV [22, 23]. All twenty rows were checked. For the SI table, the power-constrained limit obeys

$$L_{\text{published}} = \max\{L_{\text{unconstrained}}, L_{-1\sigma\ \text{expected}}\}. \tag{14.8}$$

The floor is active for the five SI points at 8, 9, 10, 11 and 12 GeV. The light-mediator rows do not activate that floor in the supplied table. Table 22 reports the reconstructed upper limits and preserves the different units of the two interaction conventions.

Table 22: Reconstructed published upper limits. SI denotes spin-independent contact scattering; the light-mediator column has different units. The last column records application of the SI sensitivity floor.

m_χ (GeV)	SI (cm^2)	Light (cm^2 MeV^4)	SI floor active
3	8.674×10^{-42}	2.907×10^{-37}	No
4	1.294×10^{-43}	7.814×10^{-39}	No
5	1.328×10^{-44}	1.447×10^{-39}	No
6	2.532×10^{-45}	4.896×10^{-40}	No
7	7.523×10^{-46}	2.241×10^{-40}	No
8	3.289×10^{-46}	1.279×10^{-40}	Yes
9	2.015×10^{-46}	8.817×10^{-41}	Yes
10	1.455×10^{-46}	6.479×10^{-41}	Yes
11	1.213×10^{-46}	5.225×10^{-41}	Yes
12	9.788×10^{-47}	4.366×10^{-41}	Yes

The descriptive coordinate

$$b = \begin{cases} \log(L_{\text{obs}}/L_{\text{med}})/\log(L_{+1}/L_{\text{med}}), & L_{\text{obs}} \geq L_{\text{med}}, \\ -\log(L_{\text{med}}/L_{\text{obs}})/\log(L_{\text{med}}/L_{-1}), & L_{\text{obs}} < L_{\text{med}} \end{cases} \tag{14.9}$$

has maximum positive values 0.668094 for SI and 0.620218 for the light mediator. It records position within plotted expected-limit bands. It is not a Gaussian significance, a discovery statistic or a likelihood for MNT. In particular, a sensitivity floor is not a collection of independent downward fluctuations. These band coordinates alone do not decide whether an underlying event sample contains a signal.

14.3.2 The prediction required for a detector test

For a specified incident dark-matter distribution and scattering model, a representative nuclear recoil rate per detector mass has the structure

$$\frac{\mathrm{d}R}{\mathrm{d}E_R} = \frac{\rho_\chi}{m_\chi} \sum_T \frac{\xi_T}{m_T} \int_{v \geq v_{\min}} \mathrm{d}^3 v \, f_{\mathrm{lab}}(\mathbf{v}) \, v \frac{\mathrm{d}\sigma_T}{\mathrm{d}E_R}. \tag{14.10}$$

Here ξ_T is the target mass fraction and f_{lab} is normalized. Exposure, efficiency, energy or signal response, backgrounds and nuisance parameters then determine bin expectations,

$$\mu_b = b_b + \mathcal{E} \int \mathrm{d}E_R \, \mathcal{R}_b(E_R) \frac{\mathrm{d}R}{\mathrm{d}E_R}, \qquad \mathcal{L} = \prod_b \frac{\mu_b^{n_b} e^{-\mu_b}}{n_b!} \, \mathcal{L}_{\mathrm{nuisance}}. \tag{14.11}$$

A node-derived dark sector would have to determine or declare m_χ, its couplings, abundance and interaction dependence. An upper-limit curve constrains only the interaction and halo assumptions under which it was constructed. No event-level likelihood or detector-response recast was performed here.

14.4 CERN: an invariant-mass ingestion check

The CERN Open Data educational histogram page displays four example dimuon rows, with energies, Cartesian momenta, charges and published pair masses [24]. Those four rows, and only those rows, were transcribed into the reproducibility inputs. In units with $c = 1$,

$$M^2 = (E_1 + E_2)^2 - |\mathbf{p}_1 + \mathbf{p}_2|^2. \tag{14.12}$$

Using rounded displayed momenta need not reproduce a separately rounded invariant mass digit for digit. The code therefore treats the last digit of each displayed input as a rounding interval, propagates conservative intervals through the squared four-vector, and tests compatibility with the published mass interval.

Table 23: Invariant-mass check on the four displayed CERN educational rows. The interval propagates the last displayed input digit as a rounding interval. All four published masses lie within their intervals.

Event	Calculated (GeV)	Published (GeV)	Input-rounding interval (GeV)
90830792	2.732339	2.73205	[2.731367, 2.733311]
90862225	3.102325	3.10256	[3.101105, 3.103545]
90644850	9.411457	9.41149	[9.411232, 9.411683]
90678594	7.747046	7.74702	[7.746664, 7.747427]

The largest absolute central-value difference is 0.000289093 GeV, and all four are compatible after input rounding. Two same-sign and two opposite-sign rows are retained; no favorable charge subset is selected. This verifies the ingestion and kinematic arithmetic. It is not a resonance measurement, a cross-section analysis or a full reprocessing of the much larger educational sample.

A genuine collider test of a derived effective interaction would instead use

$$\sigma(pp \to X) = \sum_{ij} \int \mathrm{d}x_1 \mathrm{d}x_2 \, f_i(x_1, \mu_F) f_j(x_2, \mu_F) \, \hat{\sigma}_{ij\to X}(x_1 x_2 s; \vartheta), \tag{14.13}$$

$$\mu_b = b_b + \mathcal{L}_{\mathrm{int}} \int \mathrm{d}\Phi \, \mathcal{R}_b(\Phi) \frac{\mathrm{d}\sigma}{\mathrm{d}\Phi}. \tag{14.14}$$

The common microscopic parameters ϑ must set the new interaction. Parton distributions, efficiencies, luminosity, radiative corrections and backgrounds are experimental or effective-theory inputs whose uncertainties cannot be discarded [8].

14.5 DUNE-like matter oscillations

14.5.1 Input Hamiltonian and declared forecast

DUNE planning and simulation materials describe the neutrino-oscillation program and the flux, cross-section and response inputs needed for experiment-level forecasts [26, 25]. No far-detector observation is imported into this calculation. The calculation here is explicitly a propagation benchmark, not a fit to a far-detector oscillation spectrum.

For constant electron density n_e, the flavor Hamiltonian is

$$H_\nu = \frac{1}{2E} U \, \mathrm{diag}(0, \Delta m^2_{21}, \Delta m^2_{31}) U^\dagger + \mathrm{diag}(V, 0, 0), \qquad V = \sqrt{2} G_F n_e. \tag{14.15}$$

For antineutrinos, replace $U \to U^*$ and $V \to -V$. A common mass-squared multiple of the identity has been removed because it contributes only an overall propagation phase. The transition matrix is

$$S(L) = e^{-\mathrm{i}HL}, \qquad P_{\alpha\beta} = |S_{\beta\alpha}|^2 \tag{14.16}$$

in natural units. The code restores the conversion $L/(\hbar c)$ consistently when using energy in eV and length in centimeters.

The declared inputs are $L = 1300$ km, density $2.8\,\mathrm{g\,cm^{-3}}$, electron fraction $Y_e = 0.5$, angles $(\theta_{12}, \theta_{13}, \theta_{23}) = (33, 8.5, 45)$ degrees, $\delta = -90$ degrees, and normal-ordering mass differences $(7.5 \times 10^{-5}, 2.5 \times 10^{-3})\,\mathrm{eV}^2$. These rounded illustrative values are not claimed as a current oscillation best fit. The Fermi constant and atomic mass unit used for unit conversion are reference inputs [13]. They give $V = 1.06854527 \times 10^{-13}$ eV.

14.5.2 Independent solver and conservation checks

The evolution matrix is calculated both by a matrix exponential and by diagonalizing the Hermitian Hamiltonian. Their maximum elementwise discrepancy is 1.92×10^{-15}. The largest unitarity error is 8.89×10^{-16}, and all flavor probabilities sum to one to the declared tolerance. The zero-baseline control returns the identity.

Table 24: Three-flavor, constant-density oscillation benchmark. All parameters are declared illustrative inputs; no DUNE event spectrum is fitted.

E (GeV)	$P_{\mu e}$	$P_{\mu\mu}$	$P_{\mu\tau}$	$P_{\bar{\mu}\bar{e}}$
0.5	0.133610	0.043078	0.823312	0.001018
1.0	0.037627	0.391281	0.571092	0.017526
2.0	0.078328	0.184367	0.737305	0.007893
2.5	0.078863	0.002635	0.918502	0.016014
3.0	0.067182	0.051943	0.880875	0.019312
5.0	0.030101	0.479998	0.489900	0.015080

Detector-level event counts would require, schematically,

$$\mu_b = b_b + N_T \int \mathrm{d}E\, \Phi_\mu(E)\, P_{\mu e}(E;\vartheta)\, \sigma_e(E)\, \mathcal{R}_b(E), \tag{14.17}$$

with separate neutrino and antineutrino configurations and the appropriate exposures. Matter-profile variation, energy smearing and correlated systematic uncertainties enter this stage. The propagation solver is ready to accept a derived correction to H; the current code does not invent detector counts or claim to have used unavailable response files.

15. Quantum and gravity constraints beyond rate arithmetic

15.1 Bell-local vertices and a quantum reference

For deterministic binary local responses $A_0, A_1, B_0, B_1 \in \{-1, 1\}$,

$$S = A_0(B_0 + B_1) + A_1(B_0 - B_1). \tag{15.1}$$

Exactly one parenthesis is zero and the other is ± 2, so $|S| = 2$ for every deterministic assignment. Mixtures preserve $|\mathbb{E}S| \leq 2$ by convexity. The retained code enumerates all 16 vertices as an algebraic check. This is a mathematical bound, not an MNT prediction fitted to a Bell dataset.

The quantum reference reaches the usual $2\sqrt{2}$ value for its supplied state and measurement operators. That calculation assumes the Hilbert-space and probability structure it uses. The source framework must derive or explicitly adopt that structure before it can claim a physical account of quantum correlations. Published loophole-free experiments provide the external empirical requirement [6, 7, 37]; their raw trials were not refitted in the present suite.

A conversion model must also preserve the no-signalling property of unconditioned local operations. The new quantum transfer check addresses that property for an explicit trace-preserving channel. Selecting only detected events and renormalizing their probabilities can alter the statistical sample, so selection efficiency must be included in any Bell-type detector analysis rather than treated as a post hoc correction.

15.2 Universal free fall

The MICROSCOPE final result gives a differential free-fall parameter $[-1.5 \pm 2.3\ (\text{stat}) \pm 1.5\ (\text{syst})] \times 10^{-15}$ [33]. A universally coupled metric branch predicts zero composition-dependent deviation. Quadrature of the two quoted uncertainties gives a simple summary error 2.746×10^{-15}; the zero prediction is compatible with that summary. This is not a new fit to the satellite data.

An EQEF tension or drag mechanism that couples differently to composition must calculate the corresponding differential acceleration. If it couples universally, this null comparison may be compatible but need not distinguish it from general relativity. Assigning a separate coupling per material after seeing the result would evade the shared-law test instead of passing it.

15.3 Tensor-wave speed

For the retained scalar–tensor action containing $F(\phi)R$ and no tensor-speed-changing derivative operator, the quadratic tensor action has the same coefficient multiplying its time and spatial gradients. The local tensor propagation speed equals the metric light speed in that branch. The GW170817 electromagnetic counterpart constrains a speed difference under the paper's emission and propagation assumptions [34]; zero lies within the cited interval.

The numerical check confirms membership in that interval for the chosen zero-deviation branch. It is a conditional compatibility statement shared by standard metric gravity, not a distinctive nonzero prediction. A changing F can still modify wave amplitude damping; a tensor mass term or dispersive operator is a separate interaction and must not be inferred merely from the presence of a phase field.

15.4 Why three null agreements are not three independent EQEF detections

Clock response, free fall and wave speed can all be consistent when the model retains universal metric coupling. That cross-domain structural compatibility is useful. It does not by itself select EQEF over any model with the same effective predictions. A discriminating test needs an independently derived nonzero correction, a novel relation, or a parameter value not chosen from the comparison data.

The present volumes keep these consequences together because they constrain a viable field completion. They do not multiply their separate published summaries into a global probability that MNT is correct. Shared assumptions, prior conditioning, model overlap and experimental nuisance treatments would have to be specified for a genuine joint model comparison.

16. Sensitivity, uncertainty and the avoidance of false improvement

16.1 A deficit of one part in ten million

The illustrative conversion shortfall 10^{-7} is a useful scale for discussing measurement design, but it is not a derived constant. For a Poisson count N with perfectly known potential intensity,

the fractional counting error is approximately $N^{-1/2}$. Requiring a two-sided 95-percent Gaussian-scale error smaller than $\epsilon = 10^{-7}$ gives

$$N \gtrsim \left(\frac{1.959964}{\epsilon}\right)^2 = 3.84146 \times 10^{14}. \tag{16.1}$$

For the ratio of two equally noisy independent Poisson intensities, the variance doubles and each count needs approximately 7.68292×10^{14} events under the same assumptions. These estimates exclude systematic uncertainty and do not constitute a realistic exposure forecast for any particular detector.

A different data model gives a different requirement. If each of n attempted conversions is individually known and none fails, the exact one-sided 95-percent upper bound on the failure probability is

$$p_{95} = 1 - 0.05^{1/n}. \tag{16.2}$$

At $n = 30{,}000{,}000$, this is 9.98577×10^{-8}. There is no contradiction: a known-trial failure count is not the same experiment as the ratio of two noisy intensities. Establishing which data model applies is part of deriving the observable, not a detail to be chosen after seeing a favorable bound.

16.2 Small numbers require stable arithmetic

At the optical-clock scale, directly computing $(1 + x) - 1$ with $x \sim 10^{-17}$ in ordinary double precision can produce zero. The code retains the small fractional shifts themselves and uses exact or high-precision arithmetic for the ratio correction. Similarly, a small transition probability is computed as $-\operatorname{expm1}(-\Gamma\Delta\tau)$ rather than subtracting an exponential near one, and small speed defects are written in cancellation-resistant form.

The use of extra numerical digits is not an experimental precision claim. Measured input errors still limit the physical comparison. The book prints additional digits only for reproducible algorithmic checks and labels the measured quantities with their reported uncertainties.

16.3 Nuisance parameters must stay in the model

A measured count deficit can arise from background subtraction, detector inefficiency, energy thresholds, source abundance, dead time or transmission. An EQEF interpretation cannot be established by calling their combined residual the field. For a real model, write the likelihood with nuisance parameters ν,

$$\mathcal{L}(D \mid \vartheta, \nu) = \mathcal{L}_{\text{events}}(D \mid \mu(\vartheta, \nu))\, \mathcal{L}_{\text{calibration}}(\nu), \tag{16.3}$$

and profile or marginalize with a stated procedure. Calibration constraints must come from appropriate independent information. A nuisance parameter learned from the holdout is a fit parameter for that holdout.

The deterministic numerical tests in this package deliberately do not simulate a full detector systematic model. Their purpose is to establish the transfer and timing identities before an experiment-level analysis is attempted. The physical comparisons therefore preserve their limited published-summary scope.

16.4 Multiple searches and model revisions

Trying many exponents, normalizations, particle assignments or clock laws and reporting only the best alignment inflates apparent evidence. A numerical scan can be useful for model construction, but its best result is not automatically a fresh prediction. The scope of the search, parameter count and next independent test must be recorded.

This revision does not conduct a formula search for the measured fine-structure decimal. It does not choose a clock law to reduce the DESI residual. The inverse old-n_c values are diagnostic calculations only. The new illustrative conversion laws are labeled as illustrative and are tested on their own mathematical consequences and generated data, not presented as selected laws of nature.

16.5 What would establish the next physical result

An independently specified potential rate and field response would permit an absolute efficiency or shared coupling to be estimated from one calibration setting. It could then be frozen and tested in a different setting with a separate dataset. The same response law would predict the clock correction, state dependence and detector mapping rather than obtaining each from the new residual.

A successful outcome would be evidence for that particular physical realization, not a mathematical proof of all possible domains. A disagreement would identify which frozen realization fails. The important advance is that the question would then have a well-defined numerical answer, without redefining a constant or a potential reservoir to absorb it.

17. Ten decisive requirements and the interpretation of the record

Requirement	Result at the scope actually tested
Conservation and return	The finite Hamiltonian has an exact balance; numerical drift is 3.04×10^{-13} relative. Return is part of the conservative dynamics.
Well-posed dynamics	Smooth finite-graph evolution with a positive energy bound has a unique global solution. This is not a proof for every possible infinite graph.
Clock consistency	Proper-time and reparameterized trajectories agree. Clock corrections are applied once, with detector response separate.
Conversion and threshold	A reciprocal readout is explicit and conservative; its fold is computed. Irreversible settling requires an additional reservoir or coarse-graining assumption.
Linked response and propagation	Exact memory and the full linear spectrum are derived from the same reserve parameters. Conditional geometric coefficient differences are fixed.

Requirement	Result at the scope actually tested
Quantum statistics	Coherent transfer and quantum channels pass their tests after the quantum composition and measurement rules are supplied. Those rules are not derived from the classical example.
Matter and constants	No target-free Standard Model mass spectrum or electromagnetic normalization is obtained. Reference identities and older benchmarks retain their input dependencies.
Universal gravitation	Selected metric-branch consequences are compatible with the quoted clock, free-fall and wave-speed measurements; the microscopic metric action is not uniquely selected.
Detector-level predictions	CERN four-vector, XENON limit-table and neutrino propagation checks are reproduced. Full microscopic detector likelihoods are not claimed.
Cosmology	The supplied-parameter age integral is reproduced. The fixed 13-entry DESI comparison remains strained and is not counted as a successful alignment.

There are 946 passed software and mathematical assertions, not 946 measured predictions. The number of new independently derived parameter-free physical alignments is zero in this record. There are several exact conditional predictions of the constructed model, and their scope is explicitly stated. Combining these unlike categories into an overall empirical-accuracy percentage would not produce a meaningful statistic.

The four physical selections still needed are a uniquely motivated microscopic parameter and state class; a quantum and matter representation with coupling normalization; a common dynamical metric and cosmological matching; and a frozen detector-level observable map. None requires rewriting the author's physical premises. They require equations that make those premises numerically predictive in nature.

A. Input inventory and exact numerical provenance

A.1 Inherited inputs

The baseline data directory contains six small numerical inputs from the preceding source package: the 13-entry DESI mean vector and full covariance, benchmark parameter values, the XENON limit tables and the four displayed CERN event records. They are retained with byte checksums. Their original access was a documented reading/transcription of public products, not a bulk download of detector archives. Rerunning the files verifies the recorded calculations; it does not certify that an upstream unversioned repository will remain unchanged.

The retained audit input directory records the exact printed benchmark coefficients and published comparison summaries. The revised interpretation does not overwrite those

historical numerical assumptions. Their source URLs and accessible versions are identified in the separate provenance record rather than treating earlier framework claims as independent empirical evidence.

A.2 New inputs

The revision input JSON records the seed, reservoir rates, lapse law, generated-channel rates and durations, detector efficiencies, and the three published clock summaries. The potential rates in the synthetic channels are exactly known because the data are generated from those rates. They are not inferred from their own observed counts.

The source and detector clocks are distinct in general. The generated example uses a directly declared mapping with no propagation uncertainty. The real clock comparisons use the conventions stated in the cited papers and in the published-clock section. The positive-muon comparison uses the rounded abstract Lorentz factor and does not reconstruct its beam distribution. A future uncertainty-complete historical reanalysis would need that additional information.

Table 26: Principal new supplied inputs; none is claimed as a first-principles physical constant.

Input	Value	Role
Forward attempted rate k	0.3	Illustrative proper-time rate
Efficiency η	0.9	Illustrative reservoir conversion
Return rate b	0.07	Illustrative proper-time rate
Initial expressed / total	0.2 / 1	Illustrative preparation
Lapse $q(t)$	$0.8 + 0.1\cos t$	Clock-coordinate control
Synthetic shared efficiency	0.98	Generated counting model
Negative-control D efficiency	0.90	Deliberate nonuniversality
Synthetic random seed	202609061	Reproduction setting
Optical height step	0.33 m	Published measurement setting
Muon Lorentz factor	29.33	Rounded published summary
Muon rest lifetime	2.1969803 μs	Independent measured input

A.3 Additional numerical records

The companion tables below expose intermediate results rather than only pass labels. Long time trajectories are sampled in print at regular intervals; complete CSV output is included in the archive. The shared-efficiency synthetic counts are printed in full. No unfavorable physical residual is omitted from the scorecard.

B. Verification ledger

The six suites use different assertion formats. The package normalizes them into one CSV with suite, name, status, family and numerical detail. The aggregate count is 946: 172

Table 27: Sampled exchange trajectory; the full 201 rows are in the archive.

t	τ	q	E_A	E_P	Wrong clock
0	0	0.9	0.2	0.8	0.2
2	1.69093	0.7583853	0.4597767	0.5402233	0.4931276
4	3.12432	0.7346356	0.5887486	0.4112514	0.641631
6	4.772058	0.896017	0.6768361	0.3231639	0.7168653
8	6.498936	0.78545	0.728919	0.271081	0.7549803
10	7.945598	0.7160928	0.7542496	0.2457504	0.77429
12	9.546343	0.8843854	0.7709832	0.2290168	0.7840726
14	11.29906	0.8136737	0.7813694	0.2186306	0.7890287
16	12.77121	0.7042341	0.7863895	0.2136105	0.7915395
18	14.3249	0.8660317	0.7895609	0.2104391	0.7928115
20	16.09129	0.8408082	0.7916183	0.2083817	0.7934559

Table 28: Sampled tensor-wave covariance check. The supplied equation is an illustrative effective model.

t	τ	Proper solution	Reference solution	Difference
0	0	1	1	0
1	0.8841471	0.4508991	0.4508991	$-1.654454 \times 10^{-12}$
2	1.69093	-0.4229075	-0.4229075	$-1.204536 \times 10^{-12}$
3	2.414112	-0.8419079	-0.8419079	1.907363×10^{-13}
4	3.12432	-0.7016736	-0.7016736	$-5.802026 \times 10^{-13}$
5	3.904108	-0.1252702	-0.1252702	2.940426×10^{-13}
6	4.772058	0.5110654	0.5110654	7.119860×10^{-13}
7	5.665699	0.7114447	0.7114447	1.665335×10^{-15}
8	6.498936	0.4403082	0.4403082	6.638579×10^{-13}
9	7.241212	0.01587926	0.01587926	$-1.320267 \times 10^{-12}$
10	7.945598	-0.3510013	-0.3510013	$-1.022737 \times 10^{-12}$

Table 29: Idealized counting requirements for a fractional deficit of 10^{-7}; no systematics included.

Data model	Result
Known-intensity Poisson count, 95% scale	3.84146×10^{14}
Two equal Poisson intensities, count each	7.68292×10^{14}
Known trials: 30 million, zero failures	9.98577×10^{-8}

baseline, 23 retained-audit, 325 clock-and-conversion, 277 conservative-reconstruction, 82 threshold-and-response and 67 coupled-spectrum assertions. The additional CP forward-map check is reported separately and is not added silently to that count. A count of assertions is not a count of statistically independent physical experiments.

The printed ledger groups repeated statewise assertions and lists the distinct revision checks. The complete row-level ledger remains in the machine-readable package. Every failed physical benchmark is a numerical result, not an exception suppressed to make the software appear successful.

Table 30: Assertion families. Repeated statewise checks are counted individually, not called separate experiments.

Suite / family	Count
baseline / baseline	172
legacy / legacy	23
revision / conservation	201
revision / clock covariance	4
revision / negative control	5
revision / frame covariance	9
revision / positive transfer	31
revision / entropy	31
revision / mathematical	15
revision / quantum conditional	14
revision / identifiability	1
revision / synthetic demonstration	1
revision / coordinate covariance	2
revision / relativity	6
revision / dimensionless quantities	4
revision / arithmetic	1
Total	520

Table 31: Revision verification names and recorded details. Full repeated rows are retained in the CSV.

Check	Verified	Recorded detail
proper_time_exact_ODE	True	3.099742684753437e-13
reference_time_exact_ODE	True	3.664180070472867e-12
clock_missing_factor_control	True	0.05288717766271578
exact_frame_subdivision_1	True	0.7046880897187134
exact_frame_subdivision_2	True	0.7046880897187134
exact_frame_subdivision_5	True	0.7046880897187134

Check	Verified	Recorded detail
exact_frame_subdivision_10	True	0.7046880897187134
exact_frame_subdivision_20	True	0.7046880897187134
exact_frame_subdivision_50	True	0.7046880897187134
exact_frame_subdivision_100	True	0.7046880897187134
exact_frame_subdivision_1000	True	0.7046880897187134
exact_frame_subdivision_10000	True	0.7046880897187134
markov_positive_0.0	True	D=0.8100626086328573
entropy_contracts_0.0	True	0.8100626086328573
markov_positive_0.5	True	D=0.5803702250121656
entropy_contracts_0.5	True	0.5803702250121656
markov_positive_1.0	True	D=0.4196868609084303
entropy_contracts_1.0	True	0.4196868609084303
markov_positive_1.5	True	D=0.3047792539301767
entropy_contracts_1.5	True	0.3047792539301767
markov_positive_2.0	True	D=0.22171160230844514
entropy_contracts_2.0	True	0.22171160230844514
markov_positive_2.5	True	D=0.16132869024135366
entropy_contracts_2.5	True	0.16132869024135366
markov_positive_3.0	True	D=0.11732228725541685
entropy_contracts_3.0	True	0.11732228725541685
markov_positive_3.5	True	D=0.08522514293589281
entropy_contracts_3.5	True	0.08522514293589281
markov_positive_4.0	True	D=0.061821585361548775
entropy_contracts_4.0	True	0.061821585361548775
markov_positive_4.5	True	D=0.044774238258158544
entropy_contracts_4.5	True	0.044774238258158544
markov_positive_5.0	True	D=0.032374752447939525
entropy_contracts_5.0	True	0.032374752447939525
markov_positive_5.5	True	D=0.023371146105650942
entropy_contracts_5.5	True	0.023371146105650942
markov_positive_6.0	True	D=0.01684515106240167
entropy_contracts_6.0	True	0.01684515106240167
markov_positive_6.5	True	D=0.012123580607267252
entropy_contracts_6.5	True	0.012123580607267252
markov_positive_7.0	True	D=0.00871356781591004
entropy_contracts_7.0	True	0.00871356781591004
markov_positive_7.5	True	D=0.006254930056241538
entropy_contracts_7.5	True	0.006254930056241538

Check	Verified	Recorded detail
markov_positive_8.0	True	D=0.004485012182453424
entropy_contracts_8.0	True	0.004485012182453424
markov_positive_8.5	True	D=0.0032127131389770233
entropy_contracts_8.5	True	0.0032127131389770233
markov_positive_9.0	True	D=0.002299309379004879
entropy_contracts_9.0	True	0.002299309379004879
markov_positive_9.5	True	D=0.0016443210801987754
entropy_contracts_9.5	True	0.0016443210801987754
markov_positive_10.0	True	D=0.0011751202461866214
entropy_contracts_10.0	True	0.0011751202461866214
markov_positive_10.5	True	D=0.0008393113013892943
entropy_contracts_10.5	True	0.0008393113013892943
markov_positive_11.0	True	D=0.0005991608233188051
entropy_contracts_11.0	True	0.0005991608233188051
markov_positive_11.5	True	D=0.00042753715433509545
entropy_contracts_11.5	True	0.00042753715433509545
markov_positive_12.0	True	D=0.0003049588621360476
entropy_contracts_12.0	True	0.0003049588621360476
markov_positive_12.5	True	D=0.00021745480703340078
entropy_contracts_12.5	True	0.00021745480703340078
markov_positive_13.0	True	D=0.00015501633017162616
entropy_contracts_13.0	True	0.00015501633017162616
markov_positive_13.5	True	D=0.00011048012096953868
entropy_contracts_13.5	True	0.00011048012096953868
markov_positive_14.0	True	D=7.872346580444032e-05
entropy_contracts_14.0	True	7.872346580444032e-05
markov_positive_14.5	True	D=5.6085503626996866e-05
entropy_contracts_14.5	True	5.6085503626996866e-05
markov_positive_15.0	True	D=3.9951630174228214e-05
entropy_contracts_15.0	True	3.9951630174228214e-05
two_state_detailed_balance	True	
oscillator_stable_modes	True	[0.96 2.]
oscillator_total_energy	True	1.7474910407599964e-13
interaction_energy_not_omitted	True	coupling=0.2
Kraus_completeness_0	True	s=1.0
Kraus_no_signal_0	True	0.0
Kraus_density_positive_0	True	
Kraus_completeness_0.1	True	s=0.9930244429332351

Check	Verified	Recorded detail
Kraus_no_signal_0.1	True	0.0
Kraus_density_positive_0.1	True	
Kraus_completeness_0.5	True	s=0.9656054162575665
Kraus_no_signal_0.5	True	5.551115123125783e-17
Kraus_density_positive_0.5	True	
Kraus_completeness_1	True	s=0.9323938199059482
Kraus_no_signal_1	True	0.0
Kraus_density_positive_1	True	
Kraus_completeness_2	True	s=0.8693582353988059
Kraus_no_signal_2	True	5.551115123125783e-17
Kraus_density_positive_2	True	
Kraus_completeness_5	True	s=0.7046880897187134
Kraus_no_signal_5	True	5.551115123125783e-17
Kraus_density_positive_5	True	
Kraus_completeness_10	True	s=0.49658530379140947
Kraus_no_signal_10	True	1.1102230246251565e-16
Kraus_density_positive_10	True	
lapse_efficiency_Fisher_rank_one	True	[0. 2000.]
lapse_efficiency_identical_predictions	True	
synthetic_clock_correction_changes_bias	True	26939.017043253836
synthetic_species_defect_not_hidden	True	1138.8135913255146
synthetic_calibration_not_all_channel_fit	True	0.9746444444444444
integrated_exposure_identity	True	
arithmetic_mean_not_general_efficiency	True	0.0017427059232896225
DESI_full_covariance_preserved	True	0.0
cosmic_proper_age_invariant	True	13.790692524135595
coordinate_age_is_different_label	True	1.3991328196020447
tensor_full_clock_transformation	True	2.2504775820664236e-12
identity_Hamiltonian_shift_probability	True	
quantum_time_reparametrization	True	4.583134092514981e-12
boost_mass_invariant_-0.99	True	-1.8189894035458565e-12
boost_mass_invariant_-0.5	True	2.842170943040401e-14
boost_mass_invariant_0	True	0.0
boost_mass_invariant_0.1	True	2.842170943040401e-14
boost_mass_invariant_0.9	True	-1.1368683772161603e-13

Check	Verified	Recorded detail
boost_mass_invariant_0.99	True	-4.547473508864641e-13
common_clock_ratio_0.001	True	g=0.001
common_clock_ratio_0.3	True	g=0.3
common_clock_ratio_0.99	True	g=0.99
common_clock_ratio_1.2	True	g=1.2
optical_shift_exact_arithmetic_nonzero	True	5.0168971872259797230e-18
muon_transformation_back_to_rest	True	
legacy_parameter_intervals_still_disjoint	True	conditional numerical diagnostic

C. Reproduction and verification boundaries

C.1 Numerical environment

The execution snapshots record Python, NumPy, SciPy and SymPy versions together with source and data hashes. Monte Carlo outputs reproduce with the declared seed and generator version. Floating-point last digits can vary with platform and numerical libraries; the mathematical tolerances and independent checks are supplied in the source.

The fresh numerical run preceded the final document tables. The tables and figures are generated from those outputs. The CSV datasets contain numerical trajectories, intermediate comparisons and units. They are not substitutes for the ODE or likelihood scripts. The full covariance calculation belongs to the numerical source and its recorded inputs.

C.2 Scope of independent checking

Independent computational forms are used where practical: analytic versus numerical exchange, proper-time versus reference-time propagation, eigenvalue versus matrix-exponential quantum evolution, direct covariance solve versus whitening, and floating-point versus symbolic substitutions. These are internal verification methods, not an external laboratory replication or formal machine-checked proof of all mathematics.

The separate source record inventories the supplied drafts and earlier packages used. It does not claim exhaustive retrieval of all website or archive revisions. A missing source is not assumed to contain a needed proof, nor assumed not to contain one. Author corrections in the present conversation are stated as revised premises; the explicit Markov, oscillator and channel constructions are new illustrative implementations, not attributed retrospectively to the author.

C.3 Publication status

The analysis is retrospective for already published measurements and synthetic for generated counts. The code hashes and file checksums establish reproducibility, not prospective

blinding. There is no new public preregistration or deposited withheld prediction in this package. A future physical test should freeze the microscopic law, response functions, data split, numerical tolerances and likelihood before its independent comparison.

D. Executable revision analysis

The following is the complete retained analysis script used for the conversion and clock-corrected tests. The three new reconstruction scripts follow it. Its imports refer to the package's included baseline and audit results. The retained baseline and audit scripts are supplied separately in the archive. Long code lines wrap for printing without changing the machine-readable source.

```
#!/usr/bin/env python3
"""Conservative conversion and proper-time tests. No physical target fitting.

Published summary comparisons, synthetic recovery experiments, mathematical
verification, and inherited benchmarks are separately recorded. The synthetic
calibration uses channel A only; it is not physical evidence for EQEF.
"""
from __future__ import annotations
import csv, hashlib, json, math, platform, sys
from datetime import datetime, timezone
from pathlib import Path
import numpy as np
import scipy
from scipy.integrate import quad, solve_ivp
from scipy.linalg import expm
from scipy.stats import chi2
import sympy as sp

ROOT=Path(__file__).resolve().parents[1]
OUT=ROOT/'results'; OUT.mkdir(exist_ok=True)
P=json.loads((ROOT/'data/revision_inputs.json').read_text())
B=json.loads((ROOT/'baseline/results/results.json').read_text())
L=json.loads((ROOT/'legacy/results/new_results.json').read_text())
rng=np.random.default_rng(P['seed']); checks=[]; result={}

def check(name, condition, detail='', family='mathematical'):
    checks.append({'name':name,'passed':bool(condition),'detail':str(detail),'family':family})
def save_csv(name, rows):
    if not rows: raise ValueError('empty table '+name)
    with (OUT/name).open('w',newline='') as f:
        w=csv.DictWriter(f,fieldnames=list(rows[0])); w.writeheader(); w.writerows(rows)
def digest(p): return hashlib.sha256(p.read_bytes()).hexdigest()
def q(t): return 0.8+0.1*np.cos(t)
def dq(t): return -0.1*np.sin(t)
def tau(t): return 0.8*np.asarray(t)+0.1*np.sin(t)

# 1. Exact paired transfer. Negative net changes are returns, not destruction.
```

```
rows=[]; worst=0.0
for i in range(200):
    a,p=rng.random(2)*10; f=rng.random()*p; ret=rng.random()*a
    aa,pp=a+f-ret,p-f+ret
    err=abs(aa+pp-a-p); worst=max(worst,err)
    if i<12: rows.append(dict(case=i,A_before=a,P_before=p,forward=f,returning=
    ret,A_after=aa,P_after=pp,total_error=err))
    check(f'paired_transfer_{i:03d}',aa>=-1e-14 and pp>=-1e-14 and err<1e-13,err,
    'conservation')
save_csv('paired_transfer_examples.csv',rows)
result['paired_transfer']={'cases':200,'maximum_total_error':worst,'scope':'
    closed-cell conservative bookkeeping with specified rates'}

# 2. Continuous two-reservoir exchange, exact solution vs two independent ODEs.
s=P['illustrative_exchange']; a0=s['initial_expressed']; total=s['total'];
k=s['forward_rate_per_proper_unit']*s['efficiency']; r=s['
    return_rate_per_proper_unit']; lam=k+r; ae=k*total/lam
T=s['reference_duration']; t=np.linspace(0,T,201); u=tau(t)
exact=ae+(a0-ae)*np.exp(-lam*u)
proper=solve_ivp(lambda tt,x:[k*(total-x[0])-r*x[0]],(0,float(u[-1])),[a0],rtol
    =2e-12,atol=2e-14,dense_output=True)
coord=solve_ivp(lambda tt,x:[q(tt)*(k*(total-x[0])-r*x[0])],(0,T),[a0],rtol=2e
    -12,atol=2e-14,dense_output=True)
wrong=ae+(a0-ae)*np.exp(-lam*t)
err_p=float(np.max(abs(proper.sol(u)[0]-exact))); err_c=float(np.max(abs(coord.
    sol(t)[0]-exact)))
check('proper_time_exact_ODE',err_p<1e-10,err_p,'clock covariance')
check('reference_time_exact_ODE',err_c<1e-10,err_c,'clock covariance')
check('clock_missing_factor_control',np.max(abs(wrong-exact))>0.01,float(np.max(
    abs(wrong-exact))),'negative control')
rows=[dict(t=float(tt),tau=float(uu),lapse=float(q(tt)),expressed_exact=float(aa
    ),potential_exact=float(total-aa),expressed_ODE=float(cc),wrong_clock=float(
    ww)) for tt,uu,aa,cc,ww in zip(t,u,exact,coord.sol(t)[0],wrong)]
save_csv('exchange_proper_time.csv',rows)
result['exchange']={'forward_effective_rate':k,'return_rate':r,'
    equilibrium_expressed':ae,'proper_duration':float(u[-1]),'
    proper_ODE_max_error':err_p,'coordinate_ODE_max_error':err_c,'
    wrong_clock_max_error':float(np.max(abs(wrong-exact))),'scope':'new
    illustrative closure, not a uniquely derived EQEF law'}

# 3. Frame-size covariance: a physical hazard determines per-step probability.
G=.07; duration=5.0; exact_survival=math.exp(-G*duration); rows=[]
for n in [1,2,5,10,20,50,100,1000,10000]:
    dt=duration/n; pn=-math.expm1(-G*dt); ss=math.exp(n*math.log1p(-pn)); euler
    =(1-G*dt)**n
    naive=(1-.01)**n
    check(f'exact_frame_subdivision_{n}',abs(ss-exact_survival)<3e-15,ss,'frame
    covariance')
    rows.append(dict(steps=n,proper_step=dt,negation_probability=pn,
    survival_exact_step=ss,survival_Euler=euler,survival_fixed_point01=naive))
save_csv('frame_subdivision.csv',rows)
result['frame_subdivision']={'rate':G,'duration':duration,'physical_survival':
    exact_survival,'lesson':'a fixed per-step fraction and a fixed proper-time
```

```
    rate are different hypotheses'}

# 4. Generator positivity, detailed balance, relative entropy contraction.
M=np.array([[-r,k],[r,-k]])
x0=np.array([.2,.8]); pi=np.array([k/(k+r),r/(k+r)])
prev=float('inf'); rows=[]
for tt in np.linspace(0,15,31):
    K=expm(M*tt); x=K@x0; D=float(np.sum(x*np.log(x/pi)))
    check(f'markov_positive_{tt:.1f}',np.min(K)>-1e-13 and np.max(abs(K.sum(axis
    =0)-1))<1e-12,f'D={D}','positive transfer')
    check(f'entropy_contracts_{tt:.1f}',D<=prev+1e-13,D,'entropy')
    prev=D; rows.append(dict(proper_time=tt,expressed_probability=x[0],
    potential_probability=x[1],relative_entropy=D))
check('two_state_detailed_balance',abs(r*pi[0]-k*pi[1])<1e-14)
save_csv('markov_reservoir.csv',rows)

# 5. Conservative coupled oscillators: interaction energy must be included.
wa,wp,coupling=1.0,1.4,.2
K=np.array([[wa*wa,coupling],[coupling,wp*wp]])
A=np.block([[np.zeros((2,2)),np.eye(2)],[-K,np.zeros((2,2))]])
z0=np.array([1.,0.,0.,.3]); energies=[]; rows=[]
for tt in np.linspace(0,50,101):
    z=expm(A*tt)@z0; x,y,px,py=z
    EA=.5*(px*px+wa*wa*x*x); EP=.5*(py*py+wp*wp*y*y); EI=coupling*x*y
    energies.append(EA+EP+EI)
    rows.append(dict(proper_time=tt,E_expressed=EA,E_potential=EP,E_interaction=
    EI,E_total=EA+EP+EI))
check('oscillator_stable_modes',np.min(np.linalg.eigvalsh(K))>0,np.linalg.
    eigvalsh(K))
check('oscillator_total_energy',np.ptp(energies)<1e-12,np.ptp(energies),'
    conservation')
check('interaction_energy_not_omitted',np.ptp([v['E_expressed']+v['E_potential']
     for v in rows])>1e-3,f'coupling={coupling}','negative control')
save_csv('coherent_reservoir.csv',rows)
result['coherent_reservoir']={'mode_frequencies':np.sqrt(np.linalg.eigvalsh(K)).
    tolist(),'energy_drift':float(np.ptp(energies)),'scope':'specified quadratic
     Hamiltonian; no dissipation or fundamental tension inferred'}

# 6. Channel positivity and no-signalling (conditional on Hilbert-space
    structure).
I=np.eye(2); ket=np.array([0,1,-1,0],complex)/np.sqrt(2); rho=np.outer(ket,ket.
    conj())
partial=lambda rr:np.einsum('abcb->ac',rr.reshape(2,2,2,2))
quantum_rows=[]
for tt in [0,.1,.5,1,2,5,10]:
    surv=np.exp(-G*tt)
    K0=np.diag([np.sqrt(surv),1.]); K1=np.array([[0,0],[np.sqrt(1-surv),0]])
    check(f'Kraus_completeness_{tt}',np.max(abs(K0.T@K0+K1.T@K1-I))<1e-13,f's={
    surv}','quantum conditional')
    after=sum(np.kron(I,kk)@rho@np.kron(I,kk).conj().T for kk in [K0,K1])
    sigerr=np.max(abs(partial(after)-partial(rho)))
    check(f'Kraus_no_signal_{tt}',sigerr<1e-13,sigerr,'quantum conditional')
```

```
    check(f'Kraus_density_positive_{tt}',np.linalg.eigvalsh(after).min()>-1e-13
    and abs(np.trace(after)-1)<1e-13)
    quantum_rows.append(dict(proper_time=tt,expressed_survival=surv,
    potential_population=1-surv,marginal_change=float(sigerr)))
save_csv('quantum_transfer.csv',quantum_rows)

# 7. Exact observational degeneracy and Fisher-rank test.
ridge=[]; mu=1000.; F=mu*np.ones((2,2)); eig=np.linalg.eigvalsh(F)
check('lapse_efficiency_Fisher_rank_one',np.linalg.matrix_rank(F)==1,eig,'
    identifiability')
for gg in [.72,.75,.8,.9,1.0]:
    eff=.7/gg
    ridge.append(dict(lapse=gg,efficiency=eff,predicted_ratio=gg*eff))
check('lapse_efficiency_identical_predictions',max(abs(z['predicted_ratio']-.7)
    for z in ridge)<2e-16)
save_csv('identifiability_ridge.csv',ridge)
result['identifiability']={'Fisher_eigenvalues':eig.tolist(),'
    identified_quantity':'lapse times efficiency times potential-rate
    normalization times detector response','not_identified':'absolute EQEF
    efficiency from one uncalibrated rate'}

# 8. Synthetic multi-channel universality, calibration vs held-out channels.
S=P['synthetic_universality']; name=S['names']; rates=np.array(S['potential_rate'
    ],float); tt=np.array(S['duration'],float); gg=np.array(S['lapse'],float);
    dd=np.array(S['detection_efficiency'],float)
base=rates*tt*gg*dd; eta=S['efficiency']; n=rng.poisson(eta*base)
eta_cal=n[0]/base[0]; sig_cal=math.sqrt(n[0])/base[0]
res=n[1:]-eta_cal*base[1:]; cov=np.diag(eta_cal*base[1:])+np.outer(base[1:],base
    [1:])*sig_cal**2
hold_chi=float(res@np.linalg.solve(cov,res))
def deviance(counts,exposure):
    etahat=counts.sum()/exposure.sum(); means=etahat*exposure
    return float(2*np.sum(np.where(counts>0,counts*np.log(counts/means),0)-(
    counts-means))),float(etahat)
Dgood,eta_ml=deviance(n,base); Dwrong,_=deviance(n,base/gg)
negative=n.copy(); negative[-1]=rng.poisson(S['negative_control_D_efficiency']*
    base[-1]); Dnegative,eta_negative=deviance(negative,base)
rows=[]
for j in range(4):
    rows.append(dict(channel=name[j],role='calibration' if j==0 else 'held-out
    simulation',potential_rate=rates[j],duration=tt[j],lapse=gg[j],
    detector_efficiency=dd[j],effective_exposure=base[j],injected_efficiency=eta,
    counts=int(n[j]),naive_efficiency=n[j]/(base[j]/gg[j]),
    clock_corrected_efficiency=n[j]/base[j],shot_noise_sigma=math.sqrt(n[j])/
    base[j],calibrated_prediction=eta_cal*base[j],negative_control_counts=int(
    negative[j])))
save_csv('synthetic_universality.csv',rows)
# Monte Carlo null calibration of shared-efficiency homogeneity statistic.
reps=5000; dn=[]
for ns in rng.poisson(eta_ml*base,(reps,4)):
    dn.append(deviance(ns,base)[0])
emp=(1+np.count_nonzero(np.array(dn)>=Dgood))/(reps+1)
```

```
check('synthetic_clock_correction_changes_bias',Dwrong>Dgood,Dwrong-Dgood,'synthetic demonstration')
check('synthetic_species_defect_not_hidden',Dnegative>Dgood+100,Dnegative,'negative control')
check('synthetic_calibration_not_all_channel_fit',eta_cal==n[0]/base[0],eta_cal)
result['synthetic_universality']={'injected_efficiency':eta,'calibrated_efficiency':float(eta_cal),'calibration_sigma':sig_cal,'heldout_chi2_conditional':hold_chi,'heldout_conditional_p':float(chi2.sf(hold_chi,3)),'correct_clock_homogeneity_deviance':Dgood,'correct_clock_asymptotic_p':float(chi2.sf(Dgood,3)),'correct_clock_simulated_p':emp,'null_simulations':reps,'omit_clock_deviance':Dwrong,'negative_control_deviance':Dnegative,'negative_control_p':float(chi2.sf(Dnegative,3)),'scope':'generated counts; not data from four experiments or empirical validation of EQEF'}

# 9. Weighted exposure and time-dependent efficiency.
rr=lambda z:10+2*np.sin(2*z); eff=lambda z:.95-.02*np.cos(z)
true_count=quad(lambda z:q(z)*rr(z)*eff(z),0,10,epsabs=1e-11)[0]
exposure=quad(lambda z:q(z)*rr(z),0,10,epsabs=1e-11)[0]
eff_weighted=true_count/exposure; eff_arithmetic=quad(eff,0,10)[0]/10
check('integrated_exposure_identity',abs(eff_weighted*exposure-true_count)<1e-12)
check('arithmetic_mean_not_general_efficiency',abs(eff_arithmetic-eff_weighted)>1e-5,eff_arithmetic-eff_weighted,'negative control')
result['weighted_exposure']={'counts_expectation':true_count,'effective_exposure':exposure,'weighted_efficiency':eff_weighted,'arithmetic_efficiency':eff_arithmetic}

# 10. Old DESI fixed comparator rerun; consistent data transforms preserve chi2.
desi=list(csv.DictReader((ROOT/'baseline/results/desi_fixed_benchmark.csv').open()))
C=np.loadtxt(ROOT/'baseline/data/desi_dr2_cov.txt')
# Extract by actual header names (validated below).
keys=list(desi[0]);
dvec=np.array([float(z['data']) for z in desi]); mvec=np.array([float(z['benchmark']) for z in desi])
res=dvec-mvec; chi=float(res@np.linalg.solve(C,res))
scale=.7+.03*np.arange(len(res)); A=np.diag(scale)
rp=A@res; Cp=A@C@A.T; chitr=float(rp@np.linalg.solve(Cp,rp))
check('DESI_full_covariance_preserved',abs(chi-chitr)<1e-10,chi-chitr,'coordinate covariance')
result['DESI']={'chi2_original':chi,'chi2_transformed':chitr,'difference':chitr-chi,'p_fixed_13':float(chi2.sf(chi,13)),'scope':'invertible coordinate/units audit only; not a physical EQEF modification of BAO distances'}

# 11. FLRW lapse is not an extra cosmological fluid.
BP=json.loads((ROOT/'baseline/data/benchmark_parameters.json').read_text()); Om=BP['Omega_m']; Or=BP['Omega_r']; Ol=1-Om-Or
H0=BP['H0_km_s_Mpc']*1000/BP['mpc_m']; Gyr=1e9*BP['julian_year_s']
E=lambda a:math.sqrt(Or/a**4+Om/a**3+Ol)
g_a=lambda a:.8+.2*a
age=quad(lambda a:1/(a*H0*E(a)),1e-10,1,epsabs=1e-4,epsrel=2e-12)[0]/Gyr
```

```
coordinate_age=quad(lambda a:1/(a*g_a(a)*H0*E(a)),1e-10,1,epsabs=1e-4,epsrel=2e-12)[0]/Gyr
recovered_age=quad(lambda a:g_a(a)/(a*g_a(a)*H0*E(a)),1e-10,1,epsabs=1e-4,epsrel=2e-12)[0]/Gyr
check('cosmic_proper_age_invariant',abs(age-recovered_age)<1e-11,age,'coordinate covariance')
check('coordinate_age_is_different_label',abs(coordinate_age-age)>.1,coordinate_age-age,'negative control')
result['cosmic_lapse']={'proper_age_Gyr':age,'coordinate_age_in_Gyr_units':coordinate_age,'recovered_proper_age_Gyr':recovered_age,'lapse_law':'0.8+0.2 a (illustrative coordinate choice)','scope':'same physical background; coordinate duration is not a second measured age'}

# 12. Tensor propagation transformed once, including the lapse derivative.
H=.05; Fdot=.02; kk=1.3; t2=np.linspace(0,10,101); u2=tau(t2)
def vproper(uu,v):return [v[1],-(3*H+Fdot)*v[1]-kk*kk*np.exp(-2*H*uu)*v[0]]
def vcoord(tt,v):return [v[1],-(q(tt)*(3*H+Fdot)-dq(tt)/q(tt))*v[1]-q(tt)**2*kk*kk*np.exp(-2*H*tau(tt))*v[0]]
vp=solve_ivp(vproper,(0,float(u2[-1])),[1,0],rtol=1e-11,atol=1e-13,dense_output=True)
vc=solve_ivp(vcoord,(0,10),[1,0],rtol=1e-11,atol=1e-13,dense_output=True)
terr=np.max(abs(vp.sol(u2)[0]-vc.sol(t2)[0]))
check('tensor_full_clock_transformation',terr<3e-10,terr,'clock covariance')
save_csv('tensor_clock_comparison.csv',[dict(reference_time=float(ti),proper_time=float(ui),proper_solution=float(x),reference_solution=float(y),error=float(x-y)) for ti,ui,x,y in zip(t2,u2,vp.sol(u2)[0],vc.sol(t2)[0])])
result['tensor_clock']={'maximum_solution_error':float(terr),'scope':'specified effective wave equation, not raw GW detector data'}

# 13. Quantum evolution: common phase offsets cannot fix oscillation probabilities.
Hmat=np.array([[.2,.3,.1],[.3,-.1,.2],[.1,.2,.4]],complex); init=np.array([1,0,0],complex)
S0=expm(-1j*Hmat*u2[-1]); shifted=expm(-1j*(Hmat+.137*np.eye(3))*u2[-1])
check('identity_Hamiltonian_shift_probability',np.max(abs(abs(S0)**2-abs(shifted)**2))<1e-13)
qc=solve_ivp(lambda tt,z:-1j*q(tt)*Hmat@z,(0,10),init,rtol=1e-11,atol=1e-13)
qerr=np.max(abs(qc.y[:,-1]-S0@init))
check('quantum_time_reparametrization',qerr<3e-10,qerr,'clock covariance')
result['quantum_clock']={'maximum_amplitude_error':float(qerr),'scope':'Hermitian generator identity test; clock is a laboratory evolution parameter, not photon proper time'}

# 14. Lorentz boosts preserve invariant masses, and common clock factors cancel ratios.
p0=np.array([10.,2.,3.,1.]); mass2=p0[0]**2-np.dot(p0[1:],p0[1:]); rows=[]
for beta in [-.99,-.5,0,.1,.9,.99]:
    gam=1/math.sqrt(1-beta*beta); new=p0.copy();new[0]=gam*(p0[0]-beta*p0[1]);new[1]=gam*(p0[1]-beta*p0[0]); mm=new[0]**2-np.dot(new[1:],new[1:]);
    check(f'boost_mass_invariant_{beta}',abs(mm-mass2)<1e-10,mm-mass2,'relativity')
    rows.append(dict(beta=beta,gamma=gam,invariant_mass_squared=mm,error=mm-mass2))
```

```
for g in [.001,.3,.99,1.2]:check(f'common_clock_ratio_{g}',abs((g*5)/(g*7)-5/7)<1e-15,f'g={g}','dimensionless quantities')
save_csv('invariant_mass_boosts.csv',rows)

# 15. Published clock measurements. Symbolic decimal arithmetic avoids 1+1e-17 cancellation.
c=sp.Integer(299792458); obs=P['clocks']; ch=obs['chou2010']; dphi=sp.Rational(str(ch['local_acceleration_m_s2']))*sp.Rational(str(ch['height_m']))/c**2
meas=sp.Rational(str(ch['shift'])); sig=sp.Rational(str(ch['sigma'])); r_eta=(1+meas)/(1+dphi)
chout={'predicted_fractional_shift':float(dphi),'observed_fractional_shift':float(meas),'sigma':float(sig),'residual_sigma':float((meas-dphi)/sig),'relative_efficiency_minus_one':float(r_eta-1),'interpretation':'a relative efficiency change between the two settings, conditional on GR, not absolute potential'}
bb=obs['bailey1977_positive']; ml=obs['mulan2011']; pred=bb['gamma_rounded']*ml['lifetime_us']; rel=pred/bb['lifetime_us']; sigrel=rel*math.hypot(ml['sigma_us']/ml['lifetime_us'],bb['sigma_us']/bb['lifetime_us'])
muout={'gamma_rounded':bb['gamma_rounded'],'rest_lifetime_us':ml['lifetime_us'],'predicted_lab_lifetime_us':pred,'observed_lab_lifetime_us':bb['lifetime_us'],'lifetime_sigma_us':bb['sigma_us'],'conditional_residual_sigma':(bb['lifetime_us']-pred)/math.hypot(bb['sigma_us'],bb['gamma_rounded']*ml['sigma_us']),'naive_apparent_shortfall_without_time_dilation':1-ml['lifetime_us']/bb['lifetime_us'],'moving_to_rest_efficiency_ratio':rel,'ratio_sigma_excluding_beam':sigrel,'gamma_rounding_half_last_digit_effect':.005*ml['lifetime_us']/bb['lifetime_us'],'scope':'comparison of published summaries; gamma uncertainty, beam distribution and full historical correlations not reconstructed; no exact confidence limit or particle universality claim'}
result['published_clocks']={'optical':chout,'muon':muout,'galileo':obs['galileo2018']}
check('optical_shift_exact_arithmetic_nonzero',float(dphi)>0 and r_eta!=1,sp.N(r_eta-1,20),'arithmetic')
check('muon_transformation_back_to_rest',abs((pred/bb['gamma_rounded'])-ml['lifetime_us'])<1e-14)
save_csv('published_clock_comparisons.csv',[
 dict(experiment='Chou2010 height step',quantity='fractional clock shift',observed=chout['observed_fractional_shift'],standard_error=chout['sigma'],comparison=chout['predicted_fractional_shift'],conditional_pull=chout['residual_sigma'],role='published summary, GR conditional'),
 dict(experiment='Bailey1977 positive muon',quantity='laboratory lifetime microseconds',observed=muout['observed_lab_lifetime_us'],standard_error=muout['lifetime_sigma_us'],comparison=muout['predicted_lab_lifetime_us'],conditional_pull=muout['conditional_residual_sigma'],role='rounded gamma; comparison only'),
 dict(experiment='Delva2018 Galileo',quantity='fractional redshift violation coefficient',observed=obs['galileo2018']['redshift_violation'],standard_error=obs['galileo2018']['sigma'],comparison=0,conditional_pull=obs['galileo2018']['redshift_violation']/obs['galileo2018']['sigma'],role='published fitted coefficient, not event-level refit')])

# 16. Legacy nc matches remain diagnostic, not new transport coefficients.
```

```
alpha0=L['alpha_literal']['literal_code_output']; alpha=L['alpha_literal']['reference_alpha']; nc0=1e-6
nc_alpha=nc0*alpha/alpha0; nc_scalar=nc0*(127.3/L['scalar']['mass_GeV_with_c_hs_point1'])**2
base_per_C=L['g2']['per_C_delta_a']; nc_g_low=nc0*2e-9/(1e5*base_per_C); nc_g_high=nc0*3e-9/(1e4*base_per_C)
result['legacy_normalization']={'nc_alpha_numeric_only':nc_alpha,'nc_scalar_benchmark_only':nc_scalar,'nc_historical_muon_interval':[nc_g_low,nc_g_high],'scope':'old printed numerical convention; nc is not identified with the new efficiency or proper-time transfer rate'}
check('legacy_parameter_intervals_still_disjoint',nc_alpha<nc_g_low<nc_g_high<nc_scalar, 'conditional numerical diagnostic')

# 17. Shot-noise requirements for a tiny deficit and a boundary test.
eps=1e-7; z95=1.959963984540054
result['sensitivity']={'deficit':eps,'Poisson_known_potential_counts_95':(z95/eps)**2,'two_equal_independent_Poisson_counts_each_95':2*(z95/eps)**2,'known_trials_zero_failures_95_upper_after_30_million':1-.05**(1/30_000_000),'interpretation':'different data models; ratios of noisy intensities require much larger samples than individually known conversion trials'}

result['summary']={'baseline_assertions':B['check_summary']['total'],'legacy_assertions':L['verification_summary']['total'],'new_assertions':len(checks),'new_passed':sum(x['passed'] for x in checks),'new_failed':[x for x in checks if not x['passed']],'new_independent_parameter_free_physical_alignments':0,'physical_EQEF_fit_executed':False,'record_type':'reproducible retrospective and synthetic study, not a prospective blind prediction'}
save_csv('verification_checks.csv',checks)
(OUT/'eqef_results.json').write_text(json.dumps(result,indent=2))
(OUT/'execution_record.json').write_text(json.dumps({'utc':datetime.now(timezone.utc).isoformat(),'python':sys.version,'numpy':np.__version__,'scipy':scipy.__version__,'sympy':sp.__version__,'platform':platform.platform(),'seed':P['seed'],'hashes':{str(p.relative_to(ROOT)):digest(p) for p in [Path(__file__),ROOT/'data/revision_inputs.json']}},indent=2))
print(json.dumps(result,indent=2))
raise SystemExit(0 if all(x['passed'] for x in checks) else 1)
```

E. Complete new verification ledger

Table 32: All 426 assertions added in the conservative reconstruction. R: core model; T: threshold/response; S: coupled spectrum. Numerical tolerance is an implementation criterion, not experimental uncertainty.

Suite	Check	Error / value	Tolerance	Status
R	Hamiltonian conservation, nonlinear ring	3.035×10^{-13}	1.00×10^{-9}	pass
R	Global phase momentum conservation	6.661×10^{-16}	1.00×10^{-10}	pass
R	Positive stored sector energy	0	1.00×10^{-13}	pass

Suite	Check	Error / value	Tolerance	Status
R	Global phase covariance of force	1.110×10^{-16}	2.00×10^{-14}	pass
R	Compact phase periodicity of energy	1.110×10^{-16}	1.00×10^{-14}	pass
R	Hamiltonian gradient, state 0	1.539×10^{-11}	2.00×10^{-9}	pass
R	Instantaneous total energy balance, state 0	1.532×10^{-12}	2.00×10^{-10}	pass
R	Hamiltonian gradient, state 211	2.530×10^{-11}	2.00×10^{-9}	pass
R	Instantaneous total energy balance, state 211	2.841×10^{-12}	2.00×10^{-10}	pass
R	Hamiltonian gradient, state 937	4.003×10^{-11}	2.00×10^{-9}	pass
R	Instantaneous total energy balance, state 937	2.024×10^{-12}	2.00×10^{-10}	pass
R	Time reversal	1.668×10^{-13}	2.00×10^{-8}	pass
R	Reference-time versus proper-time trajectory	6.639×10^{-13}	2.00×10^{-9}	pass
R	Exact memory elimination t=0.2, link=0	1.013×10^{-14}	2.00×10^{-8}	pass
R	Exact memory elimination t=0.2, link=1	6.518×10^{-15}	2.00×10^{-8}	pass
R	Exact memory elimination t=0.2, link=2	6.252×10^{-15}	2.00×10^{-8}	pass
R	Exact memory elimination t=0.2, link=3	1.012×10^{-14}	2.00×10^{-8}	pass
R	Exact memory elimination t=0.2, link=4	6.500×10^{-15}	2.00×10^{-8}	pass
R	Exact memory elimination t=0.2, link=5	6.236×10^{-15}	2.00×10^{-8}	pass
R	Exact memory elimination t=1, link=0	8.209×10^{-15}	2.00×10^{-8}	pass
R	Exact memory elimination t=1, link=1	3.985×10^{-15}	2.00×10^{-8}	pass
R	Exact memory elimination t=1, link=2	3.110×10^{-15}	2.00×10^{-8}	pass
R	Exact memory elimination t=1, link=3	8.212×10^{-15}	2.00×10^{-8}	pass
R	Exact memory elimination t=1, link=4	3.992×10^{-15}	2.00×10^{-8}	pass
R	Exact memory elimination t=1, link=5	3.126×10^{-15}	2.00×10^{-8}	pass
R	Exact memory elimination t=4, link=0	6.151×10^{-15}	2.00×10^{-8}	pass
R	Exact memory elimination t=4, link=1	4.448×10^{-15}	2.00×10^{-8}	pass
R	Exact memory elimination t=4, link=2	1.526×10^{-15}	2.00×10^{-8}	pass
R	Exact memory elimination t=4, link=3	6.141×10^{-15}	2.00×10^{-8}	pass
R	Exact memory elimination t=4, link=4	4.465×10^{-15}	2.00×10^{-8}	pass
R	Exact memory elimination t=4, link=5	1.548×10^{-15}	2.00×10^{-8}	pass
R	Exact memory elimination t=9, link=0	4.476×10^{-15}	2.00×10^{-8}	pass
R	Exact memory elimination t=9, link=1	1.187×10^{-15}	2.00×10^{-8}	pass
R	Exact memory elimination t=9, link=2	1.922×10^{-15}	2.00×10^{-8}	pass
R	Exact memory elimination t=9, link=3	4.420×10^{-15}	2.00×10^{-8}	pass
R	Exact memory elimination t=9, link=4	1.154×10^{-15}	2.00×10^{-8}	pass
R	Exact memory elimination t=9, link=5	1.929×10^{-15}	2.00×10^{-8}	pass
R	Exact memory elimination t=19, link=0	2.356×10^{-14}	2.00×10^{-8}	pass
R	Exact memory elimination t=19, link=1	1.166×10^{-14}	2.00×10^{-8}	pass

Suite	Check	Error / value	Tolerance	Status
R	Exact memory elimination t=19, link=2	9.361×10^{-15}	2.00×10^{-8}	pass
R	Exact memory elimination t=19, link=3	2.341×10^{-14}	2.00×10^{-8}	pass
R	Exact memory elimination t=19, link=4	1.171×10^{-14}	2.00×10^{-8}	pass
R	Exact memory elimination t=19, link=5	9.385×10^{-15}	2.00×10^{-8}	pass
R	Exact memory elimination t=37, link=0	3.150×10^{-14}	2.00×10^{-8}	pass
R	Exact memory elimination t=37, link=1	1.918×10^{-14}	2.00×10^{-8}	pass
R	Exact memory elimination t=37, link=2	9.173×10^{-15}	2.00×10^{-8}	pass
R	Exact memory elimination t=37, link=3	3.146×10^{-14}	2.00×10^{-8}	pass
R	Exact memory elimination t=37, link=4	1.917×10^{-14}	2.00×10^{-8}	pass
R	Exact memory elimination t=37, link=5	9.173×10^{-15}	2.00×10^{-8}	pass
R	Exact memory elimination t=59, link=0	9.492×10^{-15}	2.00×10^{-8}	pass
R	Exact memory elimination t=59, link=1	2.144×10^{-14}	2.00×10^{-8}	pass
R	Exact memory elimination t=59, link=2	2.609×10^{-15}	2.00×10^{-8}	pass
R	Exact memory elimination t=59, link=3	9.492×10^{-15}	2.00×10^{-8}	pass
R	Exact memory elimination t=59, link=4	2.123×10^{-14}	2.00×10^{-8}	pass
R	Exact memory elimination t=59, link=5	2.970×10^{-15}	2.00×10^{-8}	pass
R	FDT covariance 0,0	6.939×10^{-18}	1.00×10^{-14}	pass
R	FDT covariance 0,0.7	0	1.00×10^{-14}	pass
R	FDT covariance 0,3	3.469×10^{-18}	1.00×10^{-14}	pass
R	FDT covariance 0.3,0	1.388×10^{-17}	1.00×10^{-14}	pass
R	FDT covariance 0.3,0.7	6.939×10^{-18}	1.00×10^{-14}	pass
R	FDT covariance 0.3,3	0	1.00×10^{-14}	pass
R	FDT covariance 2,0	3.469×10^{-18}	1.00×10^{-14}	pass
R	FDT covariance 2,0.7	3.469×10^{-18}	1.00×10^{-14}	pass
R	FDT covariance 2,3	6.939×10^{-18}	1.00×10^{-14}	pass
R	FDT covariance 6,0	3.469×10^{-18}	1.00×10^{-14}	pass
R	FDT covariance 6,0.7	2.082×10^{-17}	1.00×10^{-14}	pass
R	FDT covariance 6,3	0	1.00×10^{-14}	pass
R	Quartic phase-speed expansion axis, ka=0.01	5.208×10^{-12}	6.67×10^{-12}	pass
R	Passive poles axis, ka=0.01	0	1.00×10^{-14}	pass
R	Pole identity axis, ka=0.01	1.355×10^{-20}	2.00×10^{-15}	pass
R	Quartic phase-speed expansion axis, ka=0.03	4.219×10^{-10}	5.40×10^{-10}	pass
R	Passive poles axis, ka=0.03	0	1.00×10^{-14}	pass
R	Pole identity axis, ka=0.03	0	2.00×10^{-15}	pass
R	Quartic phase-speed expansion axis, ka=0.1	5.208×10^{-8}	6.67×10^{-8}	pass
R	Passive poles axis, ka=0.1	0	1.00×10^{-14}	pass

Suite	Check	Error / value	Tolerance	Status
R	Pole identity axis, ka=0.1	0	2.00×10^{-15}	pass
R	Quartic phase-speed expansion axis, ka=0.3	4.216×10^{-6}	5.40×10^{-6}	pass
R	Passive poles axis, ka=0.3	0	1.00×10^{-14}	pass
R	Pole identity axis, ka=0.3	1.388×10^{-17}	2.00×10^{-15}	pass
R	Quartic phase-speed expansion axis, ka=0.7	1.247×10^{-4}	1.60×10^{-4}	pass
R	Passive poles axis, ka=0.7	0	1.00×10^{-14}	pass
R	Pole identity axis, ka=0.7	5.551×10^{-17}	2.00×10^{-15}	pass
R	Quartic phase-speed expansion axis, ka=1.0	5.177×10^{-4}	6.67×10^{-4}	pass
R	Passive poles axis, ka=1.0	0	1.00×10^{-14}	pass
R	Pole identity axis, ka=1.0	0	2.00×10^{-15}	pass
R	Quartic phase-speed expansion face diagonal, ka=0.01	1.302×10^{-12}	6.67×10^{-12}	pass
R	Passive poles face diagonal, ka=0.01	0	1.00×10^{-14}	pass
R	Pole identity face diagonal, ka=0.01	1.355×10^{-20}	2.00×10^{-15}	pass
R	Quartic phase-speed expansion face diagonal, ka=0.03	1.055×10^{-10}	5.40×10^{-10}	pass
R	Passive poles face diagonal, ka=0.03	0	1.00×10^{-14}	pass
R	Pole identity face diagonal, ka=0.03	0	2.00×10^{-15}	pass
R	Quartic phase-speed expansion face diagonal, ka=0.1	1.302×10^{-8}	6.67×10^{-8}	pass
R	Passive poles face diagonal, ka=0.1	0	1.00×10^{-14}	pass
R	Pole identity face diagonal, ka=0.1	1.735×10^{-18}	2.00×10^{-15}	pass
R	Quartic phase-speed expansion face diagonal, ka=0.3	1.054×10^{-6}	5.40×10^{-6}	pass
R	Passive poles face diagonal, ka=0.3	0	1.00×10^{-14}	pass
R	Pole identity face diagonal, ka=0.3	1.388×10^{-17}	2.00×10^{-15}	pass
R	Quartic phase-speed expansion face diagonal, ka=0.7	3.122×10^{-5}	1.60×10^{-4}	pass
R	Passive poles face diagonal, ka=0.7	0	1.00×10^{-14}	pass
R	Pole identity face diagonal, ka=0.7	0	2.00×10^{-15}	pass
R	Quartic phase-speed expansion face diagonal, ka=1.0	1.298×10^{-4}	6.67×10^{-4}	pass
R	Passive poles face diagonal, ka=1.0	0	1.00×10^{-14}	pass
R	Pole identity face diagonal, ka=1.0	0	2.00×10^{-15}	pass
R	Quartic phase-speed expansion body diagonal, ka=0.01	5.790×10^{-13}	6.67×10^{-12}	pass
R	Passive poles body diagonal, ka=0.01	0	1.00×10^{-14}	pass

Suite	Check	Error / value	Tolerance	Status
R	Pole identity body diagonal, ka=0.01	0	2.00×10^{-15}	pass
R	Quartic phase-speed expansion body diagonal, ka=0.03	4.687×10^{-11}	5.40×10^{-10}	pass
R	Passive poles body diagonal, ka=0.03	0	1.00×10^{-14}	pass
R	Pole identity body diagonal, ka=0.03	0	2.00×10^{-15}	pass
R	Quartic phase-speed expansion body diagonal, ka=0.1	5.787×10^{-9}	6.67×10^{-8}	pass
R	Passive poles body diagonal, ka=0.1	0	1.00×10^{-14}	pass
R	Pole identity body diagonal, ka=0.1	0	2.00×10^{-15}	pass
R	Quartic phase-speed expansion body diagonal, ka=0.3	4.687×10^{-7}	5.40×10^{-6}	pass
R	Passive poles body diagonal, ka=0.3	0	1.00×10^{-14}	pass
R	Pole identity body diagonal, ka=0.3	0	2.00×10^{-15}	pass
R	Quartic phase-speed expansion body diagonal, ka=0.7	1.388×10^{-5}	1.60×10^{-4}	pass
R	Passive poles body diagonal, ka=0.7	0	1.00×10^{-14}	pass
R	Pole identity body diagonal, ka=0.7	0	2.00×10^{-15}	pass
R	Quartic phase-speed expansion body diagonal, ka=1.0	5.776×10^{-5}	6.67×10^{-4}	pass
R	Passive poles body diagonal, ka=1.0	0	1.00×10^{-14}	pass
R	Pole identity body diagonal, ka=1.0	1.110×10^{-16}	2.00×10^{-15}	pass
R	Graph spectrum 4 sites	8.587×10^{-16}	1.00×10^{-13}	pass
R	Graph spectrum 7 sites	8.882×10^{-16}	1.00×10^{-13}	pass
R	Graph spectrum 12 sites	1.110×10^{-15}	1.00×10^{-13}	pass
R	Nonlinear pendulum period A=0.1	1.019×10^{-13}	1.00×10^{-10}	pass
R	Nonlinear pendulum period A=0.5	3.306×10^{-14}	1.00×10^{-10}	pass
R	Nonlinear pendulum period A=1.0	2.756×10^{-14}	1.00×10^{-10}	pass
R	Nonlinear pendulum period A=1.5707963267948966	1.407×10^{-13}	1.00×10^{-10}	pass
R	Nonlinear pendulum period A=2.5	4.964×10^{-14}	1.00×10^{-10}	pass
R	Coherent transfer formula d=0.0,t=0	0	1.00×10^{-13}	pass
R	Coherent transfer total population d=0.0,t=0	0	1.00×10^{-13}	pass
R	Coherent transfer formula d=0.0,t=0.75	4.163×10^{-17}	1.00×10^{-13}	pass
R	Coherent transfer total population d=0.0,t=0.75	0	1.00×10^{-13}	pass
R	Coherent transfer formula d=0.0,t=1.5	0	1.00×10^{-13}	pass
R	Coherent transfer total population d=0.0,t=1.5	0	1.00×10^{-13}	pass
R	Coherent transfer formula d=0.0,t=2.25	0	1.00×10^{-13}	pass

Suite	Check	Error / value	Tolerance	Status
R	Coherent transfer total population d=0.0,t=2.25	0	1.00×10^{-13}	pass
R	Coherent transfer formula d=0.0,t=3	2.220×10^{-16}	1.00×10^{-13}	pass
R	Coherent transfer total population d=0.0,t=3	1.110×10^{-16}	1.00×10^{-13}	pass
R	Coherent transfer formula d=0.0,t=3.75	2.220×10^{-16}	1.00×10^{-13}	pass
R	Coherent transfer total population d=0.0,t=3.75	2.220×10^{-16}	1.00×10^{-13}	pass
R	Coherent transfer formula d=0.0,t=4.5	2.220×10^{-16}	1.00×10^{-13}	pass
R	Coherent transfer total population d=0.0,t=4.5	2.220×10^{-16}	1.00×10^{-13}	pass
R	Coherent transfer formula d=0.0,t=5.25	2.220×10^{-16}	1.00×10^{-13}	pass
R	Coherent transfer total population d=0.0,t=5.25	4.441×10^{-16}	1.00×10^{-13}	pass
R	Coherent transfer formula d=0.0,t=6	1.665×10^{-16}	1.00×10^{-13}	pass
R	Coherent transfer total population d=0.0,t=6	5.551×10^{-16}	1.00×10^{-13}	pass
R	Coherent transfer formula d=0.0,t=6.75	5.551×10^{-17}	1.00×10^{-13}	pass
R	Coherent transfer total population d=0.0,t=6.75	0	1.00×10^{-13}	pass
R	Coherent transfer formula d=0.0,t=7.5	6.939×10^{-18}	1.00×10^{-13}	pass
R	Coherent transfer total population d=0.0,t=7.5	4.441×10^{-16}	1.00×10^{-13}	pass
R	Coherent transfer formula d=0.0,t=8.25	1.735×10^{-17}	1.00×10^{-13}	pass
R	Coherent transfer total population d=0.0,t=8.25	3.331×10^{-16}	1.00×10^{-13}	pass
R	Coherent transfer formula d=0.0,t=9	2.776×10^{-17}	1.00×10^{-13}	pass
R	Coherent transfer total population d=0.0,t=9	2.220×10^{-16}	1.00×10^{-13}	pass
R	Coherent transfer formula d=0.0,t=9.75	1.665×10^{-16}	1.00×10^{-13}	pass
R	Coherent transfer total population d=0.0,t=9.75	0	1.00×10^{-13}	pass
R	Coherent transfer formula d=0.0,t=10.5	1.110×10^{-16}	1.00×10^{-13}	pass
R	Coherent transfer total population d=0.0,t=10.5	2.220×10^{-16}	1.00×10^{-13}	pass
R	Coherent transfer formula d=0.0,t=11.25	4.441×10^{-16}	1.00×10^{-13}	pass
R	Coherent transfer total population d=0.0,t=11.25	2.220×10^{-16}	1.00×10^{-13}	pass
R	Coherent transfer formula d=0.0,t=12	6.661×10^{-16}	1.00×10^{-13}	pass
R	Coherent transfer total population d=0.0,t=12	7.772×10^{-16}	1.00×10^{-13}	pass

Suite	Check	Error / value	Tolerance	Status
R	Coherent transfer formula d=0.0,t=12.75	2.220×10^{-16}	1.00×10^{-13}	pass
R	Coherent transfer total population d=0.0,t=12.75	0	1.00×10^{-13}	pass
R	Coherent transfer formula d=0.0,t=13.5	2.220×10^{-16}	1.00×10^{-13}	pass
R	Coherent transfer total population d=0.0,t=13.5	0	1.00×10^{-13}	pass
R	Coherent transfer formula d=0.0,t=14.25	4.996×10^{-16}	1.00×10^{-13}	pass
R	Coherent transfer total population d=0.0,t=14.25	0	1.00×10^{-13}	pass
R	Coherent transfer formula d=0.0,t=15	2.776×10^{-17}	1.00×10^{-13}	pass
R	Coherent transfer total population d=0.0,t=15	6.661×10^{-16}	1.00×10^{-13}	pass
R	Coherent transfer formula d=0.3,t=0	0	1.00×10^{-13}	pass
R	Coherent transfer total population d=0.3,t=0	0	1.00×10^{-13}	pass
R	Coherent transfer formula d=0.3,t=0.75	1.388×10^{-17}	1.00×10^{-13}	pass
R	Coherent transfer total population d=0.3,t=0.75	0	1.00×10^{-13}	pass
R	Coherent transfer formula d=0.3,t=1.5	5.551×10^{-17}	1.00×10^{-13}	pass
R	Coherent transfer total population d=0.3,t=1.5	0	1.00×10^{-13}	pass
R	Coherent transfer formula d=0.3,t=2.25	0	1.00×10^{-13}	pass
R	Coherent transfer total population d=0.3,t=2.25	0	1.00×10^{-13}	pass
R	Coherent transfer formula d=0.3,t=3	6.661×10^{-16}	1.00×10^{-13}	pass
R	Coherent transfer total population d=0.3,t=3	2.220×10^{-16}	1.00×10^{-13}	pass
R	Coherent transfer formula d=0.3,t=3.75	1.110×10^{-16}	1.00×10^{-13}	pass
R	Coherent transfer total population d=0.3,t=3.75	1.110×10^{-16}	1.00×10^{-13}	pass
R	Coherent transfer formula d=0.3,t=4.5	3.331×10^{-16}	1.00×10^{-13}	pass
R	Coherent transfer total population d=0.3,t=4.5	2.220×10^{-16}	1.00×10^{-13}	pass
R	Coherent transfer formula d=0.3,t=5.25	1.110×10^{-16}	1.00×10^{-13}	pass
R	Coherent transfer total population d=0.3,t=5.25	2.220×10^{-16}	1.00×10^{-13}	pass
R	Coherent transfer formula d=0.3,t=6	1.110×10^{-16}	1.00×10^{-13}	pass
R	Coherent transfer total population d=0.3,t=6	0	1.00×10^{-13}	pass
R	Coherent transfer formula d=0.3,t=6.75	6.245×10^{-17}	1.00×10^{-13}	pass

Suite	Check	Error / value	Tolerance	Status
R	Coherent transfer total population d=0.3,t=6.75	0	1.00×10^{-13}	pass
R	Coherent transfer formula d=0.3,t=7.5	4.901×10^{-17}	1.00×10^{-13}	pass
R	Coherent transfer total population d=0.3,t=7.5	4.441×10^{-16}	1.00×10^{-13}	pass
R	Coherent transfer formula d=0.3,t=8.25	1.527×10^{-16}	1.00×10^{-13}	pass
R	Coherent transfer total population d=0.3,t=8.25	6.661×10^{-16}	1.00×10^{-13}	pass
R	Coherent transfer formula d=0.3,t=9	4.441×10^{-16}	1.00×10^{-13}	pass
R	Coherent transfer total population d=0.3,t=9	4.441×10^{-16}	1.00×10^{-13}	pass
R	Coherent transfer formula d=0.3,t=9.75	1.110×10^{-16}	1.00×10^{-13}	pass
R	Coherent transfer total population d=0.3,t=9.75	2.220×10^{-16}	1.00×10^{-13}	pass
R	Coherent transfer formula d=0.3,t=10.5	1.110×10^{-16}	1.00×10^{-13}	pass
R	Coherent transfer total population d=0.3,t=10.5	1.110×10^{-16}	1.00×10^{-13}	pass
R	Coherent transfer formula d=0.3,t=11.25	6.661×10^{-16}	1.00×10^{-13}	pass
R	Coherent transfer total population d=0.3,t=11.25	9.992×10^{-16}	1.00×10^{-13}	pass
R	Coherent transfer formula d=0.3,t=12	3.331×10^{-16}	1.00×10^{-13}	pass
R	Coherent transfer total population d=0.3,t=12	0	1.00×10^{-13}	pass
R	Coherent transfer formula d=0.3,t=12.75	1.166×10^{-15}	1.00×10^{-13}	pass
R	Coherent transfer total population d=0.3,t=12.75	8.882×10^{-16}	1.00×10^{-13}	pass
R	Coherent transfer formula d=0.3,t=13.5	1.665×10^{-16}	1.00×10^{-13}	pass
R	Coherent transfer total population d=0.3,t=13.5	2.220×10^{-16}	1.00×10^{-13}	pass
R	Coherent transfer formula d=0.3,t=14.25	1.527×10^{-16}	1.00×10^{-13}	pass
R	Coherent transfer total population d=0.3,t=14.25	3.331×10^{-16}	1.00×10^{-13}	pass
R	Coherent transfer formula d=0.3,t=15	1.978×10^{-16}	1.00×10^{-13}	pass
R	Coherent transfer total population d=0.3,t=15	8.882×10^{-16}	1.00×10^{-13}	pass
R	Coherent transfer formula d=1.0,t=0	0	1.00×10^{-13}	pass
R	Coherent transfer total population d=1.0,t=0	0	1.00×10^{-13}	pass
R	Coherent transfer formula d=1.0,t=0.75	4.163×10^{-17}	1.00×10^{-13}	pass
R	Coherent transfer total population d=1.0,t=0.75	0	1.00×10^{-13}	pass

Suite	Check	Error / value	Tolerance	Status
R	Coherent transfer formula d=1.0,t=1.5	5.551×10^{-17}	1.00×10^{-13}	pass
R	Coherent transfer total population d=1.0,t=1.5	2.220×10^{-16}	1.00×10^{-13}	pass
R	Coherent transfer formula d=1.0,t=2.25	0	1.00×10^{-13}	pass
R	Coherent transfer total population d=1.0,t=2.25	1.110×10^{-16}	1.00×10^{-13}	pass
R	Coherent transfer formula d=1.0,t=3	0	1.00×10^{-13}	pass
R	Coherent transfer total population d=1.0,t=3	0	1.00×10^{-13}	pass
R	Coherent transfer formula d=1.0,t=3.75	2.776×10^{-17}	1.00×10^{-13}	pass
R	Coherent transfer total population d=1.0,t=3.75	2.220×10^{-16}	1.00×10^{-13}	pass
R	Coherent transfer formula d=1.0,t=4.5	2.082×10^{-17}	1.00×10^{-13}	pass
R	Coherent transfer total population d=1.0,t=4.5	2.220×10^{-16}	1.00×10^{-13}	pass
R	Coherent transfer formula d=1.0,t=5.25	2.429×10^{-17}	1.00×10^{-13}	pass
R	Coherent transfer total population d=1.0,t=5.25	5.551×10^{-16}	1.00×10^{-13}	pass
R	Coherent transfer formula d=1.0,t=6	2.776×10^{-17}	1.00×10^{-13}	pass
R	Coherent transfer total population d=1.0,t=6	0	1.00×10^{-13}	pass
R	Coherent transfer formula d=1.0,t=6.75	2.776×10^{-16}	1.00×10^{-13}	pass
R	Coherent transfer total population d=1.0,t=6.75	8.882×10^{-16}	1.00×10^{-13}	pass
R	Coherent transfer formula d=1.0,t=7.5	5.551×10^{-17}	1.00×10^{-13}	pass
R	Coherent transfer total population d=1.0,t=7.5	2.220×10^{-16}	1.00×10^{-13}	pass
R	Coherent transfer formula d=1.0,t=8.25	1.665×10^{-16}	1.00×10^{-13}	pass
R	Coherent transfer total population d=1.0,t=8.25	1.110×10^{-16}	1.00×10^{-13}	pass
R	Coherent transfer formula d=1.0,t=9	1.249×10^{-16}	1.00×10^{-13}	pass
R	Coherent transfer total population d=1.0,t=9	2.220×10^{-16}	1.00×10^{-13}	pass
R	Coherent transfer formula d=1.0,t=9.75	3.003×10^{-17}	1.00×10^{-13}	pass
R	Coherent transfer total population d=1.0,t=9.75	2.220×10^{-16}	1.00×10^{-13}	pass
R	Coherent transfer formula d=1.0,t=10.5	8.327×10^{-17}	1.00×10^{-13}	pass
R	Coherent transfer total population d=1.0,t=10.5	7.772×10^{-16}	1.00×10^{-13}	pass
R	Coherent transfer formula d=1.0,t=11.25	4.441×10^{-16}	1.00×10^{-13}	pass

Suite	Check	Error / value	Tolerance	Status
R	Coherent transfer total population d=1.0,t=11.25	3.331×10^{-16}	1.00×10^{-13}	pass
R	Coherent transfer formula d=1.0,t=12	0	1.00×10^{-13}	pass
R	Coherent transfer total population d=1.0,t=12	2.220×10^{-16}	1.00×10^{-13}	pass
R	Coherent transfer formula d=1.0,t=12.75	3.331×10^{-16}	1.00×10^{-13}	pass
R	Coherent transfer total population d=1.0,t=12.75	4.441×10^{-16}	1.00×10^{-13}	pass
R	Coherent transfer formula d=1.0,t=13.5	5.551×10^{-17}	1.00×10^{-13}	pass
R	Coherent transfer total population d=1.0,t=13.5	1.776×10^{-15}	1.00×10^{-13}	pass
R	Coherent transfer formula d=1.0,t=14.25	1.180×10^{-16}	1.00×10^{-13}	pass
R	Coherent transfer total population d=1.0,t=14.25	2.220×10^{-16}	1.00×10^{-13}	pass
R	Coherent transfer formula d=1.0,t=15	5.378×10^{-17}	1.00×10^{-13}	pass
R	Coherent transfer total population d=1.0,t=15	4.441×10^{-16}	1.00×10^{-13}	pass
R	Global phase has no conversion a=0.0,t=0.1	0	1.00×10^{-13}	pass
R	Global phase has no conversion a=0.0,t=1.0	0	1.00×10^{-13}	pass
R	Global phase has no conversion a=0.0,t=8.0	0	1.00×10^{-13}	pass
R	Global phase has no conversion a=0.1,t=0.1	2.220×10^{-16}	1.00×10^{-13}	pass
R	Global phase has no conversion a=0.1,t=1.0	2.220×10^{-16}	1.00×10^{-13}	pass
R	Global phase has no conversion a=0.1,t=8.0	1.665×10^{-16}	1.00×10^{-13}	pass
R	Global phase has no conversion a=2.5,t=0.1	2.220×10^{-16}	1.00×10^{-13}	pass
R	Global phase has no conversion a=2.5,t=1.0	4.441×10^{-16}	1.00×10^{-13}	pass
R	Global phase has no conversion a=2.5,t=8.0	1.776×10^{-15}	1.00×10^{-13}	pass
R	Global phase has no conversion a=-0.7,t=0.1	2.220×10^{-16}	1.00×10^{-13}	pass
R	Global phase has no conversion a=-0.7,t=1.0	2.220×10^{-16}	1.00×10^{-13}	pass
R	Global phase has no conversion a=-0.7,t=8.0	6.661×10^{-16}	1.00×10^{-13}	pass
R	first derivative	0	0	pass
R	second derivative	0	0	pass
R	density derivative	0	0	pass
R	Bohr orbital phase is minus pi	0	0	pass
R	Kernel radial integral	0	0	pass
R	Maxwell vacuum speed	0	1.00×10^{-50}	pass
R	alpha via permittivity	1.556×10^{-61}	1.00×10^{-50}	pass
R	Planck definitions	0	1.00×10^{-50}	pass

Suite	Check	Error / value	Tolerance	Status
R	Rydberg and Hartree	0	1.00×10^{-50}	pass
R	Bohr radius and Compton	0	1.00×10^{-50}	pass
T	Readout with reciprocal feedback conserves total energy	7.178×10^{-12}	1.00×10^{-9}	pass
T	Readout phase momentum conservation	9.784×10^{-16}	1.00×10^{-11}	pass
T	Coherence gradient 0	4.366×10^{-11}	2.00×10^{-9}	pass
T	Coherence bounds 0	0	1.00×10^{-12}	pass
T	Coherence gradient 213	7.290×10^{-11}	2.00×10^{-9}	pass
T	Coherence bounds 213	0	1.00×10^{-12}	pass
T	Coherence gradient 725	1.156×10^{-10}	2.00×10^{-9}	pass
T	Coherence bounds 725	0	1.00×10^{-12}	pass
T	Coherence gradient 1400	1.770×10^{-10}	2.00×10^{-9}	pass
T	Coherence bounds 1400	0	1.00×10^{-12}	pass
T	Saddle-node stationarity	0	1.00×10^{-15}	pass
T	Saddle-node zero curvature	2.220×10^{-16}	1.00×10^{-15}	pass
T	Root count u=0.0	0	0	pass
T	Root count u=0.2	0	0	pass
T	Root count u=0.38	0	0	pass
T	Root count u=0.4	0	0	pass
T	Root count u=0.55	0	0	pass
T	Frequency FDT lambda=0.1,omega=0.05	0	1.00×10^{-11}	pass
T	Passivity lambda=0.1,omega=0.05	0	1.00×10^{-13}	pass
T	Frequency FDT lambda=0.1,omega=0.2	4.441×10^{-16}	1.00×10^{-11}	pass
T	Passivity lambda=0.1,omega=0.2	0	1.00×10^{-13}	pass
T	Frequency FDT lambda=0.1,omega=0.7	6.939×10^{-18}	1.00×10^{-11}	pass
T	Passivity lambda=0.1,omega=0.7	0	1.00×10^{-13}	pass
T	Frequency FDT lambda=0.1,omega=1.4	2.168×10^{-19}	1.00×10^{-11}	pass
T	Passivity lambda=0.1,omega=1.4	0	1.00×10^{-13}	pass
T	Frequency FDT lambda=0.1,omega=3.0	6.776×10^{-21}	1.00×10^{-11}	pass
T	Passivity lambda=0.1,omega=3.0	0	1.00×10^{-13}	pass
T	Frequency FDT lambda=0.5,omega=0.05	2.776×10^{-17}	1.00×10^{-11}	pass
T	Passivity lambda=0.5,omega=0.05	0	1.00×10^{-13}	pass
T	Frequency FDT lambda=0.5,omega=0.2	8.327×10^{-17}	1.00×10^{-11}	pass
T	Passivity lambda=0.5,omega=0.2	0	1.00×10^{-13}	pass
T	Frequency FDT lambda=0.5,omega=0.7	3.553×10^{-15}	1.00×10^{-11}	pass
T	Passivity lambda=0.5,omega=0.7	0	1.00×10^{-13}	pass
T	Frequency FDT lambda=0.5,omega=1.4	1.735×10^{-18}	1.00×10^{-11}	pass
T	Passivity lambda=0.5,omega=1.4	0	1.00×10^{-13}	pass
T	Frequency FDT lambda=0.5,omega=3.0	2.711×10^{-20}	1.00×10^{-11}	pass

Suite	Check	Error / value	Tolerance	Status
T	Passivity lambda=0.5,omega=3.0	0	1.00×10^{-13}	pass
T	Frequency FDT lambda=1.0,omega=0.05	2.776×10^{-17}	1.00×10^{-11}	pass
T	Passivity lambda=1.0,omega=0.05	0	1.00×10^{-13}	pass
T	Frequency FDT lambda=1.0,omega=0.2	1.388×10^{-17}	1.00×10^{-11}	pass
T	Passivity lambda=1.0,omega=0.2	0	1.00×10^{-13}	pass
T	Frequency FDT lambda=1.0,omega=0.7	0	1.00×10^{-11}	pass
T	Passivity lambda=1.0,omega=0.7	0	1.00×10^{-13}	pass
T	Frequency FDT lambda=1.0,omega=1.4	1.388×10^{-17}	1.00×10^{-11}	pass
T	Passivity lambda=1.0,omega=1.4	0	1.00×10^{-13}	pass
T	Frequency FDT lambda=1.0,omega=3.0	5.421×10^{-20}	1.00×10^{-11}	pass
T	Passivity lambda=1.0,omega=3.0	0	1.00×10^{-13}	pass
T	Frequency FDT lambda=2.0,omega=0.05	1.388×10^{-17}	1.00×10^{-11}	pass
T	Passivity lambda=2.0,omega=0.05	0	1.00×10^{-13}	pass
T	Frequency FDT lambda=2.0,omega=0.2	6.939×10^{-18}	1.00×10^{-11}	pass
T	Passivity lambda=2.0,omega=0.2	0	1.00×10^{-13}	pass
T	Frequency FDT lambda=2.0,omega=0.7	1.388×10^{-17}	1.00×10^{-11}	pass
T	Passivity lambda=2.0,omega=0.7	0	1.00×10^{-13}	pass
T	Frequency FDT lambda=2.0,omega=1.4	2.220×10^{-16}	1.00×10^{-11}	pass
T	Passivity lambda=2.0,omega=1.4	0	1.00×10^{-13}	pass
T	Frequency FDT lambda=2.0,omega=3.0	1.084×10^{-19}	1.00×10^{-11}	pass
T	Passivity lambda=2.0,omega=3.0	0	1.00×10^{-13}	pass
T	Frequency FDT lambda=3.0,omega=0.05	0	1.00×10^{-11}	pass
T	Passivity lambda=3.0,omega=0.05	0	1.00×10^{-13}	pass
T	Frequency FDT lambda=3.0,omega=0.2	6.939×10^{-18}	1.00×10^{-11}	pass
T	Passivity lambda=3.0,omega=0.2	0	1.00×10^{-13}	pass
T	Frequency FDT lambda=3.0,omega=0.7	6.939×10^{-18}	1.00×10^{-11}	pass
T	Passivity lambda=3.0,omega=0.7	0	1.00×10^{-13}	pass
T	Frequency FDT lambda=3.0,omega=1.4	0	1.00×10^{-11}	pass
T	Passivity lambda=3.0,omega=1.4	0	1.00×10^{-13}	pass
T	Frequency FDT lambda=3.0,omega=3.0	0	1.00×10^{-11}	pass
T	Passivity lambda=3.0,omega=3.0	0	1.00×10^{-13}	pass
T	Exponential-memory stability lambda=0.05	0	1.00×10^{-12}	pass
T	Exponential-memory stability lambda=0.3	0	1.00×10^{-12}	pass
T	Exponential-memory stability lambda=1.0	0	1.00×10^{-12}	pass
T	Exponential-memory stability lambda=2.0	0	1.00×10^{-12}	pass
T	Exponential-memory stability lambda=4.0	0	1.00×10^{-12}	pass
T	Universal scaling obeys Rydberg dependency	0	0	pass

Suite	Check	Error / value	Tolerance	Status
T	Clock generator identity q=0.3,t=0.2	0	1.00×10^{-14}	pass
T	Clock generator identity q=0.3,t=1.0	0	1.00×10^{-14}	pass
T	Clock generator identity q=0.3,t=4.0	0	1.00×10^{-14}	pass
T	Clock generator identity q=1.0,t=0.2	0	1.00×10^{-14}	pass
T	Clock generator identity q=1.0,t=1.0	0	1.00×10^{-14}	pass
T	Clock generator identity q=1.0,t=4.0	0	1.00×10^{-14}	pass
T	Clock generator identity q=2.0,t=0.2	0	1.00×10^{-14}	pass
T	Clock generator identity q=2.0,t=1.0	0	1.00×10^{-14}	pass
T	Clock generator identity q=2.0,t=4.0	0	1.00×10^{-14}	pass
S	Mode mass orthonormality lambda=1e-05	8.882×10^{-16}	2.00×10^{-13}	pass
S	Mode eigen-equation lambda=1e-05	2.665×10^{-15}	2.00×10^{-13}	pass
S	Nonnegative spectrum lambda=1e-05	0	2.00×10^{-14}	pass
S	Schur dispersion lambda=1e-05,branch=0	1.130×10^{-21}	2.00×10^{-6}	pass
S	Schur dispersion lambda=1e-05,branch=1	1.152×10^{-10}	2.00×10^{-6}	pass
S	Schur dispersion lambda=1e-05,branch=2	7.615×10^{-9}	2.00×10^{-6}	pass
S	Schur dispersion lambda=1e-05,branch=3	2.595×10^{-7}	2.00×10^{-6}	pass
S	Mode mass orthonormality lambda=0.0001	4.441×10^{-16}	2.00×10^{-13}	pass
S	Mode eigen-equation lambda=0.0001	1.776×10^{-15}	2.00×10^{-13}	pass
S	Nonnegative spectrum lambda=0.0001	0	2.00×10^{-14}	pass
S	Schur dispersion lambda=0.0001,branch=0	1.616×10^{-20}	2.00×10^{-6}	pass
S	Schur dispersion lambda=0.0001,branch=1	1.678×10^{-12}	2.00×10^{-6}	pass
S	Schur dispersion lambda=0.0001,branch=2	2.129×10^{-10}	2.00×10^{-6}	pass
S	Schur dispersion lambda=0.0001,branch=3	2.132×10^{-8}	2.00×10^{-6}	pass
S	Mode mass orthonormality lambda=0.001	4.441×10^{-16}	2.00×10^{-13}	pass
S	Mode eigen-equation lambda=0.001	9.516×10^{-16}	2.00×10^{-13}	pass
S	Nonnegative spectrum lambda=0.001	0	2.00×10^{-14}	pass
S	Schur dispersion lambda=0.001,branch=0	5.336×10^{-21}	2.00×10^{-6}	pass
S	Schur dispersion lambda=0.001,branch=1	8.011×10^{-13}	2.00×10^{-6}	pass
S	Schur dispersion lambda=0.001,branch=2	5.686×10^{-12}	2.00×10^{-6}	pass
S	Schur dispersion lambda=0.001,branch=3	3.247×10^{-10}	2.00×10^{-6}	pass
S	Mode mass orthonormality lambda=0.01	6.661×10^{-16}	2.00×10^{-13}	pass
S	Mode eigen-equation lambda=0.01	2.442×10^{-15}	2.00×10^{-13}	pass
S	Nonnegative spectrum lambda=0.01	0	2.00×10^{-14}	pass
S	Schur dispersion lambda=0.01,branch=0	8.504×10^{-19}	2.00×10^{-6}	pass
S	Schur dispersion lambda=0.01,branch=1	1.919×10^{-13}	2.00×10^{-6}	pass
S	Schur dispersion lambda=0.01,branch=2	1.080×10^{-11}	2.00×10^{-6}	pass
S	Schur dispersion lambda=0.01,branch=3	1.321×10^{-10}	2.00×10^{-6}	pass
S	Mode mass orthonormality lambda=0.1	6.661×10^{-16}	2.00×10^{-13}	pass

Suite	Check	Error / value	Tolerance	Status
S	Mode eigen-equation lambda=0.1	2.665×10^{-15}	2.00×10^{-13}	pass
S	Nonnegative spectrum lambda=0.1	0	2.00×10^{-14}	pass
S	Schur dispersion lambda=0.1,branch=0	2.537×10^{-18}	2.00×10^{-6}	pass
S	Schur dispersion lambda=0.1,branch=1	5.561×10^{-15}	2.00×10^{-6}	pass
S	Schur dispersion lambda=0.1,branch=2	4.389×10^{-13}	2.00×10^{-6}	pass
S	Schur dispersion lambda=0.1,branch=3	1.858×10^{-11}	2.00×10^{-6}	pass
S	Mode mass orthonormality lambda=1.0	8.882×10^{-16}	2.00×10^{-13}	pass
S	Mode eigen-equation lambda=1.0	1.776×10^{-15}	2.00×10^{-13}	pass
S	Nonnegative spectrum lambda=1.0	0	2.00×10^{-14}	pass
S	Schur dispersion lambda=1.0,branch=0	1.271×10^{-15}	2.00×10^{-6}	pass
S	Schur dispersion lambda=1.0,branch=1	6.236×10^{-17}	2.00×10^{-6}	pass
S	Schur dispersion lambda=1.0,branch=2	4.083×10^{-16}	2.00×10^{-6}	pass
S	Schur dispersion lambda=1.0,branch=3	1.046×10^{-12}	2.00×10^{-6}	pass
S	Mode mass orthonormality lambda=3.0	5.755×10^{-16}	2.00×10^{-13}	pass
S	Mode eigen-equation lambda=3.0	2.665×10^{-15}	2.00×10^{-13}	pass
S	Nonnegative spectrum lambda=3.0	0	2.00×10^{-14}	pass
S	Schur dispersion lambda=3.0,branch=0	3.656×10^{-15}	2.00×10^{-6}	pass
S	Schur dispersion lambda=3.0,branch=1	3.226×10^{-15}	2.00×10^{-6}	pass
S	Schur dispersion lambda=3.0,branch=2	2.980×10^{-17}	2.00×10^{-6}	pass
S	Schur dispersion lambda=3.0,branch=3	9.167×10^{-14}	2.00×10^{-6}	pass
S	Mode mass orthonormality lambda=4.0	2.220×10^{-16}	2.00×10^{-13}	pass
S	Mode eigen-equation lambda=4.0	1.120×10^{-15}	2.00×10^{-13}	pass
S	Nonnegative spectrum lambda=4.0	0	2.00×10^{-14}	pass
S	Schur dispersion lambda=4.0,branch=0	1.405×10^{-15}	2.00×10^{-6}	pass
S	Schur dispersion lambda=4.0,branch=1	0	2.00×10^{-6}	pass
S	Schur dispersion lambda=4.0,branch=2	5.804×10^{-17}	2.00×10^{-6}	pass
S	Schur dispersion lambda=4.0,branch=3	1.142×10^{-14}	2.00×10^{-6}	pass
S	Coupled acoustic expansion axis,ka=0.02	1.108×10^{-4}	4.00×10^{-4}	pass
S	Coupled acoustic expansion axis,ka=0.01	2.769×10^{-5}	1.00×10^{-4}	pass
S	Coupled acoustic expansion axis,ka=0.005	6.922×10^{-6}	2.50×10^{-5}	pass
S	Coupled acoustic expansion face,ka=0.02	1.145×10^{-4}	4.00×10^{-4}	pass
S	Coupled acoustic expansion face,ka=0.01	2.861×10^{-5}	1.00×10^{-4}	pass
S	Coupled acoustic expansion face,ka=0.005	7.151×10^{-6}	2.50×10^{-5}	pass
S	Coupled acoustic expansion body,ka=0.02	1.157×10^{-4}	4.00×10^{-4}	pass
S	Coupled acoustic expansion body,ka=0.01	2.891×10^{-5}	1.00×10^{-4}	pass
S	Coupled acoustic expansion body,ka=0.005	7.226×10^{-6}	2.50×10^{-5}	pass
S	Full ring spectrum from graph-mode decomposition	4.441×10^{-15}	3.00×10^{-13}	pass

Suite	Check	Error / value	Tolerance	Status
S	Full ring nonnegative Hessian	0	3.00×10^{-13}	pass

F. Executable conservative reconstruction

```
#!/usr/bin/env python3
"""Target-free mathematical tests of the conservative MNT/EQEF reconstruction.

This does not fit a physical EQEF parameter. Model units, initial conditions, and
all numerical checks are declared here. Reference calculations use explicit inputs.
"""
from __future__ import annotations
import csv, json, math, platform, hashlib, sys
from pathlib import Path
from datetime import datetime, timezone
import numpy as np
import scipy
from scipy.integrate import solve_ivp, quad
from scipy.linalg import expm
from scipy.special import ellipk
from scipy.optimize import brentq
import sympy as sp
import mpmath as mp
import matplotlib
matplotlib.use('Agg')
import matplotlib.pyplot as plt
ROOT=Path(__file__).resolve().parents[1]
OUT=ROOT/'results'; FIG=ROOT/'figures';OUT.mkdir(exist_ok=True);FIG.mkdir(exist_ok=True)
checks=[]
def check(name, value, limit, category='implementation'):
    value=float(value);limit=float(limit)
    checks.append({'name':name,'value':value,'limit':limit,'passed':bool(np.isfinite(value) and value<=limit),'category':category})
def save_csv(name,rows):
    if not rows:raise ValueError(name)
    with (OUT/name).open('w',newline='') as f:
        w=csv.DictWriter(f,fieldnames=list(rows[0]));w.writeheader();w.writerows(rows)
def figsave(name):
    plt.tight_layout();plt.savefig(FIG/(name+'.pdf'));plt.savefig(FIG/(name+'.png'),dpi=140);plt.close()
# --- An explicit compact-phase Hamiltonian with conservative link reservoirs ---

n=6; modes=3; I=1.0; K=1.0
B=np.zeros((n,n))
for e in range(n): B[e,e]=1.;B[(e+1)%n,e]=-1.
omega=np.array([.65,1.15,2.4]);mass=np.ones(modes);coupling=np.array
```

```
    ([.22,.13,.07])
shift=coupling/(mass*omega**2)
def unpack(y):
    return y[:n],y[n:2*n],y[2*n:2*n+n*modes].reshape(n,modes),y[2*n+n*modes:].
    reshape(n,modes)
def pieces(y):
    th,p,x,P=unpack(y);d=B.T@th;u=x-np.sin(d)[:,None]*shift
    HA=float(np.sum(p*p)/(2*I)+K*np.sum(1-np.cos(d)))
    HR=float(np.sum(P*P/(2*mass))+np.sum(.5*mass*omega**2*u*u))
    return HA,HR

def rhs(t,y):
    th,p,x,P=unpack(y);d=B.T@th;u=x-np.sin(d)[:,None]*shift
    f=-K*np.sin(d)+np.cos(d)*np.sum(coupling*u,axis=1)
    return np.r_[p/I,B@f,(P/mass).ravel(),(-mass*omega**2*u).ravel()]
angles=np.arange(n)*2*np.pi/n
th=.35*np.sin(angles);p=.08*np.cos(angles)+.015
x=np.sin(B.T@th)[:,None]*shift + .03*np.cos(angles)[:,None]*np.array
    ([1.,.5,-.4])
P=.02*np.sin(angles)[:,None]*np.array([1.,-1.,.3])
y0=np.r_[th,p,x.ravel(),P.ravel()];T=60.
sol=solve_ivp(rhs,[0,T],y0,method='DOP853',rtol=2e-12,atol=2e-14,dense_output=
    True)
if not sol.success:raise RuntimeError(sol.message)
tau=np.linspace(0,T,1201);Y=sol.sol(tau);eng=np.array([pieces(y) for y in Y.T]);
    H0=sum(pieces(y0))
conservation=float(np.max(np.abs(eng.sum(axis=1)-H0))/H0)
check('Hamiltonian conservation, nonlinear ring',conservation,1e-9)
check('Global phase momentum conservation',np.max(np.abs(np.sum(Y[n:2*n],axis=0)-
    np.sum(p))),1e-10)
check('Positive stored sector energy',max(0.,-float(eng.min())),1e-13)
shifted=y0.copy();shifted[:n]+=.938
check('Global phase covariance of force',np.max(np.abs(rhs(0,shifted)-rhs(0,y0))
    ),2e-14)
shifted=y0.copy();shifted[0]+=2*np.pi
check('Compact phase periodicity of energy',abs(sum(pieces(shifted))-H0),1e-14)
# Hamiltonian vector-field finite differences at three deterministic states.
for j in [0,211,937]:
 y=Y[:,j];f=rhs(0,y);th,p,x,P=unpack(y);gr=[]
 for k in range(len(y)):
  h=2e-6;z=y.copy();z[k]+=h;v1=sum(pieces(z));z[k]-=2*h;v0=sum(pieces(z));gr.
    append((v1-v0)/(2*h))
 gr=np.asarray(gr);qidx=np.r_[np.arange(n),np.arange(2*n,2*n+n*modes)];pidx=np.
    r_[np.arange(n,2*n),np.arange(2*n+n*modes,len(y))]
 check(f'Hamiltonian gradient, state {j}',max(np.max(np.abs(f[qidx]-gr[pidx])),
    np.max(np.abs(f[pidx]+gr[qidx]))),2e-9)
 check(f'Instantaneous total energy balance, state {j}',abs(gr@f),2e-10)
# Reversibility for an autonomous closed model.
reverse=Y[:,-1].copy();reverse[n:2*n]*=-1;reverse[2*n+n*modes:]*=-1
back=solve_ivp(rhs,[0,T],reverse,method='DOP853',rtol=2e-12,atol=2e-14)
expect=y0.copy();expect[n:2*n]*=-1;expect[2*n+n*modes:]*=-1
reverse_error=np.max(np.abs(back.y[:,-1]-expect));check('Time reversal',
    reverse_error,2e-8)
```

```
# Clock covariance: q(t)>0, tau(t) known analytically. T=60 in coordinate units.
q=lambda t:.8+.12*np.cos(.7*t)
taumap=lambda t:.8*t+.12/.7*np.sin(.7*t)
clock=solve_ivp(lambda t,y:q(t)*rhs(t,y),[0,T],y0,method='DOP853',rtol=2e-12,
    atol=2e-14,dense_output=True)
ct=np.linspace(0,T,1001);clockerr=np.max(np.abs(clock.sol(ct)-sol.sol(taumap(ct)
    )))
check('Reference-time versus proper-time trajectory',clockerr,2e-9)
# Exact generalized Langevin memory identity (bath eliminated analytically).
phase0=B.T@y0[:n];th0,p0,x0,P0=unpack(y0)
def mem(t):return np.sum(coupling**2/(mass*omega**2)*np.cos(omega*t))
memrows=[]
for t in [.2,1.,4.,9.,19.,37.,59.]:
 th,p,x,P=unpack(sol.sol(t));d=B.T@th
 for e in range(n):
  zeta=float(np.sum(coupling*((x0[e]-shift*np.sin(phase0[e]))*np.cos(omega*t)+P0
    [e]/(mass*omega)*np.sin(omega*t))))
  def integrand(s):
   aa,bb,xx,pp=unpack(sol.sol(s));ds=B.T@aa;dsv=B.T@(bb/I)
   return mem(t-s)*np.cos(ds[e])*dsv[e]
  conv=quad(integrand,0,t,epsabs=2e-10,epsrel=2e-10,limit=200)[0]
  direct=float(np.sum(coupling*(x[e]-shift*np.sin(d[e]))))
  diff=abs(zeta-conv-direct);check(f'Exact memory elimination t={t:g}, link={e}',
    diff,2e-8,'analytic identity')
  memrows.append({'proper_time':t,'link':e,'direct_reservoir_force':direct,'
    memory_noise_force':zeta-conv,'absolute_error':diff})
# Equilibrium thermal bath FDT covariance, exact expectation with Gaussian
    independent coordinates.
kbT=.4
for a in [0.,.3,2.,6.]:
 for b in [0.,.7,3.]:
  covariance=np.sum(coupling**2*kbT/(mass*omega**2)*(np.cos(omega*a)*np.cos(
    omega*b)+np.sin(omega*a)*np.sin(omega*b)))
  check(f'FDT covariance {a:g},{b:g}',abs(covariance-kbT*mem(a-b)),1e-14,'
    analytic identity')
save_csv('conservative_ring.csv',[{'proper_time':t,'expressed_energy':a,'
    reservoir_including_interaction_energy':b,'total_energy':a+b,'
    relative_total_error':(a+b-H0)/H0} for t,(a,b) in zip(tau,eng)])
save_csv('memory_identity.csv',memrows)
plt.figure(figsize=(6.6,3.8));plt.plot(tau,eng[:,0],label='Phase sector');plt.
    plot(tau,eng[:,1],label='Reserve + interaction');plt.plot(tau,eng.sum(axis=1)
    ,'--',label='Conserved total');plt.xlabel('Proper time (model units)');plt.
    ylabel('Energy (model units)');plt.legend();figsave('conservative_exchange')
# --- Exact band structure and passive nearest-neighbor damping ---
band=[];zeta=.12
for direction,v in [('axis',np.array([1.,0.,0.])),('face diagonal',np.array
    ([1.,1.,0.])/np.sqrt(2)),('body diagonal',np.ones(3)/np.sqrt(3))]:
 for ka in [.01,.03,.1,.3,.7,1.0]:
  lam=4*np.sum(np.sin(ka*v/2)**2);w0=np.sqrt(lam);gam=zeta*lam/2;wd=np.sqrt(lam-
    gam*gam)
  expected=(1-np.sum(v**4)*ka**2/24)
  check(f'Quartic phase-speed expansion {direction}, ka={ka}',abs(w0/ka-expected
    ),max(1e-13,ka**4/1500),'asymptotic')
```

```
  roots=np.roots([1.,zeta*lam,lam]);check(f'Passive poles {direction}, ka={ka}',max(0.,np.max(roots.real)),1e-14)
  check(f'Pole identity {direction}, ka={ka}',abs(wd*wd+gam*gam-lam),2e-15,'analytic identity')
  band.append({'direction':direction,'ka':ka,'laplacian_eigenvalue':lam,'omega0':w0,'phase_speed_over_cstar':w0/ka,'attenuation_rate':gam,'damped_frequency':wd})
save_csv('dispersion_predictions.csv',band)
plt.figure(figsize=(6.6,3.8));ks=np.linspace(.001,2.5,500)
for label,v in [('Axis',np.array([1.,0.,0.])),('Face diagonal',np.array([1.,1.,0.])/np.sqrt(2)),('Body diagonal',np.ones(3)/np.sqrt(3))]:
 vv=np.sqrt(4*np.sum(np.sin(ks[:,None]*v/2)**2,axis=1))/ks;plt.plot(ks,vv,label=label)
plt.xlabel(r'$|k|a$');plt.ylabel(r'$\omega/(c_*|k|)$');plt.legend();figsave('lattice_prediction')
# Finite ring graph eigenvalues independently agree with incidence representation.
for m in [4,7,12]:
 L=2*np.eye(m)-np.roll(np.eye(m),1,axis=0)-np.roll(np.eye(m),-1,axis=0)
 check(f'Graph spectrum {m} sites',np.max(np.abs(np.linalg.eigvalsh(L)-np.sort(4*np.sin(np.pi*np.arange(m)/m)**2))),1e-13)
# --- Nonlinear conservative recurrence, not a fitted particle mass ---
periods=[]
for A in [.1,.5,1.,np.pi/2,2.5]:
 exact=4/np.sqrt(2)*ellipk(np.sin(A/2)**2)
 def event(t,y):return y[0]
 event.direction=-1
 ss=solve_ivp(lambda t,y:[y[1],-2*np.sin(y[0])],[0,exact],[A,0.],rtol=1e-12,atol=1e-14,events=event,method='DOP853')
 numeric=4*ss.t_events[0][0];err=abs(numeric-exact)/exact
 check(f'Nonlinear pendulum period A={A}',err,1e-10,'model prediction')
 periods.append({'phase_amplitude':A,'period_exact':exact,'period_numeric':numeric,'period_over_small_amplitude':exact/(2*np.pi/np.sqrt(2))})
save_csv('nonlinear_period_prediction.csv',periods)
# --- Coherent conversion: a Hermitian two-mode example, not a Born-rule derivation ---
coherent=[]
for det in [0.,.3,1.]:
 g=.4;H=np.array([[det/2,g],[g,-det/2]],complex);Om=np.sqrt(g*g+(det/2)**2)
 for t in np.linspace(0,15,21):
  u=expm(-1j*H*t);psi=u@np.array([1.,0.]);pa=abs(psi[1])**2;exact=(g/Om)**2*np.sin(Om*t)**2
  check(f'Coherent transfer formula d={det},t={t:g}',abs(pa-exact),1e-13,'analytic identity')
  check(f'Coherent transfer total population d={det},t={t:g}',abs(np.vdot(psi,psi).real-1),1e-13)
  coherent.append({'detuning':det,'proper_time':t,'expressed_fraction':pa,'unconverted_fraction':1-pa,'closed_form':exact})
# State-independent real shifts have no population effect.
H=np.array([[.2,.4],[.4,-.2]],complex)
for a in [0.,.1,2.5,-.7]:
 for t in [.1,1.,8.]:
  p1=np.abs(expm(-1j*H*t)[:,0])**2;p2=np.abs(expm(-1j*(H+a*np.eye(2))*t)[:,0])
```

```
    **2
  check(f'Global phase has no conversion a={a},t={t}',np.max(abs(p1-p2)),1e-13,'
    analytic identity')
save_csv('coherent_conversion.csv',coherent)
plt.figure(figsize=(6.6,3.8))
for det in [0.,.3,1.]:
 rr=[r for r in coherent if r['detuning']==det];plt.plot([r['proper_time'] for r
     in rr],[r['expressed_fraction'] for r in rr],label=f'Detuning {det:g}')
plt.xlabel('Proper time (model units)');plt.ylabel('Expressed fraction');plt.
    legend();figsave('coherent_conversion')
# --- Symbolic corrections and exact obstructions ---
r,t,a,b,rho0,d,f=sp.symbols('r t a b rho0 d f',real=True);ph=sp.Function('phi')(
    r);gc=sp.Function('gamma')(r,t);ep=sp.Function('eps')(r)
expr=1+a*sp.tanh(r+t)+b*sp.sinh(ph)+gc
correct_r=a/sp.cosh(r+t)**2+b*sp.cosh(ph)*sp.diff(ph,r)+sp.diff(gc,r)
correct_rr=-2*a*sp.tanh(r+t)/sp.cosh(r+t)**2+b*(sp.sinh(ph)*sp.diff(ph,r)**2+sp.
    cosh(ph)*sp.diff(ph,r,2))+sp.diff(gc,r,2)
for name,ex in [('first derivative',sp.diff(expr,r)-correct_r),('second
    derivative',sp.diff(expr,r,2)-correct_rr),('density derivative',sp.diff(rho0
    *(1+d*sp.tanh(f*r)+ep),r)-rho0*(d*f/sp.cosh(f*r)**2+sp.diff(ep,r)))]:
 check(name,0 if sp.simplify(ex.rewrite(sp.exp))==0 else 1,0,'symbolic')
alpha,me,c,hb=sp.symbols('alpha me c hbar',positive=True)
E1=-me*c*c*alpha**2/2;Torb=2*sp.pi*hb/(me*c*c*alpha**2)
cycle=sp.simplify(E1*Torb/hb);check('Bohr orbital phase is minus pi',0 if cycle
    ==-sp.pi else 1,0,'symbolic')
# The distance kernel is a pair weight, not a normalizable 3D infinite-volume
    density.
x=sp.symbols('x',positive=True)
check('Kernel radial integral',0 if sp.simplify(sp.diff(x-sp.atan(x),x)-x*x/(1+x
    *x))==0 else 1,0,'symbolic')
# --- High-precision supplied-input physical reference calculations ---
mp.mp.dps=60
C=mp.mpf('299792458');HP=mp.mpf('6.62607015e-34');HB=HP/(2*mp.pi);QE=mp.mpf('
    1.602176634e-19');KB=mp.mpf('1.380649e-23');NA=mp.mpf('6.02214076e23')
G=mp.mpf('6.67430e-11');AL=mp.mpf('7.2973525643e-3');ME=mp.mpf('9.1093837139e-31'
    );MP=mp.mpf('1.67262192595e-27');MN=mp.mpf('1.67492750056e-27')
values={
 'hbar':(HB,'J s','exact h and pi'),
 'mu0':(2*AL*HP/(QE**2*C),'N A^-2','alpha and exact h,e,c'),
 'epsilon0':(QE**2/(2*AL*HP*C),'F m^-1','alpha and exact h,e,c'),
 'Rydberg_constant':(AL**2*ME*C/(2*HP),'m^-1','alpha, electron mass and exact h,
    c'),
 'Bohr_radius':(HB/(ME*C*AL),'m','alpha, electron mass and exact h,c'),
 'Hartree_energy':(ME*C*C*AL*AL,'J','alpha, electron mass and exact c'),
 'Rydberg_energy_eV':(ME*C*C*AL*AL/(2*QE),'eV','alpha and electron mass;
    infinite nuclear mass'),
 'electron_Compton_wavelength':(HP/(ME*C),'m','electron mass and exact h,c'),
 'classical_electron_radius':(AL*HB/(ME*C),'m','alpha and electron mass; not
    measured particle size'),
 'Thomson_cross_section':(8*mp.pi/3*(AL*HB/(ME*C))**2,'m^2','alpha and electron
    mass; low-energy free electron'),
 'Bohr_magneton':(QE*HB/(2*ME),'J T^-1','electron mass and exact e,h'),
 'nuclear_magneton':(QE*HB/(2*MP),'J T^-1','proton mass and exact e,h'),
```

```
 'electron_rest_energy':(ME*C*C/QE/1e6,'MeV','electron mass and exact c,e'),
 'proton_rest_energy':(MP*C*C/QE/1e6,'MeV','proton mass and exact c,e'),
 'neutron_rest_energy':(MN*C*C/QE/1e6,'MeV','neutron mass and exact c,e'),
 'proton_electron_mass_ratio':(MP/ME,'1','two measured masses; not predicted'),
 'neutron_proton_mass_ratio':(MN/MP,'1','two measured masses; not predicted'),
 'Planck_length':(mp.sqrt(HB*G/C**3),'m','G and exact h,c'),
 'Planck_time':(mp.sqrt(HB*G/C**5),'s','G and exact h,c'),
 'Planck_mass':(mp.sqrt(HB*C/G),'kg','G and exact h,c'),
 'Planck_energy':(mp.sqrt(HB*C**5/G),'J','G and exact h,c'),
 'Planck_temperature':(mp.sqrt(HB*C**5/G)/KB,'K','G and exact h,c,kB'),
 'Stefan_Boltzmann_constant':(2*mp.pi**5*KB**4/(15*HP**3*C*C),'W m^-2 K^-4','
    exact h,kB,c and pi'),
 'gas_constant':(NA*KB,'J mol^-1 K^-1','exact NA,kB'),
 'Faraday_constant':(NA*QE,'C mol^-1','exact NA,e'),
 'flux_quantum':(HP/(2*QE),'Wb','exact h,e; charged condensate interpretation
    additional'),
 'Josephson_constant':(2*QE/HP,'Hz V^-1','exact h,e; Josephson law additional'),
 'von_Klitzing_constant':(HP/QE**2,'ohm','exact h,e; Hall law additional')}
refrows=[{'quantity':k,'computed_value':mp.nstr(v,28),'unit':u,'inputs_and_scope'
    :deps,'role':'reference calculation; not independent MNT prediction'} for k
    ,(v,u,deps) in values.items()]
save_csv('reference_constants.csv',refrows)
# Identity checks use independent algebraic pathways, not agreement to fitted
    reference digits.
EPS=values['epsilon0'][0];MU=values['mu0'][0]
identities={'Maxwell vacuum speed':MU*EPS*C*C-1,'alpha via permittivity':QE
    **2/(4*mp.pi*EPS*HB*C)/AL-1,'Planck definitions':values['Planck_mass'][0]*
    values['Planck_length'][0]*C/HB-1,'Rydberg and Hartree':2*HP*C*values['
    Rydberg_constant'][0]/values['Hartree_energy'][0]-1,'Bohr radius and Compton'
    :values['Bohr_radius'][0]*AL*2*mp.pi/values['electron_Compton_wavelength'
    ][0]-1}
for k,v in identities.items():check(k,abs(v),1e-50,'reference identity')
# Standard frozen background (same input values as prior benchmark, no re-fit).
H0_kms=70.;Om=.3;H0_SI=H0_kms*1000/3.0856775814913673e22;secGyr=365.25*86400*1e9
age=2/(3*H0_SI*np.sqrt(1-Om))*np.arcsinh(np.sqrt((1-Om)/Om))/secGyr
fermi=float(HB**2/(2*ME)*(3*mp.pi**2*mp.mpf('1e28'))**(mp.mpf(2)/3)/QE)
newresults={
 'edition':'Conservative reconstruction, 6 September 2026',
 'construction_status':'A complete finite dynamical model, not a demonstrated
    microscopic theory of all observed sectors',
 'fixed_model_inputs':{'nodes':n,'reservoir_modes_per_link':modes,'I':I,'K':K,'
    omega':omega.tolist(),'mass':mass.tolist(),'coupling':coupling.tolist(),'
    proper_duration':T,'initial_state':y0.tolist(),'parameter_selection':'
    illustrative model units; no empirical target optimized'},
 'ring':{'initial_total_energy':H0,'relative_energy_error':conservation,'
    reversal_max_error':float(reverse_error),'clock_max_error':float(clockerr),'
    max_memory_identity_error':max(z['absolute_error'] for z in memrows)},
 'predictions':{'pendulum_period_ratio_pi_over_2':next(z['
    period_over_small_amplitude'] for z in periods if abs(z['phase_amplitude']-
    np.pi/2)<1e-9),'small_k_axis_phase_coefficient':-1/24,'
    small_k_body_diagonal_phase_coefficient':-1/72,'axis_body_coefficient_ratio'
    :3.,'damping_coefficient_zeta':zeta,'role':'conditional mathematical
    predictions of the specified realization; no claimed new physical detection'
```

```
    },
 'reference_recalculations':{'flat_70_03_age_Gyr':age,'fermi_at_1e28_m3_eV':
    fermi,'Bohr_orbital_phase_radians':str(cycle)},
 'new_physical_parameter_free_alignments':0,
 'checks':{'total':len(checks),'passed':sum(r['passed'] for r in checks),'failed'
    :[r for r in checks if not r['passed']]}}
(OUT/'reconstruction_results.json').write_text(json.dumps(newresults,indent=2))
save_csv('reconstruction_checks.csv',checks)
(OUT/'execution_environment.json').write_text(json.dumps({'time_utc':datetime.
    now(timezone.utc).isoformat(),'python':sys.version,'numpy':np.__version__,'
    scipy':scipy.__version__,'sympy':sp.__version__,'script_sha256':hashlib.
    sha256(Path(__file__).read_bytes()).hexdigest(),'platform':platform.platform
    ()},indent=2))
print(json.dumps(newresults,indent=2))
if newresults['checks']['failed']:sys.exit(1)
```

G. Executable threshold and causal-response checks

```
#!/usr/bin/env python3
"""Additional target-free checks: conservative threshold coupling and response.
No fitted measurements or experimentally selected parameters are used.
"""
from pathlib import Path
import json,csv
import numpy as np
from scipy.integrate import solve_ivp
from scipy.linalg import expm
import sympy as sp
ROOT=Path(__file__).resolve().parents[1];OUT=ROOT/'results';OUT.mkdir(exist_ok=
    True)
checks=[]
def check(name,error,tol,kind='analytic or implementation'):
 e=float(error);checks.append(dict(name=name,error=e,tolerance=float(tol),passed
    =bool(np.isfinite(e) and e<=tol),kind=kind))
def csvout(name,rows):
 with (OUT/name).open('w',newline='') as f:
  w=csv.DictWriter(f,fieldnames=rows[0]);w.writeheader();w.writerows(rows)
# Phase-feedback readout, with time-independent parameters; no external work
    omitted.
N=4;I=1.;K=.5;M=1.2;ED=.4;u0=.05;lc=.5
B=np.eye(N)-np.roll(np.eye(N),1,axis=0)
def coherence(th):
 return abs(np.exp(1j*th).sum())**2/N**2
def dc(th):
 return -2/N**2*np.sum(np.sin(th[:,None]-th[None,:]),axis=1)
def energy(y):
 th,p,z,v=y[:N],y[N:2*N],y[-2],y[-1]
 return np.sum(p*p)/(2*I)+K*np.sum(1-np.cos(B.T@th))+v*v/(2*M)+ED*((z*z-1)
    **2/4-(u0+lc*coherence(th))*z)
def rhs(t,y):
 th,p,z,v=y[:N],y[N:2*N],y[-2],y[-1]
 return np.r_[p/I,-K*B@np.sin(B.T@th)+ED*lc*z*dc(th),v/M,-ED*(z**3-z-u0-lc*
```

```
    coherence(th))]
y0=np.r_[[-.25,0.,.25,0.],[.05,-.03,.04,-.02],-1.,0.]
sol=solve_ivp(rhs,[0,35],y0,method='DOP853',rtol=2e-12,atol=2e-14,dense_output=
    True)
if not sol.success:raise RuntimeError(sol.message)
t=np.linspace(0,35,1401);Y=sol.sol(t);E=np.array([energy(y) for y in Y.T]);err=
    float(np.max(np.abs(E-E[0])))
check('Readout with reciprocal feedback conserves total energy',err,1e-9)
check('Readout phase momentum conservation',np.max(abs(Y[N:2*N].sum(axis=0)-sum(
    y0[N:2*N]))),1e-11)
for j in [0,213,725,1400]:
 th=Y[:N,j];h=1e-6;grad=[]
 for k in range(N):
  a=th.copy();a[k]+=h;b=th.copy();b[k]-=h;grad.append((coherence(a)-coherence(b)
    )/(2*h))
 check('Coherence gradient '+str(j),np.max(abs(np.array(grad)-dc(th))),2e-9)
 check('Coherence bounds '+str(j),max(0,-coherence(th),coherence(th)-1),1e-12)
# Prove fold and its dimensionless threshold, independent of any measured
    constant.
uc=2/(3*np.sqrt(3));zc=-1/np.sqrt(3)
check('Saddle-node stationarity',abs(zc**3-zc-uc),1e-15)
check('Saddle-node zero curvature',abs(3*zc*zc-1),1e-15)
thresholds=[]
for u in [0.,.2,.38,.4,.55]:
 roots=np.roots([1.,0.,-1.,-u]);real=sorted(float(x.real) for x in roots if abs(
    x.imag)<1e-10)
 check('Root count u='+str(u),abs(len(real)-(3 if abs(u)<uc else 1)),0)
 thresholds.append(dict(tilt=u,real_stationary_points=';'.join(f'{r:.12g}' for r
     in real),stable_points=';'.join(f'{r:.12g}' for r in real if 3*r*r-1>0)))
csvout('threshold_stationary_points.csv',thresholds)
csvout('threshold_feedback_trajectory.csv',[dict(proper_time=a,readout_z=y[-2],
    coherence=coherence(y[:N]),total_energy=e) for a,y,e in zip(t,Y.T,E)])
# Linear response: real and imaginary components, force spectrum and fluctuation
     relation.
# A causal exponential memory M(t)=(zeta/tb) exp(-t/tb), t>=0.
# This is a declared limiting bath spectrum, separate from the finite three-mode
     example.
zeta=.12;tb=.7;response=[]
for lam in [.1,.5,1.,2.,3.]:
 for w in [.05,.2,.7,1.4,3.]:
  Mt=zeta/(1-1j*w*tb);D=lam-w*w-1j*w*lam*Mt;chi=1/D
  noise=2*.4*lam*Mt.real;S=noise*abs(chi)**2
  fdt=2*.4/w*chi.imag
  check(f'Frequency FDT lambda={lam},omega={w}',abs(S-fdt),1e-11)
  check(f'Passivity lambda={lam},omega={w}',max(0.,-chi.imag),1e-13)
  response.append(dict(laplacian_eigenvalue=lam,frequency=w,susceptibility_real=
    chi.real,susceptibility_imaginary=chi.imag,noise_spectrum=noise,
    phase_spectrum=S,FDT_prediction=fdt))
csvout('frequency_response.csv',response)
# All modes have a pole in the left half-plane in the exponential-memory
    embedding.
# dQ=V, dV=-lambda Q-lambda Z, dZ=-(Z-zeta V)/tb
for lam in [.05,.3,1.,2.,4.]:
```

```
 A=np.array([[0.,1.,0.],[-lam,0.,-lam],[0.,zeta/tb,-1/tb]])
 eig=np.linalg.eigvals(A)
 check(f'Exponential-memory stability lambda={lam}',max(0.,float(max(eig.real)))
    ,1e-12)
# Same scaling in constants is not consistent with their defining algebra.
s=sp.symbols('s',positive=True)
# Rydberg(alpha,me,c,h) scales s^2*s*s/s = s^3 when all supplied quantities
    scale s.
check('Universal scaling obeys Rydberg dependency',0 if sp.simplify((s**2*s*s/s)-
    s**3)==0 else 1,0)
# Hamiltonian additive scalar produces unchanged observables; norm multiplying
    is not conversion.
H=np.array([[.1,.3],[.3,-.1]],complex);rho=np.array([[1.,0.],[0.,0.]],complex)
for q in [.3,1.,2.]:
 for tau in [.2,1.,4.]:
  U=expm(-1j*H*q*tau);V=expm(-1j*(q*H)*tau)
  check(f'Clock generator identity q={q},t={tau}',np.max(abs(U-V)),1e-14)
res={'fixed_readout_parameters':{'nodes':N,'I':I,'K':K,'M':M,'ED':ED,'u0':u0,'
    coherence_coupling':lc,'duration':35.},'threshold':{'critical_tilt':uc,'
    critical_negative_well_coordinate':zc,'trajectory_energy_absolute_error':err,
    'initial_energy':float(E[0]),'minimum_z':float(Y[-2].min()),'maximum_z':
    float(Y[-2].max())},'response':{'zeta':zeta,'memory_time':tb,'kBT':.4,'role':
    'declared exponential-memory model, not fitted to finite-bath parameters or
    measurements'},'checks':{'total':len(checks),'passed':sum(r['passed'] for r
    in checks),'failed':[r for r in checks if not r['passed']]}}
(OUT/'additional_results.json').write_text(json.dumps(res,indent=2));csvout('
    additional_checks.csv',checks)
print(json.dumps(res,indent=2))
if res['checks']['failed']:raise SystemExit(1)
```

H. Executable coupled-spectrum checks

```
#!/usr/bin/env python3
"""Linearized spectrum of the same conservative phase-reserve Hamiltonian.
The coefficients are copied from the frozen six-node demonstration, not from
    measurements.
"""
from pathlib import Path
import json,csv
import numpy as np
from scipy.linalg import eigh
ROOT=Path(__file__).resolve().parents[1];OUT=ROOT/'results';OUT.mkdir(exist_ok=True)
I=K=1.;m=np.ones(3);Om=np.array([.65,1.15,2.4]);c=np.array([.22,.13,.07])
A0=float(sum(c*c/(m*Om**2)));A1=float(sum(c*c/(m*Om**4)))
checks=[]
def check(name,e,tol):
 e=float(e);checks.append(dict(name=name,error=e,tolerance=tol,passed=bool(np.
    isfinite(e) and e<=tol)))
def normal(lam):
 S=np.zeros((4,4));S[0,0]=lam*(K+A0);S[0,1:]=S[1:,0]=-np.sqrt(lam)*c;S[1:,1:]=np.diag
    (m*Om**2)
 M=np.diag(np.r_[I,m]);v,U=eigh(S,M)
 return v,U,S,M
rows=[]
```

```
for lam in [1e-5,1e-4,1e-3,.01,.1,1.,3.,4.]:
 v,U,S,M=normal(lam)
 check(f'Mode mass orthonormality lambda={lam}',np.max(abs(U.T@M@U-np.eye(4))),2e-13)
 check(f'Mode eigen-equation lambda={lam}',np.max(abs(S@U-M@U@np.diag(v))),2e-13)
 check(f'Nonnegative spectrum lambda={lam}',max(0.,-float(min(v))),2e-14)
 for j,w2 in enumerate(v):
  # Original eliminated-bath dispersion, away from bare poles.
  D=K*lam-I*w2-lam*sum((c*c/(m*Om**2))*w2/(Om**2-w2))
  scale=1+abs(K*lam)+abs(I*w2)
  check(f'Schur dispersion lambda={lam},branch={j}',abs(D)/scale,2e-6)
  rows.append(dict(laplacian_eigenvalue=lam,branch=j,squared_frequency=w2,frequency=
    np.sqrt(max(0,w2)),resolved_weight=float(I*U[0,j]**2)))
# Three directional limits of the actual coupled acoustic branch.
low=[]
for direction,unit in [('axis',np.array([1.,0,0])),('face',np.array([1.,1.,0])/np.
    sqrt(2)),('body',np.ones(3)/np.sqrt(3))]:
 angular=sum(unit**4);coef=-(angular/24+A1/(2*I))
 for ka in [.02,.01,.005]:
  lam=float(4*sum(np.sin(.5*ka*unit)**2));v,_,_,_=normal(lam)
  ratio=np.sqrt(v[0])/(np.sqrt(K/I)*ka);estimate=(ratio-1)/(ka*ka)
  check(f'Coupled acoustic expansion {direction},ka={ka}',abs(estimate-coef),max(1e
    -6,ka*ka))
  low.append(dict(direction=direction,ka=ka,phase_speed_ratio=ratio,
    estimated_quadratic_coefficient=estimate,analytic_quadratic_coefficient=coef))
# Full six-node ring has an exact common phase zero mode and free cycle-reserve modes
    .
N=6;B=np.eye(N)-np.roll(np.eye(N),1,axis=0);L=B@B.T
S=np.zeros((24,24));S[:N,:N]=(K+A0)*L
for a in range(3):
 sl=slice(N+a*N,N+(a+1)*N);S[:N,sl]=-c[a]*B;S[sl,:N]=-c[a]*B.T;S[sl,sl]=m[a]*Om[a
    ]**2*np.eye(N)
M=np.diag(np.r_[np.ones(N)*I,np.repeat(m,N)]);vals,U=eigh(S,M)
expected=[0.,*list(Om**2)]
for lam in np.linalg.eigvalsh(L)[1:]:expected.extend(normal(lam)[0])
check('Full ring spectrum from graph-mode decomposition',np.max(abs(vals-np.sort(
    expected))),3e-13)
check('Full ring nonnegative Hessian',max(0.,-float(min(vals))),3e-13)
for name,data in [('coupled_spectrum.csv',rows),('coupled_acoustic_dispersion.csv',
    low),('spectral_checks.csv',checks)]:
 with (OUT/name).open('w',newline='') as f:
  w=csv.DictWriter(f,fieldnames=data[0]);w.writeheader();w.writerows(data)
r={'frozen_parameters':dict(I=I,K=K,m=m.tolist(),Omega=Om.tolist(),coupling=c.tolist
    ()),'counterterm_coefficient':A0,'reserve_inertia_coefficient':A1,'
    full_ring_squared_frequencies':vals.tolist(),'directional_coefficients':{x['
    direction']:x['analytic_quadratic_coefficient'] for x in low},'checks':dict(total
    =len(checks),passed=sum(x['passed'] for x in checks),failed=[x for x in checks if
     not x['passed']])}
(OUT/'spectral_results.json').write_text(json.dumps(r,indent=2));print(json.dumps(r,
    indent=2))
if r['checks']['failed']:raise SystemExit(1)
```

External references

[1] W. Hoeffding, “Probability Inequalities for Sums of Bounded Random Variables,” *Journal of the American Statistical Association* **58**, 13–30 (1963). doi:10.1080/01621459.1963.10500830.

[2] K. G. Wilson, “Confinement of quarks,” *Physical Review D* **10**, 2445 (1974). doi:10.1103/PhysRevD.10.2445.

[3] J. Kogut and L. Susskind, “Hamiltonian formulation of Wilson’s lattice gauge theories,” *Physical Review D* **11**, 395 (1975). doi:10.1103/PhysRevD.11.395.

[4] A. M. Gleason, “Measures on the Closed Subspaces of a Hilbert Space,” *Journal of Mathematics and Mechanics* **6**, 885–893 (1957). doi:10.1512/iumj.1957.6.56050; original-paper record and abstract.

[5] G. Lindblad, “On the generators of quantum dynamical semigroups,” *Communications in Mathematical Physics* **48**, 119–130 (1976). doi:10.1007/BF01608499.

[6] J. S. Bell, “On the Einstein Podolsky Rosen paradox,” *Physics Physique Fizika* **1**, 195–200 (1964). doi:10.1103/PhysicsPhysiqueFizika.1.195.

[7] J. F. Clauser, M. A. Horne, A. Shimony and R. A. Holt, “Proposed Experiment to Test Local Hidden-Variable Theories,” *Physical Review Letters* **23**, 880 (1969); erratum **24**, 549 (1970). doi:10.1103/PhysRevLett.23.880.

[8] S. Navas et al. (Particle Data Group), “Review of Particle Physics,” *Physical Review D* **110**, 030001 (2024), with the 2025 update. doi:10.1103/PhysRevD.110.030001; official review index. Particle conventions, kinematics, cosmology and statistical methods are used as external effective-physics references.

[9] E. Witten, “An SU(2) anomaly,” *Physics Letters B* **117**, 324–328 (1982). doi:10.1016/0370-2693(82)90728-6.

[10] H. B. Nielsen and M. Ninomiya, “A no-go theorem for regularizing chiral fermions,” *Physics Letters B* **105**, 219–223 (1981). doi:10.1016/0370-2693(81)91026-1.

[11] M. Lüscher, “Exact chiral symmetry on the lattice and the Ginsparg–Wilson relation,” *Physics Letters B* **428**, 342–345 (1998). arXiv:hep-lat/9802011; doi:10.1016/S0370-2693(98)00423-7.

[12] H. Neuberger, “More about exactly massless quarks on the lattice” (1998). arXiv:hep-lat/9801031.

[13] National Institute of Standards and Technology, *2022 CODATA Recommended Values of the Fundamental Physical Constants*, released 2024. Official all-constants text table. Accessed 6 September 2026. Exact SI definitions and measured reference constants retain their respective roles.

[14] J. Garriga and V. F. Mukhanov, "Perturbations in k-inflation" (1999). arXiv:hep-th/9904176.

[15] J. D. Bekenstein, "Black Holes and Entropy," *Physical Review D* **7**, 2333 (1973). doi:10.1103/PhysRevD.7.2333.

[16] S. W. Hawking, "Particle creation by black holes," *Communications in Mathematical Physics* **43**, 199–220 (1975). doi:10.1007/BF02345020.

[17] N. Aghanim et al. (Planck Collaboration), "Planck 2018 results. VI. Cosmological parameters," *Astronomy & Astrophysics* **641**, A6 (2020). arXiv:1807.06209; doi:10.1051/0004-6361/201833910.

[18] M. Abdul-Karim et al. (DESI Collaboration), "DESI DR2 Results II: Measurements of Baryon Acoustic Oscillations and Cosmological Constraints" (2025). arXiv:2503.14738v2. Compressed distance-vector interpretation and sample definitions.

[19] DESI DR2 BAO likelihood data distributed in *CobayaSampler/bao_data*, directory `desi_bao_dr2`. Repository directory; GC-combined mean vector; GC-combined covariance. Accessed 6 September 2026; local input bytes recorded separately.

[20] Gravitational Wave Open Science Center, *GW150914*, catalog GWTC-1-confident, version 3. Versioned event record. Accessed 6 September 2026. The numerical calculation uses catalog source-parameter summaries, not raw strain.

[21] T. Baka et al., "Testing general relativity with gravitational waves: Improving and extending modified dispersion relation tests," *Physical Review D* **113**, 064064 (31 March 2026). doi:10.1103/bgvh-c1wj; arXiv:2511.00497.

[22] E. Aprile et al. (XENON Collaboration), "First Search for Light Dark Matter in the Neutrino Fog with XENONnT," *Physical Review Letters* **134**, 111802 (2025). arXiv:2409.17868; public release doi:10.5281/zenodo.14522707.

[23] XENONnT Collaboration, *light_wimp_data_release*. Official public repository; SI limit CSV; Light-mediator limit CSV. Accessed 6 September 2026.

[24] CERN Open Data Portal, *Histogram visualization: educational dimuon example*. Displayed CSV example; associated educational sample record 700. Accessed 6 September 2026. Only the four displayed example rows are used in this edition.

[25] T. Alion et al., "Experiment Simulation Configurations Used in DUNE CDR" (2016). arXiv:1606.09550.

[26] B. Abi et al. (DUNE Collaboration), "Deep Underground Neutrino Experiment (DUNE), Far Detector Technical Design Report, Volume II: DUNE Physics" (2020). arXiv:2002.03005.

[27] Fermi National Accelerator Laboratory, "DUNE will use liquid-argon time projection chamber technology both near and far" (May 2026). Official experiment-status report. Accessed 6 September 2026.

[28] A. Einstein, “Zur Elektrodynamik bewegter Körper,” *Annalen der Physik* **17**, 891–921 (1905). doi:10.1002/andp.19053221004. Relativistic clock comparisons are used as an established reference, not as a claimed derivation from EQEF.

[29] C. W. Chou, D. B. Hume, T. Rosenband and D. J. Wineland, “Optical Clocks and Relativity,” *Science* **329**, 1630–1633 (2010). doi:10.1126/science.1192720; NIST-hosted primary paper. Figure 3 supplies the height-step comparison used here.

[30] J. Bailey et al., “Measurements of relativistic time dilatation for positive and negative muons in a circular orbit,” *Nature* **268**, 301–305 (1977). doi:10.1038/268301a0. Published positive-muon lifetime and rounded abstract Lorentz factor; no full beam-distribution reanalysis.

[31] D. M. Webber et al. (MuLan Collaboration), “Measurement of the Positive Muon Lifetime and Determination of the Fermi Constant to Part-per-Million Precision,” *Physical Review Letters* **106**, 041803 (2011). arXiv:1010.0991; doi:10.1103/PhysRevLett.106.041803. Independent rest-lifetime input.

[32] P. Delva et al., “Gravitational Redshift Test Using Eccentric Galileo Satellites,” *Physical Review Letters* **121**, 231101 (2018). arXiv:1812.03711; doi:10.1103/PhysRevLett.121.231101.

[33] P. Touboul et al., “MICROSCOPE Mission: Final Results of the Test of the Equivalence Principle,” *Physical Review Letters* **129**, 121102 (2022). arXiv:2209.15487.

[34] B. P. Abbott et al., “Gravitational Waves and Gamma-rays from a Binary Neutron Star Merger: GW170817 and GRB 170817A,” *Astrophysical Journal Letters* **848**, L13 (2017). arXiv:1710.05834.

[35] R. Aliberti et al., “The anomalous magnetic moment of the muon in the Standard Model: an update” (2025). arXiv:2505.21476. Reference prediction and hadronic-input qualifications.

[36] D. P. Aguillard et al. (Muon $g-2$ Collaboration), “Measurement of the Positive Muon Anomalous Magnetic Moment to 127 ppb” (2025). arXiv:2506.03069. Experimental world-average comparison as reported in the cited release.

[37] L. K. Shalm et al., “Strong Loophole-Free Test of Local Realism,” *Physical Review Letters* **115**, 250402 (2015). arXiv:1511.03189.

[38] Bureau International des Poids et Mesures, *The International System of Units (SI)*, ninth edition (2019), version 4.01, June 2026. doi:10.59161/AUEZ1291. Exact defining constants and current unit conventions.

[39] P. J. Mohr, D. B. Newell, B. N. Taylor and E. Tiesinga, “CODATA recommended values of the fundamental physical constants: 2022,” *Reviews of Modern Physics* **97**, 025002 (2025). doi:10.1103/RevModPhys.97.025002; arXiv:2409.03787.

[40] E. Noether, "Invariante Variationsprobleme," *Nachrichten von der Gesellschaft der Wissenschaften zu Göttingen, Mathematisch-Physikalische Klasse*, 235–257 (1918). English translation by M. A. Tavel, "Invariant Variation Problems," arXiv:physics/0503066.

[41] R. Zwanzig, "Nonlinear generalized Langevin equations," *Journal of Statistical Physics* **9**, 215–220 (1973). doi:10.1007/BF01008729.

[42] H. Mori, "Transport, Collective Motion, and Brownian Motion," *Progress of Theoretical Physics* **33**, 423–455 (1965). doi:10.1143/PTP.33.423.

[43] R. Kubo, "The fluctuation-dissipation theorem," *Reports on Progress in Physics* **29**, 255–284 (1966). doi:10.1088/0034-4885/29/1/306.

[44] R. P. Feynman and F. L. Vernon, Jr., "The theory of a general quantum system interacting with a linear dissipative system," *Annals of Physics* **24**, 118–173 (1963). doi:10.1016/0003-4916(63)90068-X.

[45] A. O. Caldeira and A. J. Leggett, "Path integral approach to quantum Brownian motion," *Physica A* **121**, 587–616 (1983). doi:10.1016/0378-4371(83)90013-4.

[46] E. H. Lieb and D. W. Robinson, "The finite group velocity of quantum spin systems," *Communications in Mathematical Physics* **28**, 251–257 (1972). doi:10.1007/BF01645779.

[47] D. N. Page and W. K. Wootters, "Evolution without evolution: Dynamics described by stationary observables," *Physical Review D* **27**, 2885–2892 (1983). doi:10.1103/PhysRevD.27.2885.

[48] C. Rovelli, "Time in quantum gravity: An hypothesis," *Physical Review D* **43**, 442–456 (1991). doi:10.1103/PhysRevD.43.442.

[49] V. Gorini, A. Kossakowski and E. C. G. Sudarshan, "Completely positive dynamical semigroups of N-level systems," *Journal of Mathematical Physics* **17**, 821–825 (1976). doi:10.1063/1.522979.

[50] N. Bohr, "On the constitution of atoms and molecules," *Philosophical Magazine*, series 6, **26**, 1–25 (1913). doi:10.1080/14786441308634955.

[51] E. Schrödinger, "Quantisierung als Eigenwertproblem," *Annalen der Physik* **384**, 361–376 (1926). doi:10.1002/andp.19263840404.

[52] P. A. M. Dirac, "The quantum theory of the electron," *Proceedings of the Royal Society A* **117**, 610–624 (1928). doi:10.1098/rspa.1928.0023.

[53] J. Schwinger, "On Quantum-Electrodynamics and the Magnetic Moment of the Electron," *Physical Review* **73**, 416–417 (1948). doi:10.1103/PhysRev.73.416.

[54] G. H. Derrick, "Comments on Nonlinear Wave Equations as Models for Elementary Particles," *Journal of Mathematical Physics* **5**, 1252–1254 (1964). doi:10.1063/1.1704233.

[55] C. N. Yang and R. L. Mills, "Conservation of Isotopic Spin and Isotopic Gauge Invariance," *Physical Review* **96**, 191–195 (1954). doi:10.1103/PhysRev.96.191.

[56] S. Weinberg, “A Model of Leptons,” *Physical Review Letters* **19**, 1264–1266 (1967). doi:10.1103/PhysRevLett.19.1264.

[57] D. J. Gross and F. Wilczek, “Ultraviolet Behavior of Non-Abelian Gauge Theories,” *Physical Review Letters* **30**, 1343–1346 (1973). doi:10.1103/PhysRevLett.30.1343.

[58] H. D. Politzer, “Reliable Perturbative Results for Strong Interactions?” *Physical Review Letters* **30**, 1346–1349 (1973). doi:10.1103/PhysRevLett.30.1346.

[59] L. Wolfenstein, “Neutrino oscillations in matter,” *Physical Review D* **17**, 2369–2374 (1978). doi:10.1103/PhysRevD.17.2369.

[60] A. Einstein, “Die Grundlage der allgemeinen Relativitätstheorie,” *Annalen der Physik* **354**, 769–822 (1916). doi:10.1002/andp.19163540702.

[61] C. Barceló, S. Liberati and M. Visser, “Analogue Gravity,” *Living Reviews in Relativity* **8**, 12 (2005); updated review, arXiv:gr-qc/0505065, version 4 (2024). Analogue propagation geometry is distinguished from autonomous Einstein dynamics.

[62] T. Jacobson, “Thermodynamics of Spacetime: The Einstein Equation of State,” *Physical Review Letters* **75**, 1260–1263 (1995). doi:10.1103/PhysRevLett.75.1260; arXiv:gr-qc/9504004.

[63] F. W. Hehl, P. von der Heyde and G. D. Kerlick, “General relativity with spin and torsion and its deviations from Einstein’s theory,” *Physical Review D* **10**, 1066–1069 (1974). doi:10.1103/PhysRevD.10.1066.

[64] M. Planck, “Ueber das Gesetz der Energieverteilung im Normalspectrum,” *Annalen der Physik* **309**, 553–563 (1901). doi:10.1002/andp.19013090310.

[65] C. M. Wilson, G. Johansson, A. Pourkabirian, M. Simoen, J. R. Johansson, T. Duty, F. Nori and P. Delsing, “Observation of the dynamical Casimir effect in a superconducting circuit,” *Nature* **479**, 376–379 (2011). doi:10.1038/nature10561; arXiv:1105.4714.

[66] C.-P. Ma and E. Bertschinger, “Cosmological Perturbation Theory in the Synchronous and Conformal Newtonian Gauges,” *Astrophysical Journal* **455**, 7–25 (1995). arXiv:astro-ph/9506072.

[67] J. F. Navarro, C. S. Frenk and S. D. M. White, “A Universal Density Profile from Hierarchical Clustering,” *Astrophysical Journal* **490**, 493–508 (1997). doi:10.1086/304888; arXiv:astro-ph/9611107.

[68] C. Pitrou, A. Coc, J.-P. Uzan and E. Vangioni, “Precision big bang nucleosynthesis with improved Helium-4 predictions,” *Physics Reports* **754**, 1–66 (2018). doi:10.1016/j.physrep.2018.04.005; arXiv:1801.08023.